Dissertation Thesis

Multifunctional Carbon Based Felt

Study programme:	P3106 Textile Engineering
Study branch:	Textile Technics and Materials Engineering

Author:	**Yuanfeng Wang, M.Eng.**
Thesis Supervisor:	prof. Ing. Jiří Militký, CSc.
	Department of material engineering

Liberec 2024

Declaration

I hereby certify, I, myself, have written my dissertation as an original and primary work using the literature listed below and consulting it with my thesis supervisor and my thesis counsellor.

I acknowledge that my dissertation is fully governed by Act No. 121/2000 Coll., the Copyright Act, in particular Article 60 – School Work.

I acknowledge that the Technical University of Liberec does not infringe my copyrights by using my dissertation for internal purposes of the Technical University of Liberec.

I am aware of my obligation to inform the Technical University of Liberec on having used or granted license to use the results of my dissertation; in such a case the Technical University of Liberec may require reimbursement of the costs incurred for creating the result up to their actual amount.

At the same time, I honestly declare that the text of the printed version of my dissertation is identical with the text of the electronic version uploaded into the IS/STAG.

I acknowledge that the Technical University of Liberec will make my dissertation public in accordance with paragraph 47b of Act No. 111/1998 Coll., on Higher Education Institutions and on Amendment to Other Acts (the Higher Education Act), as amended.

I am aware of the consequences which may under the Higher Education Act result from a breach of this declaration.

May 22, 2024   Yuanfeng Wang, M.Eng.

Acknowledgement

During my doctoral studies, I received guidance from many individuals. I am sincerely grateful to them.

Firstly, I extend my sincere gratitude to my supervisor, prof. Jiří Militký. Throughout these years, his guidance and encouragement have propelled me forward. I am deeply thankful for his patience and vast knowledge, which have been instrumental in solving academic challenges and thesis writing.

I would also like to express my gratitude for the strong support provided by the Department of Materials Engineering, both in the laboratory and in experimental materials. I am grateful to prof. Jakub Wiener for generously sharing his expertise. I extend my thanks to colleagues Dr. Blanka Tomková, Dr. Miroslava Pechočiaková, Assoc. prof. Dr. Dana Křemenáková, Dr. Mohanapriya Venkataraman, Dr. Veronika Tunáková, and Ms. Kateřina Nohýnková and Assoc. prof. Martina Viková for their assistance. I would also like to express my gratitude to Vice Dean Dr. Iva Mertová, Ms. Bohumila Keilová, and Ms. Hana Musilová for their dedication to student affairs. Special thanks to colleagues doc. Jiří Chvojka, Mr. Pavel Holec, and Dr. Tomáš Kalous from the Department of Nonwovens and Nanofibrous Materials for their assistance in experiments.

I am particularly grateful to Dr. Josef Večerník and Assoc. prof. Amorn Chaiyasat for their invaluable support during my internship. Their profound knowledge has been enlightening. I am grateful for the companionship and assistance provided by the lovely members of our team, including Mr. Kai Yang, Ms. Xiuling Zhang, Mr. Shi Hu, Ms. Dan Wang, Mr. Xiaodong Tan, Ms. Qingyan Peng, Dr. Tao Yang, Dr. Xiaoman Xiong, and Dr. Muhammad Zaman Khan.

I also like to thank my parents for their unwavering support throughout my journey. Additionally, I am thankful to the Technical University of Liberec for providing me with the opportunity to pursue my doctoral studies. Lastly, I extend my deepest gratitude to all those who have contributed to my academic journey.

Abstract

Pyrolysis has emerged as a strategy for processing waste textiles, with the conversion of high-carbon-content textile waste into carbonaceous materials being beneficial for recovering its economic value while mitigating the environmental impact of textile waste. Carbon felt is widely used due to its lightweight nature and internal 3D conductive network. However, limited research exists on directly using waste textile felts as a precursor to produce carbon felt. The aim of this thesis is to carbonize acrylic-based waste felts under controlled conditions to produce carbon felt and enable its multifunctional applications.

To achieve the conversion of acrylic-based felts into flexible carbon felts with excellent performance, this study aims to investigate the impact of different loading tension methods and PTFE coatings during the pyrolysis process on the shrinkage rate, mechanical properties, electrical properties, and thermal properties of the resulting carbon felt. The results indicate that applying edge load to the samples during the carbonization stage helps to reduce the shrinkage rate of the final product, allowing the carbon felt to gain flexibility and form a well-structured conductive network.

To study the impact of PTFE coating on the pyrolysis of acrylic -based felts, acrylic -based felts were coated with different concentrations of PTFE and subsequently subjected to pyrolysis. By examining the morphology, mechanical properties, and electrical properties of PTFE-coated samples, we found that higher coating concentrations had a greater impact on the performance of the resulting carbon felt. Although high coating concentrations increased the material's modulus and electrical conductivity, they also led to a loss of flexibility in the carbon felt, which could severely limit its application scope.

By characterizing the morphology and structure of carbon felts prepared at different carbonization temperatures under an edge loading mode, it was found that increasing the carbonization temperature promoted higher crystallinity within the fibers and the formation of an ordered graphite structure. The formation of a dense, highly conductive network and high porosity was achieved. EMI shielding results demonstrated that the resulting carbon felt achieved a high EMI shielding effectiveness of 55 dB and a specific shielding effectiveness

of 2676.9 dBcm^{2}g^{-1}, surpassing many carbon composites. Additionally, the carbon felt exhibited excellent heating efficiency and high heating rates in resistive heating tests. Structural stability was investigated through a custom-designed experiment. The results showed that even under heating conditions, the carbon felt could maintain internal conductive pathway stability through multiple bending cycles.

This work also investigated the feasibility of converting acrylic -based filter felts into carbon felts for use in respiratory filtration layers. The excellent electrical conductivity of carbon felt allows it to be used not only as a respiratory filtration layer but also for high-temperature electrical disinfection. The design of the mask body and the corresponding electrode configuration enabled controlled resistive heating performance, ensuring the reliability of high-temperature disinfection of the carbon felt. Filtration efficiency and antibacterial testing results showed that the carbon felt achieved over 90% filtration efficiency for inhalable particles and effectively inhibited microbial growth due to its antibacterial properties.

Flexible carbon felt offers lower manufacturing costs and exhibits good chemical and structural stability. Functional testing results indicate that it demonstrates significant potential for applications in wearable heaters, flexible EMI shielding, respiratory filters, and other related fields.

Abstrakt

Pyrolýza se běžně používá jako strategie pro zpracování odpadních textilií, přičemž přeměna textilního odpadu s vysokým obsahem uhlíku na uhlíkaté materiály je potřebná pro přípravu ekonomicky výhodných produktů s vyšší užitnou hodnotou („upcycling") a zároveň zmírňuje dopad textilních odpadů na životní prostředí. Uhlíkové plsti jsou široce používána pro svoji relativně nízkou hmotnost a vysokou elektrickou vodivosti díky vnitřní 3 D vodivé síti. Přímé použití odpadních textilních plstí jako prekurzoru k výrobě uhlíkových plsti je však zkoumáno jen omezeně. Cílem této dizertační práce je optimalizace karbonizace odpadních plstí na bázi acrylic za kontrolovaných podmínek pro výrobu uhlíkových plstí a realizaci jejích multifunkčních aplikací. Byl zkoumán vliv různých metod zatížení odpadních plstí na bázi akrylových vláken s PTFE zátěrem na proces smršťování při pyrolýze. Byly hodnoceny mechanické vlastnosti, elektrické vlastnosti a tepelné vlastnosti finální uhlíkové plsti. Výsledky naznačují, že aplikace okrajového zatížení na vzorky během fáze karbonizace pomáhá snížit rychlost smrštění konečného produktu, což umožňuje uhlíkové plsti získat pružnost a vytvořit dobře strukturovanou vodivou síť. Pro studium vlivu zátěru PTFE na pyrolýzu plstí na bázi akrylových vláken byly plsti potaženy různými koncentracemi PTFE a následně podrobeny pyrolýze. Zkoumáním morfologie, mechanických vlastností a elektrických vlastností vzorků potažených PTFE bylo zjištěno, že vyšší koncentrace povlaku měly pozitivní dopad na mechanické a elektrické vlastnosti výsledné uhlíkové plsti. Vysoké koncentrace povlaku však vedly také ke ztrátě pružnosti uhlíkové plsti, což by mohlo vážně omezit jejich použitelnost. Zkoumáním morfologie a chování uhlíkových plstí připravených při různých teplotách karbonizace v režimu zatížení okraje bylo zjištěno, že zvýšení teploty karbonizace podpořilo růst krystalinity ve vláknech a tvorbu uspořádané grafitické struktury. Bylo dosaženo vytvoření husté, vysoce vodivé sítě s vysokou porozitou. Výsledky stínění elektromagnetického záření (EMI) prokázaly, že výsledná uhlíková plsť dosáhla vysoké účinnosti stínění EMI 55 dB a specifické účinnosti stínění 2676,9 dBcm^{2}g^{-1}, čímž překonala mnoho uhlíkových kompozit. Kromě toho uhlíková plsť vykazovala vynikající účinnost ohmického ohřevu a vysoké rychlosti ohřevu. Strukturální stabilita byla zkoumána pomocí speciálně navrženého experimentu. Výsledky ukázaly, že si uhlíková plsť udržela stabilitu vnitřních vodivých drah po více cyklech ohybu. Bylo také zkoumáno využití připravených

uhlíkových plstí pro tvorbu filtračních vrstev použitelných v respirátorech a filtračních maskách (filtrace vzduchu). Vynikající elektrická vodivost uhlíkové plsti umožnila její použití nejen jako respirační filtrační vrstvu, ale také pro vysokoteplotní elektrickou dezinfekci kontaminantů a mikrobů/virů. Konstrukce masky a vhodná konfigurace elektrod umožnila řízený odporový ohřev, zajišťující spolehlivost vysokoteplotní dezinfekce uhlíkové plsti. Účinnost filtrace a výsledky antibakteriálních testů ukázaly, že uhlíková plsť dosáhla více než 90 % účinnosti filtrace pro inhalovatelné částice a účinně inhibovala výskyt mikrobů. Flexibilní uhlíkové plsti mají obecně nižší výrobní náklady a vykazují dobrou chemickou a strukturální stabilitu. Výsledky funkčních testů ukázaly, že připravené uhlíkové plsti mají významný potenciál pro aplikace v oděvních ohřívačích, flexibilním stínění EMI, respiračních filtrech a dalších typech funkčních materálů.

Klíčová slova: odpadní plsti na bázi akrylu, zátěr PTFE, speciální pyrolýza, elektrická vodivost, EMI stínění, ohmický ohřev, respirační filtry.

Table of Contents

iii

List of Figures

List of Tables

List of Symbols

Symbols		Description
M_0	[mN cm]	Bending moment
F_m	[mN]	Bending force
k	[cm]	Constant for bending moment calculation
E	[MPa]	Modulus
σ	[MPa]	Stress
ε		Strain
φ	[%]	Porosity
ρ_{bulk}	[g/cm^3]	Bulk density
ρ_{fiber}	[g/cm^3]	Fiber density
R_{et}	[m^2 Pa/W]	Evaporation resistance
P_m	[Pa]	Saturation water vapor pressure
P_a	[Pa]	Water vapor pressure
q_s	[W/m^2]	Heat loss of the measurement head with the sample
q_0	[W/m^2]	Heat loss of the measurement head without the sample
R_v	[Ω]	Volume resistance
r_v	[Ω.m]	Volume resistivity
γ	[S/m]	Conductivity
t	[m]	Thickness
S	[m^2]	Surface area of electrode
C_{down}		Particle concentration in the downstream
C_u		Particle concentration in the upstream
SE_T	[dB]	Total EMI shielding effectiveness
P_T	[W]	Transmittance power
P_I	[W]	Incident power
SE_A	[dB]	Shielding effectiveness from absorption
SE_R	[dB]	Shielding effectiveness from reflection
R		Reflection component of the incident power

T	Transmission component of the incident power
S_{11}	Input reflection coefficient
S_{21}	Forward transmission
I_D	Peak intensity of the D band
I_G	Peak intensity of the G band
R^2	Coefficients of determination

List of Abbreviations

Abbreviations	Description
EMI	Electromagnetic Interference
PP	Polypropylene
PTFE	Polytetrafluoroethylene
SEM	Scanning Electron Microscope
EDX	Energy-dispersive X-ray Spectroscopy
DEHS	Dioctyl sebacate
XRD	X-ray Diffractometer
TGA	Thermogravimetric Analysis
CFU	Colony-forming Units
E. coli	Escherichia coli
S. aureus	Staphylococcus aureus
USB	Universal Serial Bus
SARS-CoV-2	Severe Acute Respiratory Syndrome Coronavirus 2
RNA	Ribonucleic Acid
COVID-19	Coronavirus Disease 2019

Chapter 1 Introduction

The flourishing of smart textile materials has spurred the development of flexible and lightweight conductive fiber materials. Carbon materials are undoubtedly the preferred choice for meeting the aforementioned performance requirements. Carbon fibers can be prepared by carbonizing or graphitizing polymers with high carbon content [1]. Approximately 90% of carbon fiber production comes from acrylic precursors, though cellulose and pitch are also used as precursors for carbon fiber [2]. This is because acrylic exhibits high carbonization yield, excellent fiber-forming properties, and unique thermal chemical characteristics, allowing for the synthesis of large graphite planes during pyrolysis. acrylic-based carbon fiber production involves thermal oxidation stabilization of the fibers in air conditions within the temperature range of 200-400 °C, followed by carbonization of the fibers at high temperatures between 800 °C and 1700 °C [3].

Carbon fibers are primarily used in two forms. One uses bundles of carbon fibrous filaments to create carbon fabric composites, typically with a resin matrix. In this application, carbon fibers mainly provide their exceptional mechanical properties to the composite material. Another form is carbon felt, in which fibers are combined through processes such as condensing, pressing, and needle punching. In addition to the inherent properties of carbon fibers, carbon felt also possesses a stable three-dimensional network structure, excellent flexibility and high porosity, which has led to its widespread application [4][5].

The manufacturing process of carbon felt include the formation of felt via needle punching and high-temperature carbonization. Most carbon felt manufacturing directly uses pre-carbonized fibers as raw materials, requiring only the felting process to produce carbon felt [6][7]. There has also been a study reporting the use of pre-oxidized acrylic fibers to produce felt, followed by carbonization [8]. acrylic felt is widely used in fiber filtration materials. Using waste acrylic felt as a precursor for carbon felt not only saves on raw material costs but also eliminates the need for fiber opening, carding, and felting processes. More importantly, this strategy transforms waste fibers into high-value materials, effectively alleviating the environmental impact of solid fiber waste. However, there are relatively few

reports on the preparation of carbon felt through the carbonization of acrylic felt. This is because fibers tend to shrink during pyrolysis, and using already-formed fiber assemblies as carbonization raw materials often leads to the production of hard or brittle carbon materials. Therefore, controlling the pyrolysis of waste acrylic felt through certain measures during experimental processes to produce flexible and conductive carbon felt holds significant research value.

As an industrial textile, acrylic felt typically undergoes functional finishing treatments, which leads to complex material composition. This complexity poses challenges when using it as a precursor for carbon fiber production, but it also opens up new avenues for exploration. Some studies have shown that using mixed fibers as precursors for carbon felt optimizes its mechanical properties[9]. Compared to pure acrylic felt precursors, acrylic felt with polymer coatings may exhibit different properties after carbonization, yet research in this area is lacking.

Furthermore, as a fiber material with excellent electrical conductivity, carbon felt possesses significant advantages in terms of lightweight and flexibility over metals. Its potential applications in resistive heating, electromagnetic shielding, filtration, and other areas are also worthy of research consideration.

Chapter 2 Objectives

This work aims to investigate the parameters involved in the preparation process of carbon felt from acrylic felt and explore the multifunctionality of carbon felt. The specific objectives of this study are as follows:

2.1 Pyrolysis of acrylic-based felt coated by layer of PTFE

Investigation of different loading modes to acrylic-based felt during the carbonization stage and their impact on the shrinkage rate, mechanical properties, electrical conductivity, and thermal conductivity of the resulting samples. Preparation of carbon felt derived from acrylic-based felt with PTFE coatings and evaluation the impact of the coatings on shrinkage and mechanical properties.

2.2 Flexible carbon felt characterization and properties

Comprehensive study of the EMI shielding efficiency, mechanical properties and resistive heating behavior of the resulting carbon felts. Testing of the structural stability of the samples after multiple bending cycles through a custom-designed experiment.

2.3 Special application of the prepared carbon felt

Design of carbon felt as a filtration layer for respirator filtration system. Examination of the breathability and vapor permeability of the carbon felt. Disinfection of the carbon felt via resistive heating after filtration.

Chapter 3 State of the art

3.1 Carbon materials

Carbon materials are a class of materials composed of carbon elements that exhibit exceptional performance due to their unique hybridization orbitals and diverse structures. Carbon possesses four valence electrons, which can form strong covalent bonds with other elements through hybridization orbitals. Carbon's hybridization orbitals include sp^3, sp^2, and sp hybridization, corresponding to carbon structures such as diamond, graphite, and acetylene, respectively. The different hybridization states of carbon atoms in carbon allotropes is shown in Figure 3.1. These different hybridization orbitals lead to the rich and varied physical and chemical properties of carbon materials.
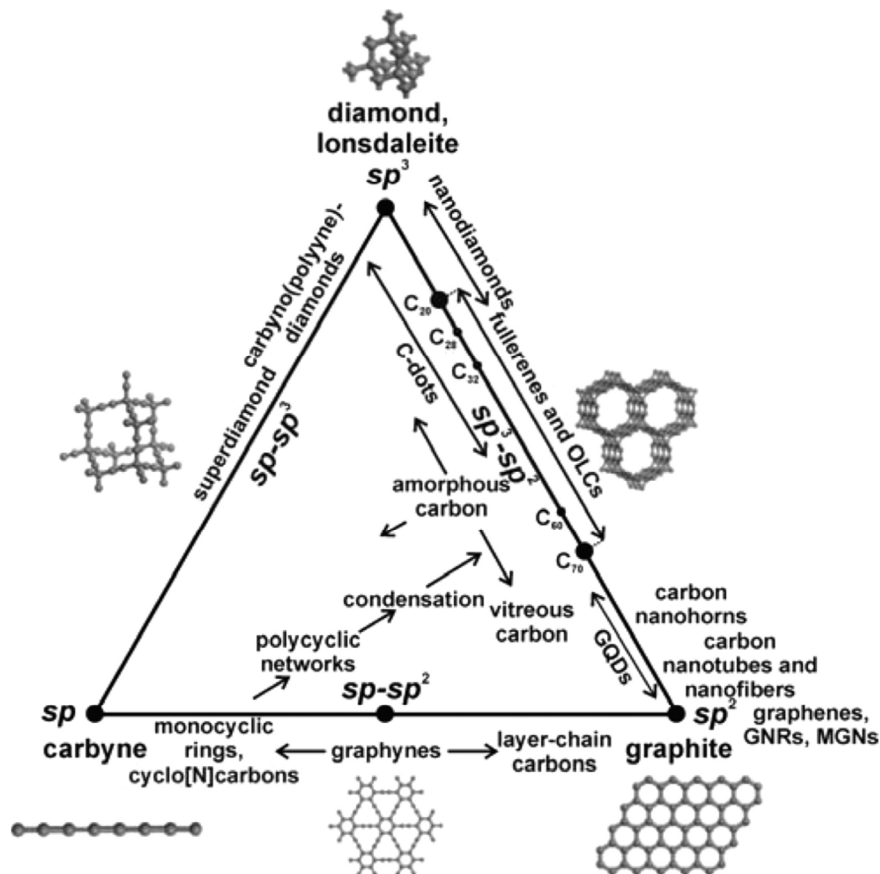
Figure 3.1 The hybridization states of carbon atoms in carbon allotropes[10]

The formation of two completely opposite electron density lobes on each atom is a result of sp hybridization, which leads to the creation of linear atomic chains. Single sp hybridized linear carbon chains have been recently synthesized and characterized [11]. In sp^2 hybridization, each carbon atom combines one 2s orbital and two 2p orbitals to form three coplanar hybrid orbitals spaced 120 degrees apart. These three hybrid orbitals overlap with the hybrid orbitals of adjacent carbon atoms, forming a planar hexagonal carbon network. This planar structure is known as a graphene layer. In graphite, these graphene layers are stacked together via van der Waals forces to form a multi-layer structure. Each carbon atom retains one unhybridized 2p orbital, which overlaps with the unhybridized 2p orbitals of neighboring carbon atoms to form π bonds. These π bonds contribute to graphite's excellent electrical and thermal conductivity. The sp^2 hybridized structure of graphite provides it with several advantageous properties, such as high electrical and thermal conductivity and mechanical strength. These characteristics enable graphite to be widely used in various applications, including batteries, electrodes, lubricants, and high-performance materials [12]. The carbon atoms in diamond are sp^3 hybridized, resulting in each carbon atom being bonded to four other carbon atoms in a tetrahedral arrangement. This configuration endows diamond with exceptional hardness and abrasion resistance. Diamond is an electrical insulator due to the involvement of all valence electrons in covalent bonding, leaving no free electrons. Diamond finds extensive applications in both industrial and optical domains [13].

Carbon atoms in graphite group carbon materials exhibit sp^2 hybridization and possess layered structures, which have drawn significant attention due to their exceptional properties. In addition to graphite, the graphite group also includes turbostratic carbon, which is a type of amorphous carbon composed of carbon layers stacked in a manner that is not exactly parallel [14]. Carbon materials primarily composed of turbostratic carbon include carbon fiber, carbon nanofiber, and carbon black. Carbon fiber is widely used for lightweight structures due to its combination of low density, high strength, and high modulus. The preferential alignment of carbon layers along the fiber axis results in high strength and high modulus in this direction [15]. Graphene and carbon nanotubes also belong to the graphite family. Graphene is a single-atom-thick planar graphite structure. As a true two-dimensional

material, it possesses unique structural characteristics, leading to many exceptional properties such as outstanding electrical, mechanical, and high thermal conductivity. When graphene is rolled into a tubular form, it can produce carbon nanotubes. This one-dimensional carbon material can consist of one or more layers of graphene rolled into a seamless cylinder. As a result, carbon nanotubes can exhibit many excellent properties similar to those of graphene. Additionally, due to the specificity of one-dimensional structures, such as a large aspect ratio, the material properties display high anisotropy [16]. The graphite group also includes activated carbon, a porous carbon formed by subjecting turbostratic carbon to an activation reaction that consumes part of the carbon. The activation process creates surface pores, thereby increasing the specific surface area, which enhances the adsorption capacity of activated carbon [17].

3.2 Carbon materials from textile waste

Human daily life is inseparable from textiles, especially with the evolution of fashion trends and the pursuit of multifunctional textiles, leading to a significant increase in textile production [18]. Correspondingly, textile waste is inevitably generated in large quantities. It has been reported that the textile industry is the second-largest industrial polluter, accounting for 10% of global carbon emissions [19]. In addition to the chemical-laden wastewater generated during production processes, the handling of solid fiber waste is also a challenging issue. Currently, the predominant methods for handling solid fiber waste are landfill disposal and incineration [20]. According to data from the United States Environmental Protection Agency in 2018, textile waste accounted for 5.8% of the total municipal solid waste disposed of in landfills, amounting to approximately 17 million metric tons [21]. The majority of non-biodegradable fiber waste is ultimately directed to landfill sites, perpetually contaminating soil and groundwater systems. For instance, discarded polyester fiber products emit substantial quantities of microplastic fibers into the environment, with approximately 0.5 million metric tons of microplastic fibers flowing into the oceans annually. These detrimental substances eventually find their way into the human body through bioaccumulation [22]. Another factor contributing to environmental pollution is the presence of dyes retained on

fibers. These dyes contain toxins and carcinogens such as naphthols, azo dyes, nitrites, and heavy metals [23].

The environmental issues caused by non-biodegradable textile waste are becoming increasingly severe, prompting the textile industry to adopt and implement environmentally conscious strategies in the production and disposal processes of textile products. Researchers are actively seeking novel and sustainable solutions to replace the current landfill disposal methods. By developing innovative technologies and implementing strategies for recycling, reusing, and repurposing, the environmental impact of textile waste can be mitigated, while efforts can be made to restore its economic value [24].

Thanks to the prosperity of the fossil fuel industry, most carbon materials are produced using fossil-derived precursors under typically harsh synthesis conditions or high energy requirements, such as arc discharge techniques and chemical vapor deposition [25]. Recently, there has been an increased focus on developing new pathways for carbon materials that are more environmentally friendly. Polymer molecules in textile fibers typically contain a high carbon content, which can yield solid carbon products through pyrolysis under certain conditions. The strategy of producing carbon materials from textile waste not only reduces the production cost of carbon materials but also serves as a method of managing textile waste, thereby contributing to the valorization of textile waste. A considerable amount of research has been conducted on the preparation of carbon materials using textile waste as a carbon source, including cotton [26], polyester [27], acrylic [28][29], flax [30], and blended fabrics [31]. Table 3.1 summarizes the properties and performance of carbon materials obtained from textile waste as a raw material through different pyrolysis processes, as well as their applications.

Table 3.1 The properties and applications of carbon materials derived from the pyrolysis of textile waste

Textile waste type	Pyrolysis condition	Activation method	Properties		Application	Ref.
			BET surface area (m^2/g)	Total pore volume (cm^3/g)		

Polyester	900 °C; 10 °C min^{-1}; nitrogen; 75–90 min	Impregnated with MgCl$_2$ (1:1–5:1)	1307–1364	2.91–3.56	-	[32]
Acrylic	700 °C; 5 °C min^{-1}; nitrogen; 120 min	With steam at 900 °C for 120 min	752	0.39	-	[29]
Jute	700 °C; 10 °C min^{-1}; nitrogen; 90 min	Impregnated with H$_3$PO$_4$	1539	1.62	-	[33]
Polyester	650 °C; 10 °C min^{-1}; nitrogen; 1440 min	Impregnated with FeCl$_3$ (1:1)	1415	1.45	Used as adsorbent for Eriochrome Black T	[34]
Polyester	900 °C; 10 °C min^{-1}; nitrogen; 60 min	Mixed with Mg(Ac)$_2$ (7:3)	951	1.68	Used as adsorbent for Cr(VI)	[35]
Cotton	700 °C; 10 °C min^{-1}; nitrogen; 1440 min	Impregnated with FeCl$_3$ (1.62:1)	837.4	0.69	Used as adsorbent for iodine	[36]
Flax	800 °C; nitrogen; 60 min	Impregnated with ZnCl$_2$	1020	0.96	Used as adsorbent for iodine and methylene blue	[37]
Cotton	500 °C; 10 °C min^{-1}; nitrogen; 60 min	Impregnated with ZnCl$_2$, H3PO4, and FeCl3	1854.7	-	Used as adsorbent capacity for Cr(VI)	[38]
Denim fabric	300-500 °C; 5 °C min^{-1}; nitrogen;60-120 min	Impregnated with H3PO4	1582	1	Used as adsorbent for Remazol Brilliant Blue R	[39]
Carpet tile	265 °C; helium; 30 min;	Ball-milling of pyrolyzed sample	-	-	Recover nylon from carpet tile waste	[40]

Wool	100 °C; 2 °C min⁻¹; argon; 120 min	Mixed with 10 wt% conductive carbon black (Super P) and 10 wt% polyacrylic acid	152	0.15	Used as anode for sodium-ion battery	[41]
Acrylic	1200 °C; 150–450 °C h−1; charcoal; 0-60 min	-	280	-	Used as adsorbent for methylene blue	[42]
Acrylic	800-1200 °C; 300 °C h⁻¹; charcoal;	-	278	-	EMI shielding	[43]
Acrylic and Kevlar blended	1000 °C; 300 °C/h; charcoal	-	329	0.13	EMI shielding	[9]
Kevlar	500 °C; 10 °C min⁻¹; nitrogen	Ball milling	-	-	Conductive polymer fillers	[44]
Kevlar	800-1100 °C; 300 °C/h; Charcoal; Ammonium bicarbonate; nitrogen	-	-	-	Joule Heating	[45]

Most studies have focused on the preparation of activated carbon from textile waste for the adsorption of water pollutants. The basic strategy for this type of work involves pyrolyzing a mixture of textile waste feedstock and metal salts, where the cations or anions in the metal salts act as templates and catalysts during the synthesis process to alter the pore structure, as shown in Figure 3.2 [34]. Activated carbon derived from textile waste has been found to exhibit better adsorption performance than activated carbon obtained from the pyrolysis of other biomasses. For instance, the adsorbent prepared from polyester textile waste by Xu et

al. [34] showed approximately twice the adsorption capacity for chrome black T compared to activated carbon sourced from rice husks. Mesoporous activated carbon synthesized from the pyrolysis of mixed magnesium compound-containing waste polyester textiles exhibited 150% higher adsorption of $Cr(VI)$ compared to other biomass-derived adsorbents [35].
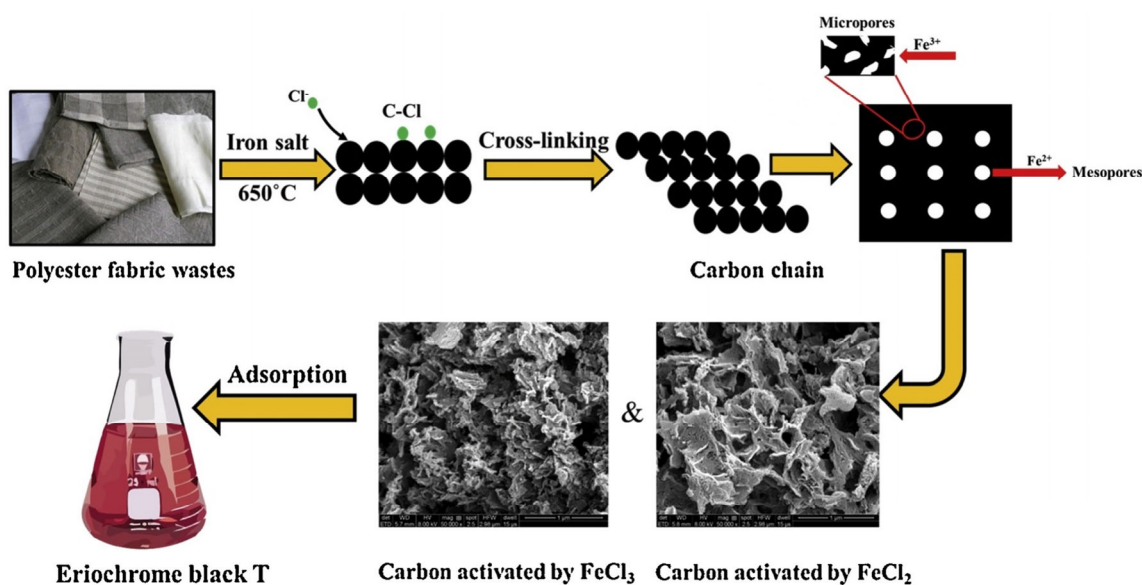
Figure 3.2 Schematic diagram of synthesizing activated carbon materials using polyester textile waste mixed with metal salts [34]

In addition to serving as a precursor for activated carbon adsorbents, textile waste has also been used as a source for conductive fiber assemblies. Conductive fiber assemblies have a wide range of applications, encompassing electronic textiles, sensors, energy storage, heated textiles, and electromagnetic shielding, among others. For example, Zhu et al. used wool from old clothes as a low-cost and easily collectible precursor to prepare high-performance hard carbon for sodium-ion batteries [41]. The satisfactory electrochemical performance and simple synthesis process demonstrated a promising manufacturing pathway for anode materials. Baheti' group team developed a porous conductive activated carbon mesh from acrylic fiber waste and applied it to electromagnetic interference (EMI) shielding materials. Benefiting from the amount of nomadic charges in the network, uniform dispersion of graphite layers, extended free path of electrons, and large surface area, its absorption and multiple internal reflections of electromagnetic radiation were enhanced. Later, they developed activated carbon fabric from a mixture of acrylic and aramid fiber waste [9]. They

examined the EMI shielding efficiency and thermal performance of the carbonized nonwoven fabric and analyzed the conductive mechanism of the blended carbon fabric (Figure 3.3). The EMI shielding efficiency of the carbonized fabric was satisfactory, but its mechanical performance was less than ideal, primarily exhibiting brittleness and fragility [46]. The primary challenge in the current application of carbonized fabric derived from textile waste lies not in its conductivity but in its mechanical performance, making it crucial to address this issue.
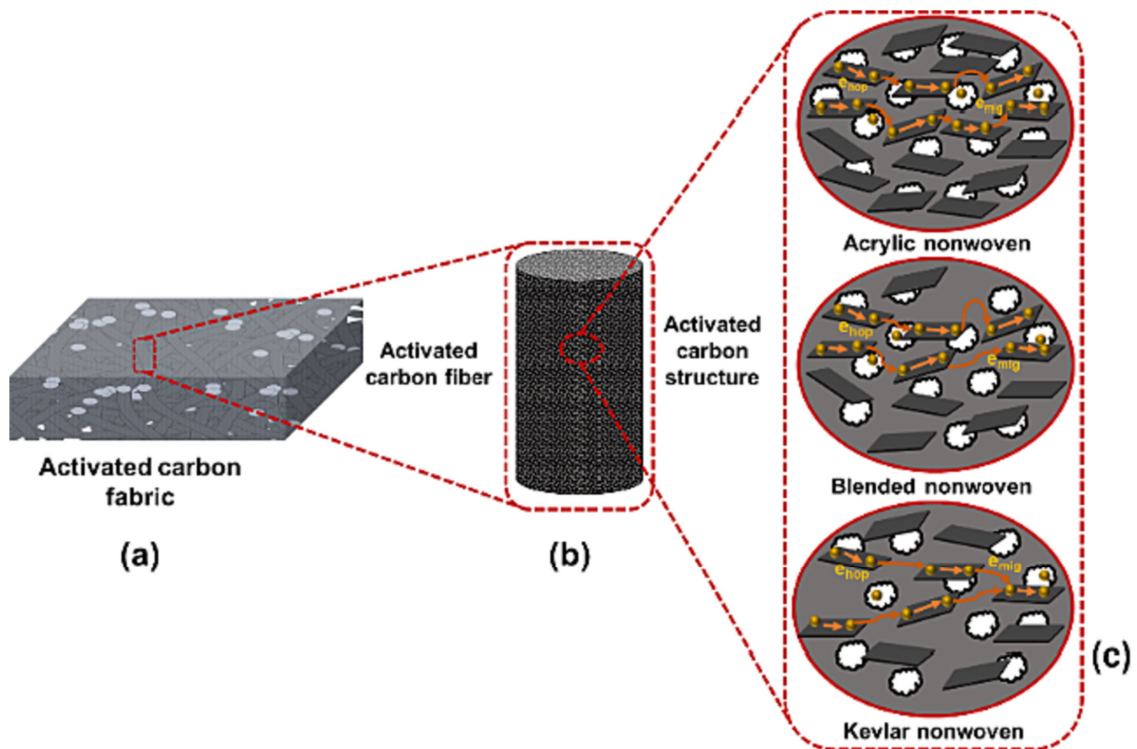
Figure 3.3 Mechanism of conductive network in carbonized acrylic and Kevlar blended nonwoven fabrics [9]

3.3 Mechanical properties of carbonized fiber networks

Mechanical performance is a critical factor in determining the practical utility of materials. The mechanical properties of carbonized fabric can be enhanced through three approaches: utilizing precursors with superior mechanical attributes, modifying technical parameters in the fabrication process, and employing a blend of raw materials [47]. For the technical

pathway of using textile waste as a precursor for preparing carbon fabric, altering the mechanical properties of the precursor fibers is evidently not feasible. Utilizing mixed fibers as feedstock necessitates processes such as fiber opening and blending, introducing additional steps, while the resulting enhancements in mechanical performance are modest [9]. Therefore, adjusting the mechanical performance of the resulting product from the perspective of technical parameters in the carbon fabric preparation process holds more promise.

Acrylic (or polyacrylonitrile) precursor is the primary material used in the preparation of conductive carbonized fiber materials. The production of carbon fibers using acrylic-based fibers typically involves three processes: stabilization, carbonization, and graphitization. The stabilization process conducted in the atmosphere can alter the chemical structure of the fibers, transitioning from a chain structure to a stable ladder polymer, thereby preventing melting. Typically, during the stabilization process, the ladder polymer forms as the acrylic-based precursor fibers change color from white to yellow to black. The stabilization process usually occurs at a heat treatment temperature of 180–300°C, and stabilization temperatures that are too high or too low can greatly impact the properties of the final carbon fibers. Two important reactions occur during the stabilization process: dehydrogenation and cyclization, as shown in Figure 3.4 [48]. These reactions are key to forming the thermally stable ladder polymer structure.

Dehydrogenation forms stable carbon-carbon double bonds, and this reaction involves two basic steps: oxidation followed by dehydration. The reaction requires oxygen to proceed, so air is typically used as the gas atmosphere, which is why stabilization needs to occur in air. Cyclization is the process of forming rings. In this process, the triple bond structure (C≡N) in the nitrile groups of acrylics is converted into a double bond structure(C=N), forming a stable ladder polymer with adjacent groups. The resulting ring structure is known as a six-membered pyridine ring[49]. Cyclization is the most important reaction in stabilization because it changes the molecular structure within the fibers and increases rigidity [50]. There is no distinct sequence between dehydrogenation and cyclization [51].
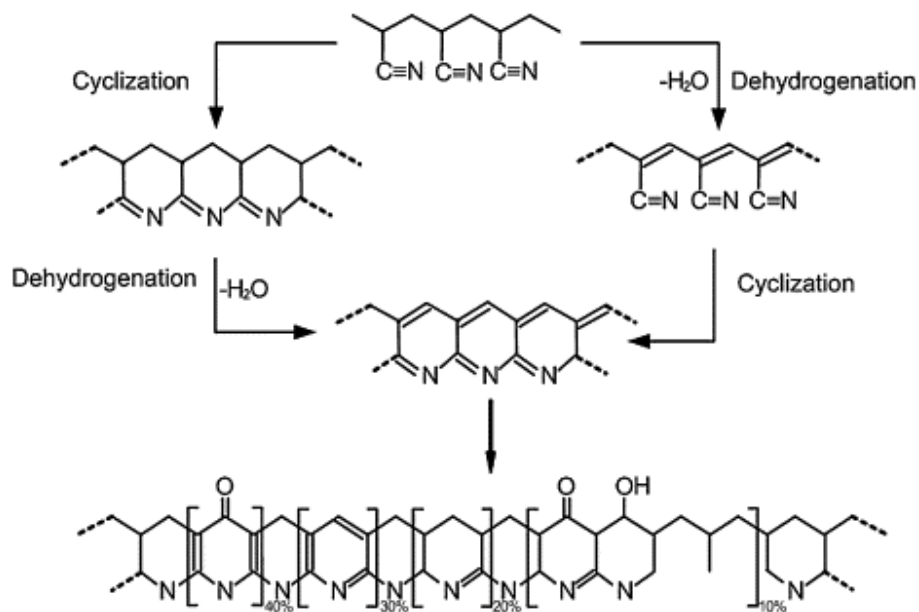
Figure 3.4 Reactions involved in stabilization of acrylic [48]

The carbonization and graphitization processes occur at high temperatures ranging from 800 to 3000 °C, resulting in fibers with carbon content as high as 95% [52]. Carbonization at lower temperatures produces carbon fibers with high tensile strength and low modulus, while high-temperature carbonization and graphitization yield high-modulus fibers [53]. The molecular structural changes during carbonization are illustrated in Figure 3.5. In this process, the molecular structure transitions from a ladder structure to a hexagonal lattice structure of carbon atoms, forming a graphite structure.
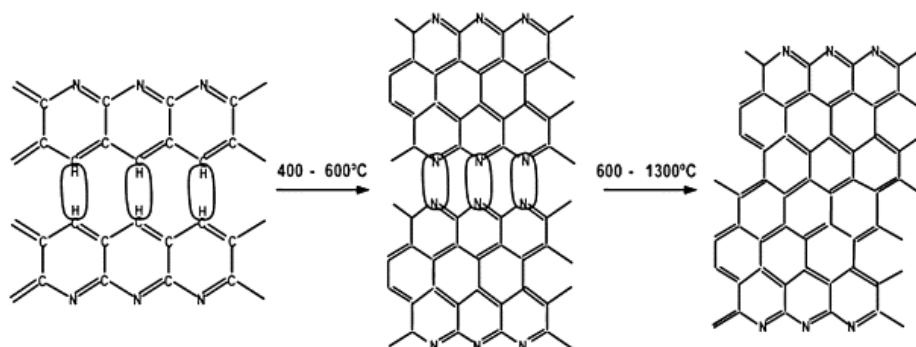
Figure 3.5 Changes in molecular structure during the carbonization process [48]

It is well known that applying appropriate tension to acrylic fibers during the during the carbon fiber production process facilitates the preferred orientation of the fibers, thereby enhancing the strength and tensile modulus of the resulting carbon fibers. The influence of tension, especially during the stabilization process, on carbon fibers has been extensively studied [54][55][56]. Furthermore, the tensile stress also alleviates the contraction of the fibers due to high temperatures [48].

In traditional carbon fiber production using acrylic precursor filaments, the application of tension only requires control of the two ends of the filament during the high-temperature treatment process. The method of applying tension is not feasible for the already-formed acrylic precursor felt. This is because the fiber arrangement within the felt is non-directional and there is significant entanglement between fibers. The thermal degradation process of the fiber material inevitably leads to shrinkage and even breakage. Therefore, preserving the fiber morphology of the original felt to some extent during production to ensure the mechanical properties of the resulting carbon felt is a challenge. In this area, current research is relatively limited. Baheti et al. found that applying pre-tension on the felt during the stabilization process mitigates the shrinkage rate of the resulting carbon web [43]. However, this study did not provide a specific method for applying pre-tension, and the resulting samples were relatively brittle and fragile. Other studies have also presented various methods of applying tension to acrylic nanofiber webs during the stabilization process, including vertical loaded hanging [57], both-sides hanging [58], borders fixation [59], and sandwiching between graphite plates [60]. Applying vertical tensile force during the stabilization phase has been found to help control the shrinkage rate of the fibers and aid in the orientation of macromolecular chains within the fibers, thereby leading to the development of high tensile modulus fibers. The authors believed that the technique of applying tensile force to electrospun acrylic fibers during the stabilization process was effective in producing relatively large-sized stabilized fiber mats compared to other techniques [57]. Ehrmann et al. studied the impact of edge fixation on samples during the stabilization process. They found that the change in the area of the fixed samples was smaller as the stabilization temperature and heating rate increased, as shown in Figure 3.6 [59].

The use of a metal substrate to provide single-sided or double-sided support during the stabilization process for electrospun acrylic fiber mats has been proposed by Storck et al. [61]. The results indicate that stabilization and carbonization within a double-sided metal-supported sandwich structure preserve the original fiber morphology and even accelerate the carbonization process. However, the carbonization temperature in this work was only 500 ℃, significantly lower than the typical preparation temperature for carbon felt. The same research team further increased the carbonization temperature and utilized different metal and metalloid substrates for the sandwich structure [62]. However, their study was primarily focused on finding the optimal balance between carbonization, crystallinity, and intact nanofibers, and did not investigate the mechanical properties such as the flexibility of the resulting samples. It can be stated that current research primarily focuses on applying tension during the stabilization process of fiber mats, while there is a lack of reporting on tension application during the carbonization stage. Furthermore, no studies have been found regarding the mechanical properties such as tensile strength and flexibility of the carbon felt or carbon nanofiber network obtained after applying tension. Applying tension to samples during the carbonization phase has research value as a potential means of enhancing the mechanical properties of carbon felt. Identifying an appropriate method could enable the direct preparation of carbon felt from textile waste felt precursors without brittle limitations, thereby avoiding additional processing steps such as opening and mixing.
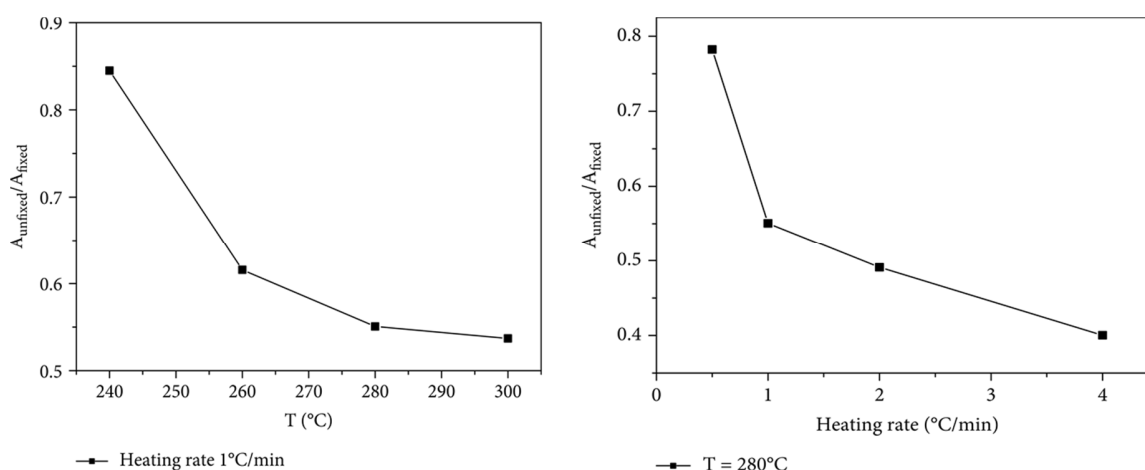
Figure 3.6 The impact of edge fixation on the area of stabilized samples [59]

3.4 Applications of carbonized fiber networks

Carbonized fiber networks, due to their 3D network structure, high specific surface area, tunable pore structure, and excellent electrical and thermal conductivity, have a wide range of applications.

3.4.1 Electromagnetic interference shielding

Various issues arising from EMI have been extensively documented, prompting widespread interest in the development of EMI shielding materials [63][64][65][66][67]. Given the diversity of contemporary electronic products and the wide range of usage scenarios, lightweight and flexible conductive materials are better suited for meeting the practical application requirements of EMI shielding compared to traditional heavy and rigid metal plates [68][69]. Therefore, the investigation and development of flexible multifunctional materials, characterized good EMI shielding capabilities, are warranted due to their promising potential applications in safeguarding both the human body and electronic components [70].

EMI shielding is the attenuation of electromagnetic energy caused by reflection at the shield surface and absorption and multiple reflections within the shield. The shielding of electromagnetic waves is divided into three components: reflection loss, absorption loss, and internal multiple reflection loss, as shown in Figure 3.7 [71]. Generally, conductive shielding materials exhibit predominantly reflection-based shielding effects, such as traditional metals and graphene [72]. The incident electromagnetic wave causes free electrons or holes in the conductor to oscillate, generating an induced field on the conductor's surface that forms a reflected wave [73]. However, the reflected electromagnetic waves may cause secondary electromagnetic pollution to nearby electronic devices or individuals, which is particularly concerning. Therefore, recent EMI shielding research primarily focuses on reflection.

The absorption of electromagnetic waves in a material is mainly related to eddy current loss and dielectric loss. When the electric field of the electromagnetic wave acts on the conductor, it generates eddy currents within the conductor. Eddy currents are circular motions of electric currents that, when flowing through resistance, produce heat, thus consuming the energy of the electromagnetic wave [71]. The electromagnetic wave in the material causes oscillations

of electric dipoles. These oscillations lead to the conversion of energy within the material into heat, a process known as dielectric loss [74]. Although this phenomenon is not as pronounced as eddy current loss in non-magnetic conductors, it is still present at high frequencies and plays a role in the absorption of electromagnetic wave energy.
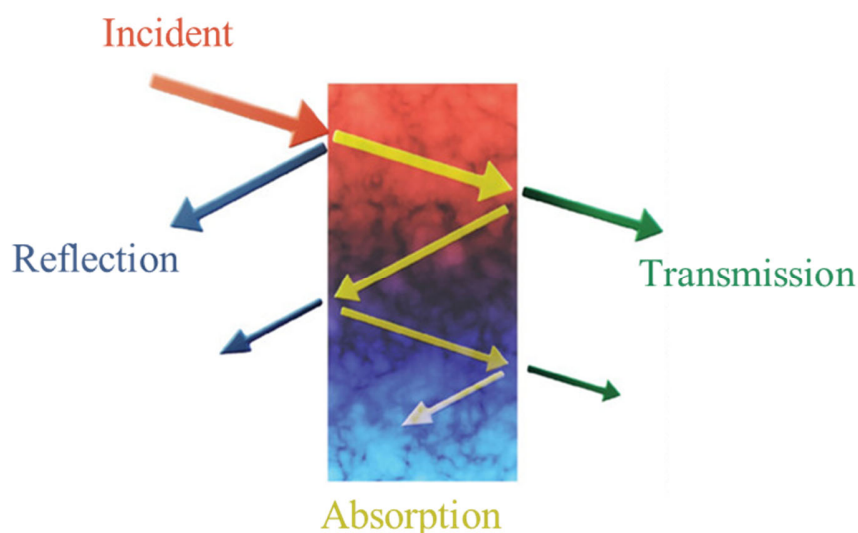
Figure 3.7 Schematic illustrations of main EMI shielding mechanisms [71]

Recently, carbon fiber materials have garnered attention for their applications in EMI shielding. Carbon fibers can form conductive networks that enhance the electrical conductivity of materials, enabling EMI shielding. Lu et al. used a pre-fabricated film method and hot-press composite process to prepare carbon fiber felt composites with a sandwich structure [75]. Carbon fibers formed a highly conductive network during the compounding process with the substrate. The resulting composites achieved a maximum EMI shielding effectiveness of 45 dB. The EMI shielding behavior of carbon fiber felt made from three types of chopped carbon fibers via wet laying was studied [76]. It was found that a higher fiber packing density can enhance the absorption of electromagnetic waves due to the formation of a denser conductive network. When electromagnetic waves strike the surface of the carbon fiber felt, reflection occurs due to impedance mismatch at the interfaces. They also discovered that fiber felts with a higher magnetic field density have a larger internal surface area, which facilitates increased polarization loss and ohmic loss. Hu et al. prepared

carbon fiber felt using waste carbon fibers that were environmentally friendly and decorated with cationic polyacrylamide [77]. Thanks to the construction of rich effective pathways within the 3D interconnected network of carbon fibers, its conductivity reached as high as 140.06 S/m, with efficient EMI shielding effectiveness of 66.15 dB. In addition, the carbon felt also exhibited advantages such as flexibility, light weight, and sustainable reusability.

In recent years, carbon felt materials have become a common candidate for new EMI shielding materials due to their exceptional 3D conductive network, light weight, and outstanding chemical stability [70][78][79][80]. Despite extensive research and commercial availability of carbon felt production, simplifying its preparation process and using sustainable precursors could lead to more unique and widespread applications in the field of wearable flexible shielding materials.

3.4.2 Separation and filtration

Air pollution and the prevalence of respiratory diseases have prompted research into respirator filtration materials. The efficiency of a filter system for a specific aerosol can be estimated using multiple input parameters, including particle size, flow speed through the filter, filter thickness, filter surface properties, and fiber diameter. The overall effectiveness of a filter system results from the interaction of various mechanisms, each of which is more significant in different size ranges and flow scenarios. Three standard filtration processes are detailed below [81][82]:

1 Impaction: This filtration mechanism occurs when particles deviate from their original airflow path due to inertia, causing them to collide with the filter material. The efficiency of impaction increases with larger particle size, higher density, and faster speed.

2 Interception: Particles following the airflow around the filter structure can be captured through interception when they pass close enough to the filter fibers. This occurs when the distance between the particle's center and the fiber surface is within one particle radius. Unlike impaction, intercepted particles do not deviate from their original flow path. The likelihood of interception increases with increasing particle size.

3 Brownian diffusion: For very small particles that are not significantly influenced by inertia or gravity, filtration is achieved through Brownian diffusion. This mechanism occurs when random diffusive motion brings particles into contact with the filter, removing them from the airflow. The rate of diffusive motion increases as particle size decreases and temperature rises. Low airflow velocity also enhances filtration by diffusion.

Each filtration mechanism operates most effectively within a specific particle size range. There is also a narrow range of particle sizes where none of the filtration mechanisms are dominant, as illustrated in Figure 3.8.
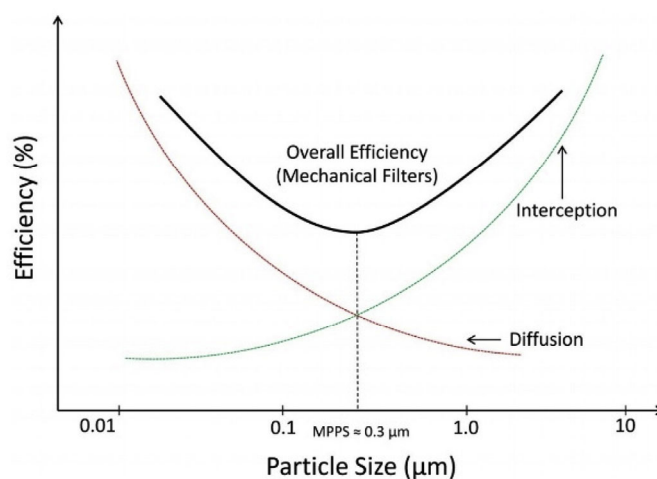
Figure 3.8 Filtration efficiency curves for common filtration mechanisms [81]

Carbonized fiber networks, due to their high porosity, can be used in adsorption and filtration materials. Lorimier et al. investigated the filtration performance of activated carbon fibers against alumina particles under different conditions. The initial filtration efficiency of the activated carbon fiber felt was 74% at a pressure drop below 210 Pa [83]. Hayashi et al. examined the filtration efficiency of cellulose-derived activated carbon fibers against NaCl aerosols. The results showed a strong agreement between the experimental measurements and theoretical predictions for the filter efficiency. They also highlighted the various potential applications of this filter [84]. Due to the brittleness and short fiber length of activated carbon fibers, it is challenging to produce nonwoven fabrics through carding and needling processes. To address this issue, Kim and colleagues used a wet-laid nonwoven process to manufacture

activated carbon fiber nonwoven fabrics for use as gas filtration layers in masks [85]. They evaluated the ammonia removal efficiency, mechanical properties, and particulate filtration performance of the prepared active carbon fiber nonwoven fabric. Another study used multi-layer commercial super activated carbon fiber fabrics and polypropylene nonwoven fabrics to produce washable and reusable masks [86]. These masks exhibited good breathability and water resistance. Xiong and colleagues reported a multifunctional mask made of carbon fibers and carbon nanofibers, offering excellent comfort and pathogen resistance [87]. The fluorination treatment of the carbon nanofibers imparted hydrophobicity. The resulting mask demonstrated better heat dissipation efficiency compared to commercial polypropylene (PP) nonwoven fabrics. Additionally, they proposed a disinfection method using resistive heating to kill viruses and bacteria in the mask.

Even though many studies have used carbon fibers or activated carbon fibers as respirator filter layers, demonstrating excellent performance, two issues still hinder their large-scale application. The first is that the cost of carbon fiber filter layers is generally higher than that of ordinary polymer fibers. The second is the complexity of the manufacturing process due to the brittleness and length of carbon-based fibers. Many industrial filtration nonwoven materials are made from acrylic (or polyacrylonitrile). If discarded acrylic felt can be used as a precursor for preparing carbon felt, it would simultaneously address the above two issues. Additionally, since the precursor was originally intended for filtration, it is believed that the resulting carbon felt will meet the required filtration performance.

Chapter 4 Experimental materials and methods

4.1 Materials

The needle-punched acrylic-based dust filter felt used as the precursor in this work was purchased from Zhejiang Hengze Filter Material Co., Ltd, China. The density of the felt is $500g/m^2$ and the thickness is 2.0- 2.1 mm, where the acrylic-based fibers have a diameter of 12-16 μm. One side of the felt is coated with polytetrafluoroethylene (PTFE) at a thickness of about 0.1 mm. The Scanning Electron Microscope (SEM) images of the acrylic-based felt are shown in Figure 4.1. The other chemicals used are of reagent grade and have not been further purified prior to use.
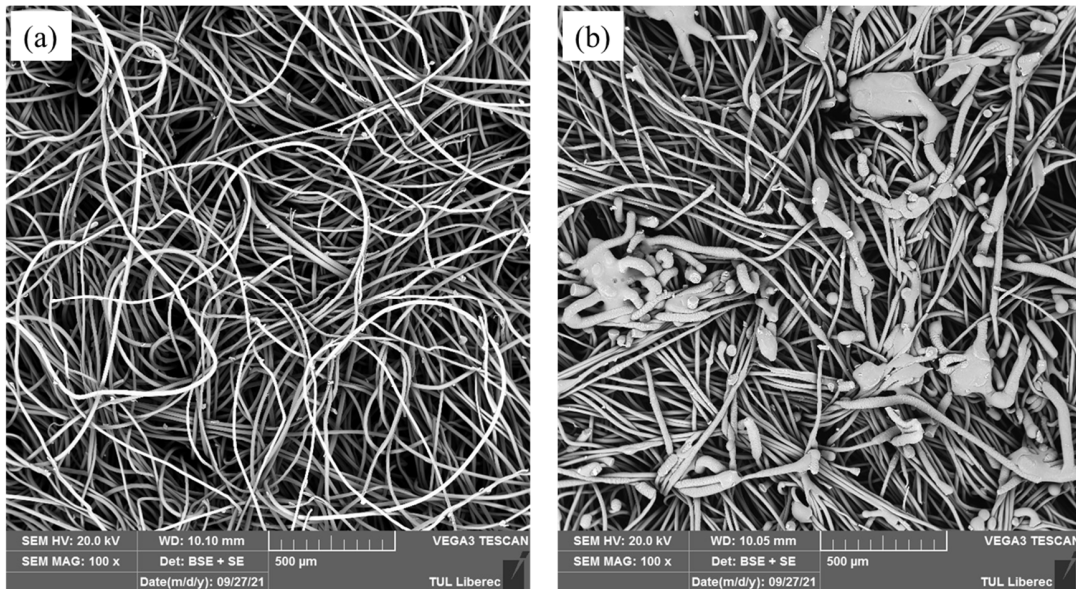
Figure 4.1. SEM images of acrylic-based felt material, (a) without PTFE, (b) with PTFE

4.2 Sample preparation

4.2.1 Carbon felt prepared by different loading mode

The precursor material for carbon felt, acrylic-based felt, was washed and cut into squares pieces before the experiment. First, the acrylic-based felt was stabilized in an air atmosphere using a muffle furnace at a temperature of 200°C for 2 hours. During the stabilization process, the sample was placed between two metal plates to maintain its original flat shape.

Subsequently, the carbonization of the stabilized acrylic-based felts was carried out in a muffle furnace under nitrogen atmosphere at a temperature of 800-1100 °C for 30-90 min with a heating rate of 10 °C/min. The samples were labeled as AC_x, where x represented the carbonization temperature.

It is well known that fibers inevitably shrink during the carbonization process and a commonly employed solution is to apply appropriate tension to the fibers. Here, during the carbonization process, two modes were used to apply tension to the fibers in the felt. One is simply placing cylindrical blocks weighing 66g at each of the four corners of the sample, termed as the edge loading. Another mode is to use a flat crucible with weight of 540g as a load to completely cover the sample surface, termed as uniform loading. Samples without any loading were also prepared as control samples. The diagram of different loading modes is shown in Figure 4.2 [88].

In the first mode, on the one hand, the loading of the four corners ensures that the sample remained flat during the carbonization process. On the other hand, the proper weight of the cylindrical block enables its movement with the shrinkage of the sample, continuously applying tension to the fibers during the shrinkage of the sample without breaking the sample. In the second mode, the sample was uniformly loaded and the fibers were subjected to both horizontal tension and vertical pressure during the shrinkage process.

No loading   Edge loading   Uniform loading
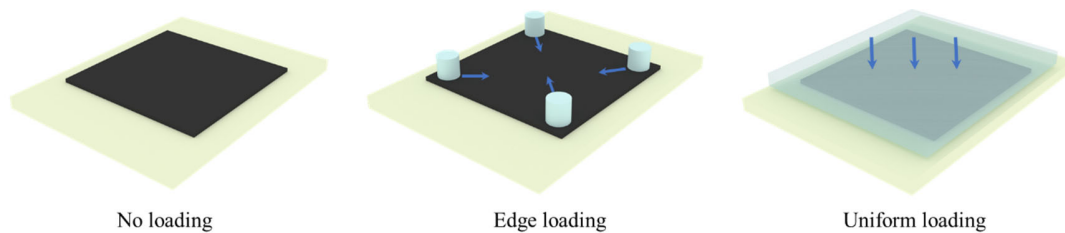
Figure 4.2 Schematic diagram of different loading modes for the preparation of carbon felts.

4.2.2 Carbon felt prepared from acrylic-base felt with PTFE coating.

To study the impact of the PTFE coating on carbonization, the acrylic-based felt was first subjected to a coating process. Dip-pad-dry method was used for the PTFE coating of acrylic-

base felt. Briefly, a PTFE dispersion of 60wt% was diluted with deionized water to 3wt%, 6wt%, 12wt% and 30wt%, respectively. The felt was then immersed in PTFE dispersions of different concentrations. After thorough saturation, excess dispersion was removed using pressure rollers. Finally, the samples were dried and cured in an oven at 120 ℃.

The PTFE-coated acrylic felt was carbonized using an edge loading method under the same experimental conditions as described in the previous section, with a temperature of 800 °C and a duration of 30 min.

4.3 Characterizations

4.3.1 Morphology

The surface morphology of the carbon felts obtained in this study was examined via scanning electron microscopy (SEM) using a VEGA3 TESCAN instrument operated at an acceleration voltage of 10 kV. Prior to testing, the sample surfaces were subjected to a metal sputtering treatment with a thickness of 10 nm. The surface elements of the resulting carbon felts were analyzed using an Oxford X-max 20 energy dispersive X-ray spectrometer (EDX).

4.3.2 Mechanical properties

The tensile properties and stiffness of the samples were tested to study the mechanical properties of the obtained carbon felt.

In order to investigate the flexibility of the carbon felts, the stiffness of the samples was evaluated by means of a TH-5 instrument (Czech Republic), following the guidelines outlined in the standard ČSN 80 0858. The specimens utilized for the study were rectangular in shape, with a length and width of 5 and 2.5 cm, respectively. During the testing process, one end of the specimen was bent to 60°, and the bending force was measured by the instrument. The bending moment was then computed using Equation (1),

$$M_0 = F_m \times k \tag{1}$$

where M_0 [mN cm] is bending moment, F_m [mN] is bending force measured by the instrument. The constant k for a sample with a width of 2.5 cm is 0.604 cm [89].

The tensile properties of the samples were tested using the dynamometer LaborTech 2.050 (LaborTech, Czech Republic) in accordance with the EDANA 20.2-89 standard. Samples with a width of 1 cm and a clamping length of 5 cm was stretched to fracture, and the tensile force and elongation were recorded. The tensile stress [MPa] was then calculated as the ratio of the breaking force to the cross-sectional area of the sample. The calculation of modulus E [MPa] was as follows,

$$E = \lim_{\varepsilon \to 0} \frac{d\sigma}{d\varepsilon} \tag{2}$$

where σ [MPa] is the tensile stress and ε is the strain, near origin of the stress-strain curve. In the above experiment, measurements were realized five times, and the average was taken. Standard deviation was used as error bars.

4.3.3 Porosity

By measuring the bulk density and fiber density of the carbon felt and utilizing the definition of porosity, which is the ratio of the pore volume to the total volume, the porosity φ [%] of the carbon felt was calculated using Equation (3),

$$\varphi = 1 - \frac{\rho_{\text{bulk}}}{\rho_{\text{fiber}}} \tag{3}$$

where ρ_{bulk} is the bulk density[g/cm^3] of carbon felt and ρ_{fiber} is the density [g/cm^3] of fiber, respectively. The volume of the carbon fiber was determined through the immersion method, which involves immersing the fibers in water-filled containers and measuring the resulting change in water level[90]. The thickness of the carbon felt was measured using a thickness gauge (D-2000-T, SCHMIDT). The testing head size was 20 cm², and the applied pressure was 1 kPa. The bulk volume of carbon felt was determined by multiplying the sample area by the thickness. The mass of the samples was measured using an electronic balance.

4.3.4 Air and water vapor permeability

The air permeability of carbon felts was measured by FX-3300 air permeability tester (TESTEST AG, Switzerland). The testing was carried out at various pressure differences,

ranging from 60 to 260 Pa, with increments of 10 Pa. Each pressure condition underwent five tests, and the average value was calculated.

The evaporation resistance R_{et} [m^2 Pa/W] were determined using the Permetest Instrument (SENSORA, Czech Republic) according to ISO 11092. A semi-permeable membrane was placed between the testing head and the sample to preserve the dryness of the sample. The heat losses were determined by measuring the change in heat flow value before and after the sample covered the testing head. The water vapor resistance R_{et} can be calculated using Equation (4)[92]

$$R_{et} = \frac{P_m - P_a}{q_s^{-1} - q_0^{-1}}$$

(4)

where P_m is the saturation water vapor pressure [Pa] at ambient temperature, P_a is the water vapor pressure [Pa] in the room, q_s is the heat loss [W/m^2] of the measurement head with the sample, and q_0 is the heat loss [W/m^2] of the measurement head without the sample.

4.3.5 Thermal properties

The thermal properties of carbon felts were studied by measuring the thermal conductivity [Wm^{-1}K^{-1}] and thermal resistivity [Km^{2}W^{-1}] of the samples using Alambeta Instrument (SENSORA, Czech Republic) according to Standard EN 31092. For each sample, the measurement was repeated five times.

4.3.6 Electrical conductivity

The volume electrical resistance R_v [Ω] of the obtained carbon felts was measured in accordance with the ASTM D257-14 standard, using an Agilent 5313A resistance meter under conditions of 55% relative humidity and 23 °C temperature. After conducting ten measurements on each sample using a circular electrode, the volume resistivity r_v [Ω.m] and conductivity γ [S/m] were calculated.

$$r_v = R_v \frac{S}{t}$$

(5)

$$\gamma = \frac{1}{r_v}$$

(6)

Where t [m] is the material thickness and S [m^2] is the surface area of measurement electrodes.

4.3.7 Resistive heating

The electrical heating performance of the carbon felt samples was studied by connecting samples to a power source and applying varying voltages. An infrared camera (FLIR E6, USA) was used to record the temperature of the samples, with an emissivity of 0.95 [93].

4.3.8 Filtration efficiency

The gas filtration performance of the sample was evaluated using the MPF 1000 HEPA (PALAS GmbH, Germany) filtration instrument with Dioctyl sebacate (DEHS aerosols) as the dust. To investigate the penetration of aerosol particles, a scanning mobility particle sizer was employed. The filtration efficiency was obtained from Equation (7).

$$\text{Filtration efficiency} = 1 - \frac{C_{down}}{C_{up}} \tag{7}$$

where C_{down} and C_{up} are the particle concentration in the downstream and the upstream, respectively [91].

4.3.9 EMI shielding effectiveness

EMI shielding effectiveness testing was conducted in the frequency range of 30 MHz to 3 GHz using the coaxial transmission line method, following ASTM 4935–10, designed for evaluating flat materials. Experimental apparatus included a coaxial specimen holder (EM-2107A, Electro-Metrics, Inc.) with input and output signals connected to a vector network analyzer (Rhode & Schwarz ZNC3). The analyzer was specifically configured for generating and receiving electromagnetic signals. The total EMI shielding effectiveness (SE_T) was characterized by the ratio of transmitted power to incident power and is typically presented as follow.

$$SE_T[dB] = -10\log\frac{P_T}{P_I} = SE_A + SE_R \tag{8}$$

Where P_T and P_I refer to the transmittance power and incident power, respectively. SE_A and SE_R are used to describe the shielding effectiveness resulting from absorption and reflection (including secondary reflections), respectively. They can be calculated from the total

reflection (R) and transmission (T) components of the incident power, along with the scattering parameters (S_{11} and S_{21}), using Equation (9-12) [78][94] [95].

$$R = |S_{11}|^2 \tag{9}$$

$$T = |S_{21}|^2 \tag{10}$$

$$SE_R[dB] = -10\log(1 - R) \tag{11}$$

$$SE_A[dB] = -10\log(\frac{T}{1-R}) \tag{12}$$

4.3.10 Structural stability

To evaluate the structural stability of the carbon felts under different types of deformation, a custom testing method was developed. In simple terms, when the structure of a conductor undergoes physical damage, its conductive network can be partially disrupted. Leveraging this fact, the real-time monitoring of the resistance of a sample in a bent state can be used to investigate whether its structure has been damaged. As shown in Figure 4.3, one end of the sample was fixed at point A, while the other end was clamped at point B. During the testing process, point A remained stationary, while point B rotated the sample in a circular motion. As the sample end moved from point B to point C, the sample underwent a transition from a straight state to a bent state, as depicted in Phase I and Phase II in the Figure 4.3. During the aforementioned motion process, both ends of the sample were consistently connected to an ohmmeter, and the resistance value of the sample was recorded. In the present work, one end of the sample was kept in motion at 200 rpm for 20 min. The same stability testing was also applied to the resistive heating of the carbon felt by replacing the ohmmeter with a power supply.
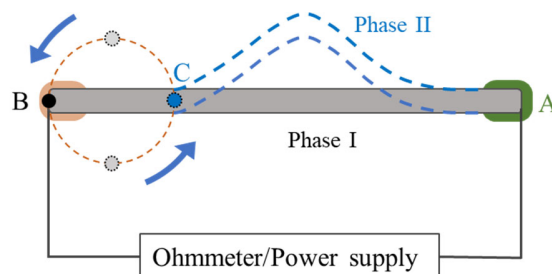
Figure 4.3 Schematic diagram of the structural stability test

4.3.11 Raman spectra

Raman spectroscopic analysis was performed utilizing a DXR Raman microscope (Thermo Scientific, USA) equipped with an excitation laser emitting at a wavelength of 532 nm and operating at a laser power of 8.0 mW. The specimens were scrutinized under an Olympus MPlan microscope with a magnification of 50, employing a spectrograph aperture set at 50 μm. Spectral data were acquired across the range of 3500-50 cm^{-1} prior to baseline correction.

4.3.12 XRD

The crystal structure of the carbon felt was analyzed using an analytical X'Pert PRO MRD X-ray diffractometer with a Cu-Kα1 radiation source.

4.3.13 TGA

The Thermogravimetric analysis (TGA) was conducted up to 800 °C with a heating rate of 10 °C/min in an N_2 atmosphere using the TGA/SDTA851e instrument (Mettler-Toledo).

4.3.14 Antibacterial properties

To evaluate the antibacterial properties of the obtained samples, Escherichia coli strain (CCM 7395) and Staphylococcus aureus strain (CCM2446) obtained from Masaryk University in Brno were utilized. Samples sized 1×2 cm were added to 25 ml of bacterial inoculum and thoroughly homogenized by agitation. Samples were taken after homogenization at 2, 5, and 24 hours, transferred to petri dishes, and then poured with PCA agar (BioRad). Subsequently, the samples were cultured at 37°C for 48 hours. Finally, colony-forming units (CFU) were counted. Additionally, bacterial inoculum not mixed with samples was extracted and cultured as a control.

Chapter 5 Results and discussion

5.1 Effect of different load modes during carbonization on the properties of carbon felt

5.1.1 Effect of different load modes on sample shrinkage and morphology.

In the preparation of flexible fibrous materials, the overall morphology of the sample is a crucial factor that cannot be overlooked. This factor is intricately linked to the structural stability and reproducibility of the resultant product. Hence, this study initiates with an examination of the shrinkage behavior of the samples under various loading conditions. Figure 5.1 and 5.2 illustrate the variations in mass, dimensions and size of the samples prepared under different loading conditions, respectively. Evidently, samples without loading exhibit significant alterations in both mass and size after carbonization. In contrast, both loading modes mitigate the shrinkage of resulting carbon samples, particularly notable at a temperature of 1000 ℃. However, the variation in thickness of the samples follows a distinct trend compared to the changes in mass and size.
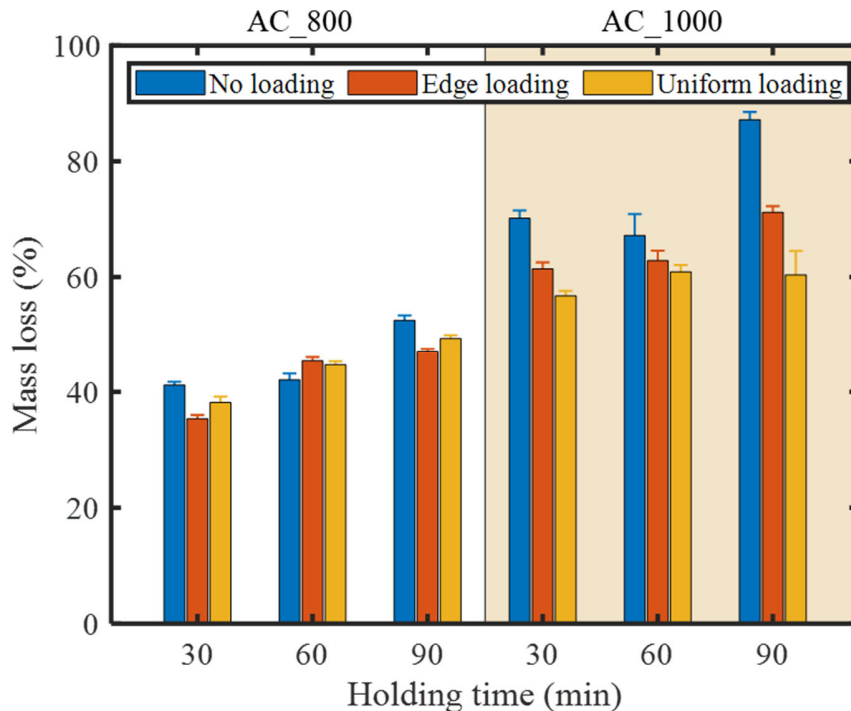
Figure 5.1 Mass loss of the obtained carbon felts under different loading modes
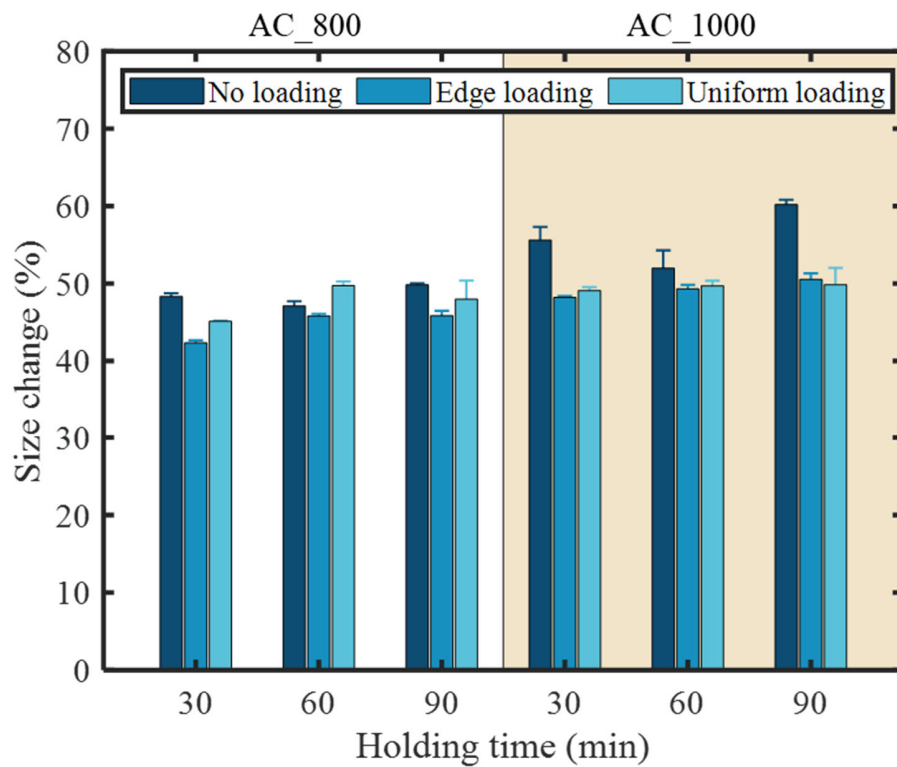
Figure 5.2 Size change of the obtained carbon felts under different loading modes

In Figure 5.3, it can be found that samples subjected to no load and edge loading exhibit similar thickness, whereas the samples under uniform loading show a pronounced reduction in thickness. This phenomenon can be readily comprehended as a consequence of the complete cover of the samples throughout the preparation process, leading to their thinning due to the pressure applied from above
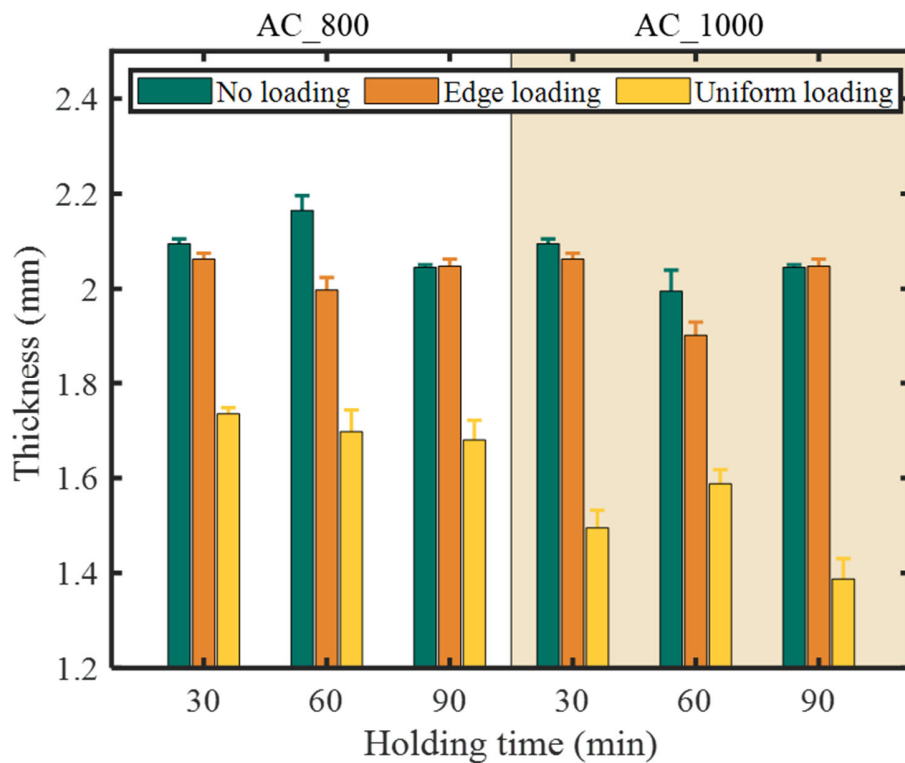
Figure 5.3 Thickness change of the obtained carbon felts under different loading modes

Furthermore, photographs of the carbon felt obtained under different loading conditions are presented in the Figure 5.4. It can be observed that the unloaded sample exhibit irregular deformations after carbonization. This is attributed to the uneven shrinkage of the fibers under the heated conditions, resulting in unpredictable deformations of the fiber assembly. Such unpredictability of the visual morphological changes is unacceptable for the preparation of stable and reproducible specimens. Later, the flexibility of the samples was observed by placing the handle of a knife onto the inclined specimens. Observably, samples with no load and edge loading displayed bending when subjected to pressure, showcasing excellent flexibility, whereas samples under uniform loading appear relatively rigid. In summary, while samples with no load do exhibit favorable flexibility, they are also accompanied by shrinkage and uncontrollable product morphology. Both loading modes decelerate the shrinkage, with the edge loading mode particularly preserving the flexibility of the samples. Therefore, in terms of the morphological appearance of the obtained samples, the edge loading mode proves more conducive to achieving the desired sample characteristics.
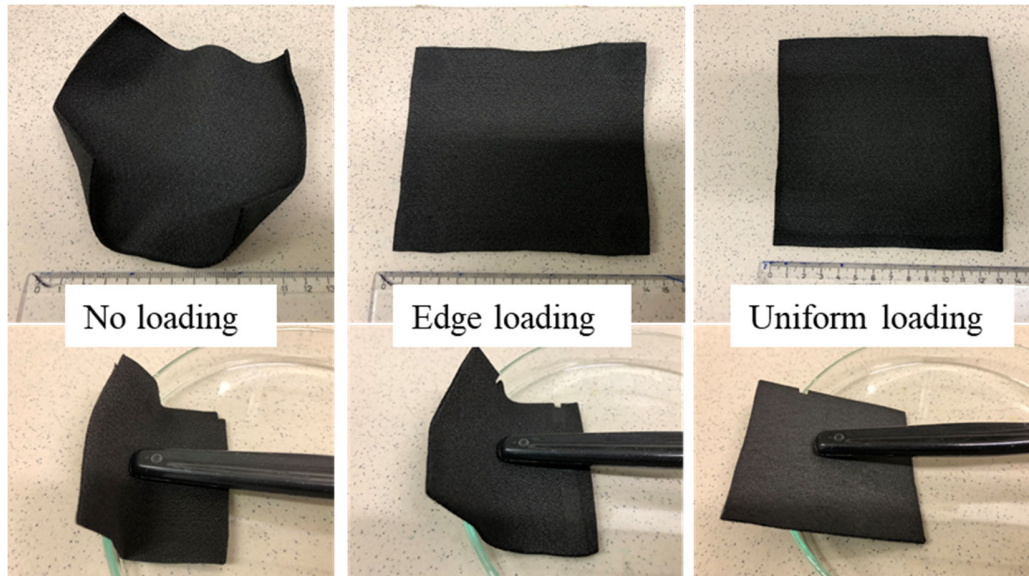
Figure 5.4 Photographs of the obtained carbon felts under different loading modes

5.1.2 Effect of different load modes on mechanical properties

The investigation of the mechanical properties of the obtained carbon felt is of paramount importance due to its highly porous nature. In view of the potential applications of carbon felt, this study examined the stiffness and tensile properties of the samples. The stiffness of the prepared samples under different conditions is shown in the Figure 5.5. It can be observed that across varying carbonized temperatures, the unloaded samples consistently exhibited the lowest bending moment. Compared to samples under uniform loading, significantly reduced bending moments were found on the edge loading samples. This phenomenon arises due to the inevitable occurrence of shrinkage deformation and curling during the heating process of the fibers. In contrast to samples under edge loading, fibers in uniform loaded carbon felts experience more external force confinement, thereby restricting fiber shrinkage deformation and curling. Researchers have established theoretical models to explore the effective stiffness of nonwoven fibrous webs [96]. The outcomes have revealed that the interplay of fiber stretching, fiber bending, and crosslink rotation deformation exerts a profound influence on the overall mechanical behavior of nonwoven fibrous networks. Among these, a significant reduction in the stiffness of the fibrous network was observed when the fiber curvature exceeded $\pi/3$. As a result, this observation provides a plausible explanation for the reduced stiffness found in edge-loaded samples, as they experience fewer fiber deformations and

curling phenomena. Furthermore, it can be observed that longer carbonization time and higher carbonization temperatures lead to further reductions in the stiffness of the resulting samples. This is also be attributed to the influence of carbonization process parameters on the shrinkage of the fibers obtained.
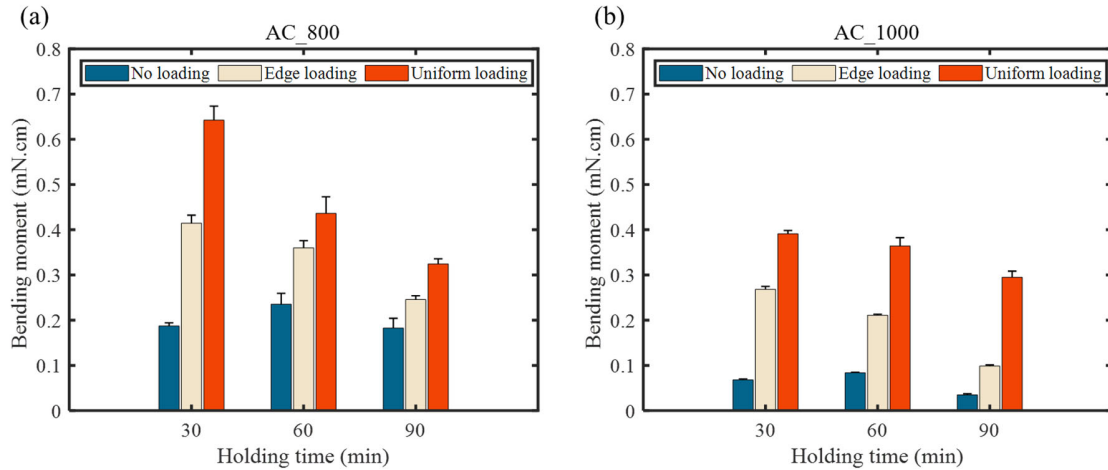
Figure 5.5 Stiffness of the obtained carbon felts under different loading modes at 800℃ (a) and 1000℃ (b)

Subsequently, the tensile properties of the samples were studied, and the breaking stress and breaking elongation of the specimens are displayed in the Figure 5.6. It is evident that the unloaded samples subjected to a holding time of 30 min exhibit the highest tensile stress, whereas an increase in the holding time to 90 min results in the lowest tensile stress. For carbonization temperatures of 800 ℃ and 1000 ℃, the carbonization duration leads to a significant decrease in tensile stress, ranging from 0.97 MPa to 0.44 MPa and from 0.85 MPa to 0.17 MPa, respectively. On the other hand, the tensile stress of the other two loaded samples demonstrates a relatively stable behavior, remaining within the range of 0.6 MPa to 0.9 MPa regardless of the carbonization temperature and duration. In the realm of nonwoven textiles, the principal mechanism governing tensile fracture primarily involves the fracture of fibers and inter-fiber slippage. During the process of tensile loading, individual carbon fibers may undergo fracture due to external stresses, consequently leading to the overall fracture of the fiber assembly. In the carbonization process, applying tension to the fibers is widely acknowledged as an effective means of enhancing the tensile performance of carbon

fibers [54]. In this study, the improved tensile properties observed in the loaded samples may be attributed to this particular factor, leading to greater stability in their tensile behavior. In the case of unloaded samples, extended carbonization adversely affects the molecular alignment within the fibers, resulting to a weakening of the mechanical properties. Furthermore, the breaking elongation results in Figure 5.6 (b) indicate that sample subjected to edge loading exhibit superior breaking elongation compared to the uniform loading sample. This is attributed to the pressure applied by uniform loading during the carbonization process, which imparts greater brittleness to the fiber assembly. In samples subjected to edge loading, the majority of fibers remain unexposed to direct compressive forces during the preparation process, leading to the development of carbon felt with enhanced elasticity and flexibility.
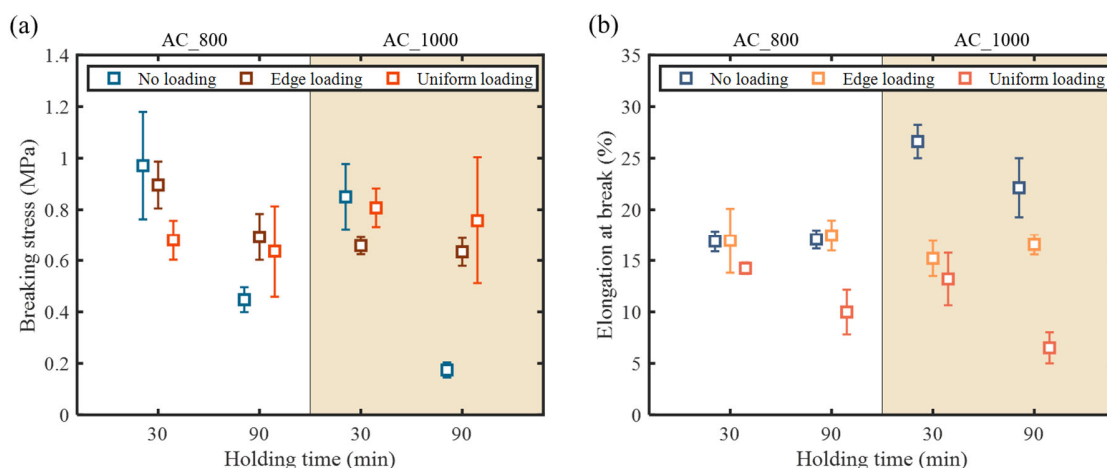
Figure 5.6 Breaking stress (a) and elongation (b) of the obtained carbon felts under different loading modes

5.1.3 Effect of different load modes on thermal properties

Understanding the thermal transport performance of carbon felts is crucial for numerous engineering applications. By modulating thermal conductivity, materials can be designed to meet specific thermal management requirements in various applications, such as heat dissipation in electronic devices. Thermal conductivity, measured as the rate at which heat is transferred through a material per unit area and unit thickness under a specified temperature gradient, is an intrinsic property of materials. As depicted in Figure 5.7 (a), it is observed that among the samples prepared using three different loading modes, the thermal conductivity is

highest for the edge-loaded sample, followed by the uniform loaded sample, with the unloaded sample having the lowest thermal conductivity. (Major influence has pore size and their amount) The thermal conduction in carbon fibers primarily occurs through lattice vibrations. Within the lattice, carbon atoms oscillate around their equilibrium positions, generating phonons (lattice vibrational quanta). These phonons propagate within the lattice, carrying thermal energy [97]. It has been found that the thermal conductivity of carbon fibers gradually increases asymptotically with the enhanced preferential orientation degree of the crystalline segments within the fibers [98]. During the carbon felt preparation process, edge loading provides the fibers with the appropriate tension, optimizing the preferred orientation of the internal crystalline phases within the fibers, thereby enhancing the overall thermal conductivity of the fiber assembly but porosity effect is more important. With the increase in carbonization temperature from 800 ℃ to 1000 ℃, there is an observed elevation in the thermal conductivity of the samples. This phenomenon can be attributed to the enhanced interatomic bonding among carbon atoms at higher carbonization temperatures, thereby leading to an improvement in material crystallinity. Greater crystallinity is conventionally correlated with superior thermal conductivity, as it facilitates more efficient heat transfer between crystalline regions. Thermal resistance is determined by both the thermal conductivity and thickness of the material, and it serves as an indicator of the ability to impede the flow of heat through a unit area of the material. From Figure 5.7 (b), it can be observed that the thermal resistance of the unloaded sample is almost 40% higher than that of the loaded samples, while the difference in thermal resistance between the two loaded samples is not as significant as the difference in thermal conductivity. This is primarily attributed to the varying thicknesses of the samples under different loading modes, as demonstrated in the previous section. Generally, the thermal properties of the samples, reveals that the edge loading mode enhances the thermal conductivity of the samples by optimizing the orientation of internal crystalline phases within the fibers and changing real porosity.
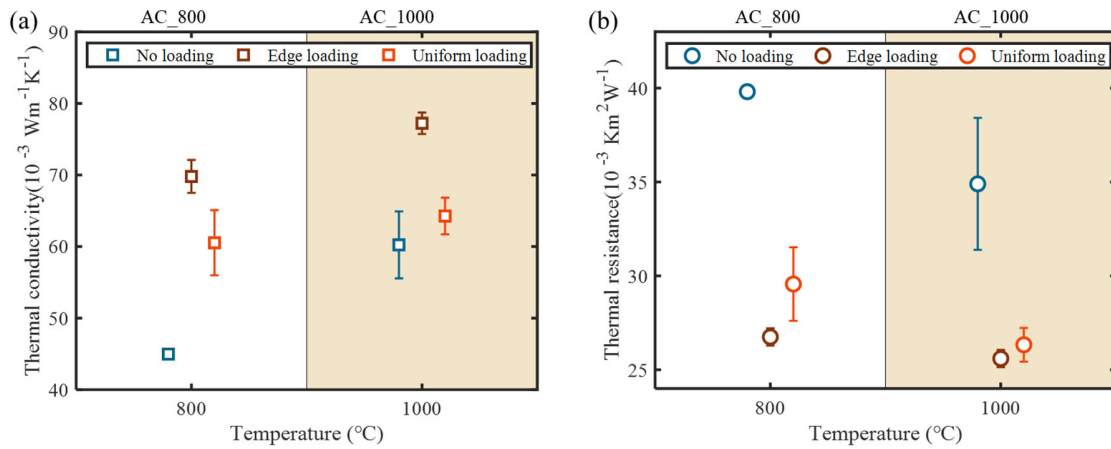
Figure 5.7 Thermal conductivity (a) and resistivity (b) of the obtained carbon felts under different loading modes

5.1.4 Effect of different load modes on electrical properties

The volume electrical conductivity of carbon felt samples obtained under different loading conditions in this study is presented in the Figure 5.8. At a carbonization temperature of 800 ℃, the samples exhibited relatively lower electrical conductivity, with no significant differences among different loading modes. As the temperature increased to 1000 ℃, it was observed that the edge-loaded samples exhibited the highest electrical conductivity. As mentioned earlier, edge loading provides the fibers with the appropriate tension, thereby ensuring a more homogeneous electrical connection within the fiber assembly. However, it should be noted that, when the carbonization time was extended to 90 minutes, there was a sharp decrease in the electrical conductivity of the samples. This could be attributed to the prolonged carbonization time causing damage to the fibers, consequently disrupting the internal conductive pathways within the carbon felt and reduction of porosity.
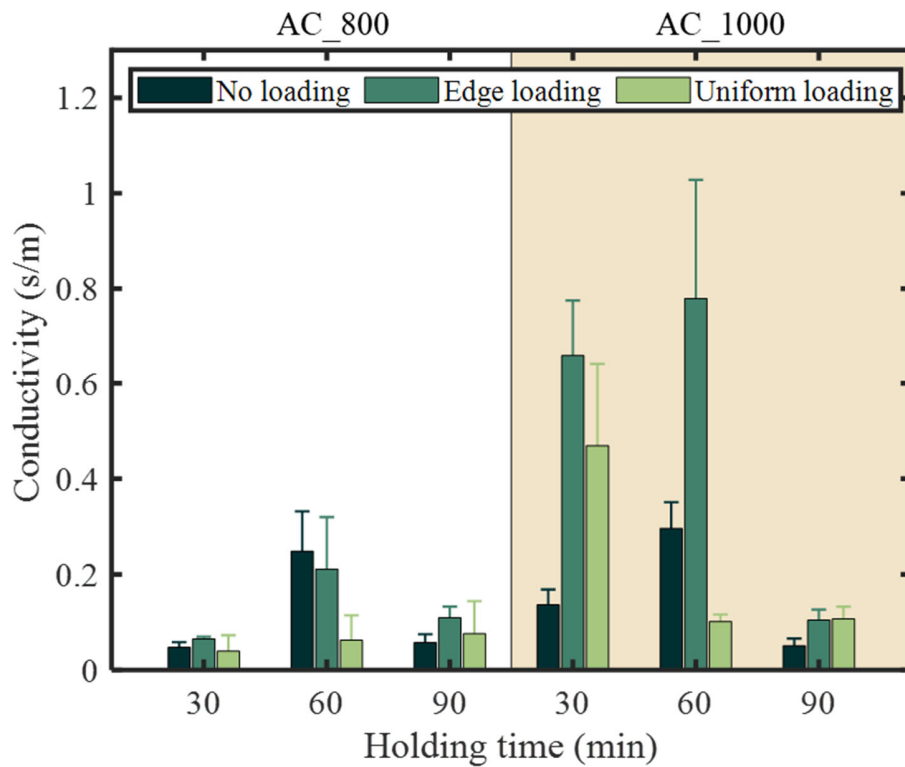
Figure 5.8 Electrical conductivity of the obtained carbon felts under different loading modes

Thus far, through an examination of the performance of samples obtained under various loading modes, it has become apparent that the edge loading mode is more conducive to achieving the desired sample characteristics. Therefore, subsequent sections used the edge-loading mode to prepare samples and conduct research.

5.2 Effect of PTFE coating on the properties of carbon felt

As an industrial dust filter felt, the surface is typically treated with hydrophobic treatments to improve applicability. In this thesis, one side of the acrylic-based felt was coated with PTFE, with a mass content of approximately 0.5% of the total felt weight. One of the challenges in processing waste textiles is the mixture of various fibers, due to the lack of efficient methods for separating different fibers. For pyrolyzed fiber waste, such mixed fibers or fiber coatings may introduce uncertainties in the performance of the resulting carbon materials. We investigated the effects of a PTFE coating on the properties of acrylic-based carbon felt. Since the raw material had PTFE coating only on one side and was very thin, its

impact on acrylic fibers during pyrolysis may have been minimized. Therefore, we coated the raw material with a PTFE dispersion to form a PTFE layer on the fiber surface, followed by sequential stabilization and carbonization, to examine its impact on the properties of the resulting carbon felt.

5.2.1 Effect of PTFE coating on sample shrinkage and morphology

The morphology of the PTFE coating on the acrylic-base felt was first observed, and SEM images are shown in Figure 5.9. The surface of the original acrylic-based felt fibers was smooth, with large gaps between the fibers. After coating with a 60% concentration PTFE dispersion, the fiber surfaces were observed to be evenly covered. Due to the high viscosity resulting from the high concentration of the dispersion, the gaps between the fibers were filled with a significant amount of PTFE chunks formed as a result of cracking upon drying.
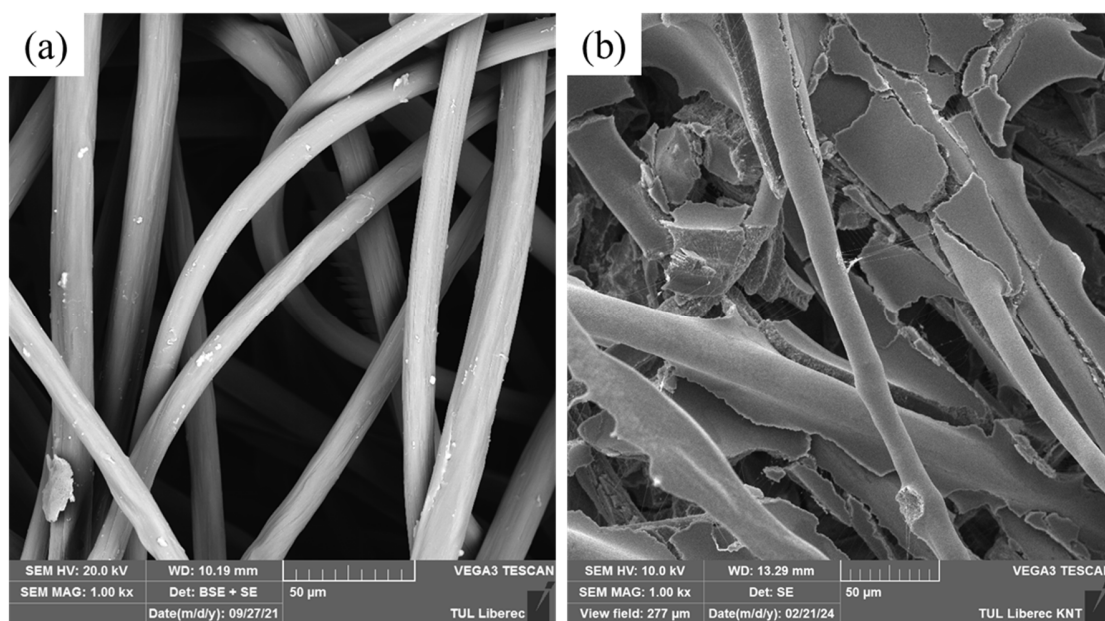
Figure 5.9 The morphology of the acrylic-base felt without PTFE coating (a) and with PTFE coating

After coating the acrylic-based felt, EDX testing was conducted on the surface, and the result is shown in Figure 5.10. The EDX spectrum obtained after the 60% PTFE dispersion coating revealed the presence of 10.4% fluorine on the fiber surface, confirming the existence of the PTFE coating.
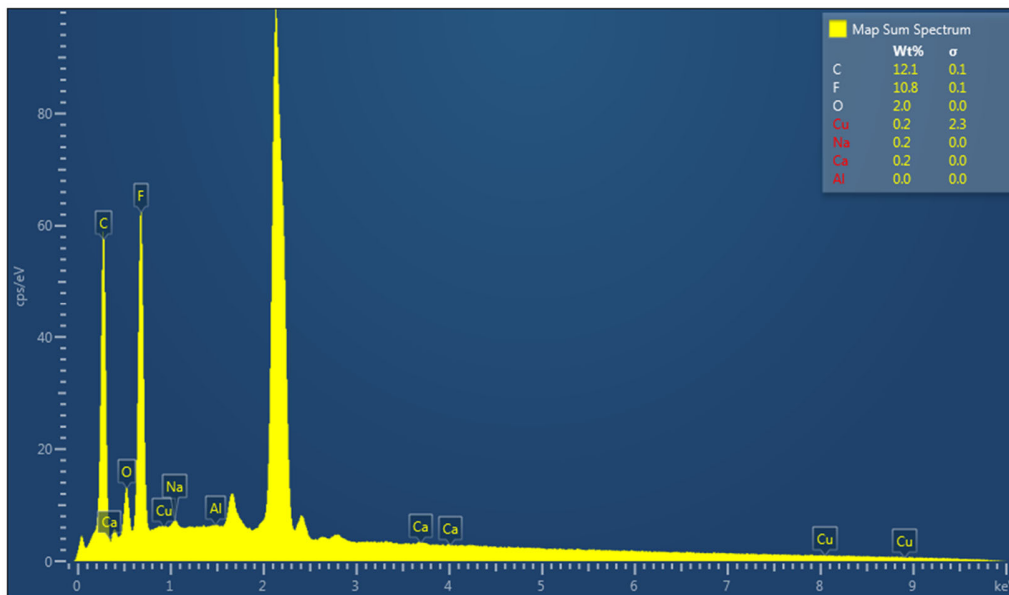
Figure 5.10 The EDX spectrum of the acrylic-base felt with PTFE coating

Figure 5.11 shows the morphology of carbon felt fibers prepared from uncoated and coated acrylic felt. The surface of carbon felt fibers made from uncoated acrylic felt was clean, with some wrinkles distributed along the fiber axis. Similar wrinkles were also found in the coated samples. However, the surface of carbon felt fibers from coated acrylic felt exhibited the presence of small particles. These may be minor residues from the decomposition of PTFE or small bubbles formed at the acrylic-PTFE interface during pyrolysis due to incomplete gas release.
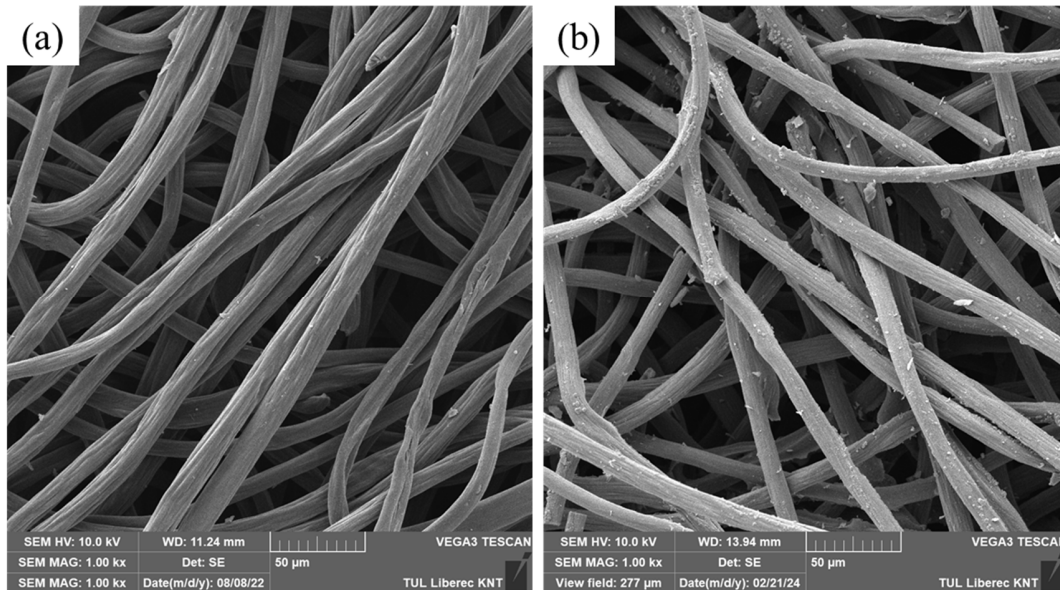
Figure 5.11 The morphology of the obtained carbon felts from precursor without PTFE coating (a) and with PTFE coating

Photographs of the samples obtained after carbonization of acrylic-based felt with PTFE coatings of different concentrations are shown in Figure 5.12 (a). It can be clearly observed that the size of the samples increases with the concentration of the PTFE coating. Notably, when the PTFE concentration reaches 30% and 60%, the change in sample size becomes more pronounced. The quantified results of the changes in sample mass and size are shown in Figure 5.12(b). The loss in sample mass did not change significantly in the range of low concentration PTFE coatings (0%–12%). When PTFE reached 30%, a notable decrease in mass loss was observed, which further decreased as the concentration increased to 60%. This indicated that mass loss in the carbon felt was only reduced when the PTFE coating fully enveloped the fibers. In contrast, the changes in sample size followed the variations in PTFE concentration, decreasing accordingly. Notably, when PTFE concentrations were increased to 30% and 60%, the decrease in sample size changes became more pronounced. As PTFE concentration increased, the change in sample size exhibited a different trend compared to mass loss. This may be due to the initially high porosity of the felt, where higher PTFE concentrations not only enveloped the fiber surfaces but also filled the gaps between the fibers. The filling of the original gaps between fibers with PTFE inhibited the heat-induced

shrinkage of the acrylic felt, resulting in a significant difference in the variation of sample size.
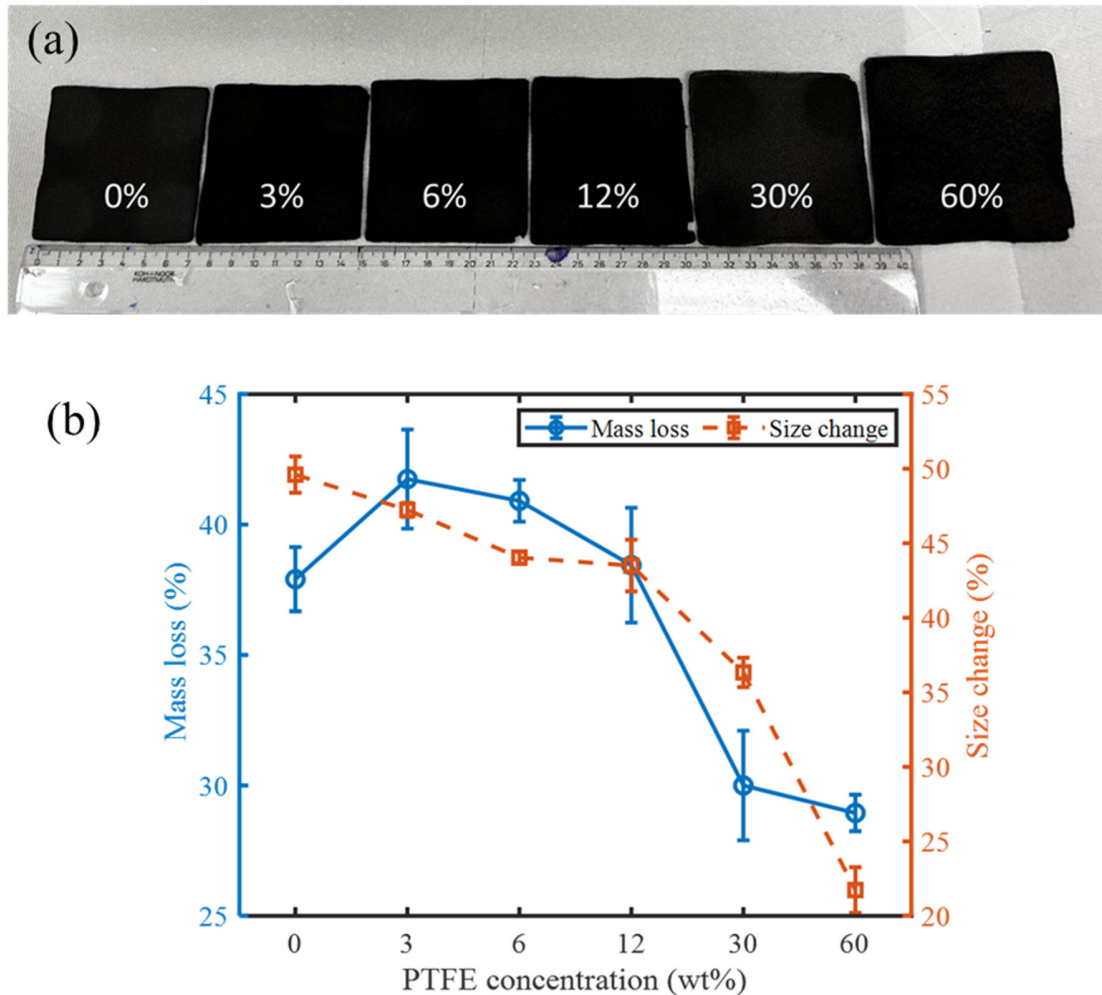
Figure 5.12 Shrinkage of the carbon felts obtained with different concentration PTFE coating. (a) Photographs of the samples. (b) Mass loss and size change

To further investigate the effect of PTFE on acrylic-based felt during pyrolysis, we conducted TGA on the samples, and the results are shown in Figure 5.13. The thermal decomposition of exposed acrylic fibers mainly occurred between 300°C and 500°C. However, the decomposition of pure PTFE occurred around 600°C. Therefore, within the range of 300°C to 500°C, the surface of the fibers remained enveloped by an undecomposed PTFE layer, hindering the release of gaseous products produced during the pyrolysis of acrylic. This could be the reason for the reduction in mass loss in samples with high PTFE coating concentrations.

Additionally, during the acrylic decomposition stage, the undecomposed PTFE between the fibers acted as a support structure, maintaining the original structure of the felt and slowing down changes in sample size.
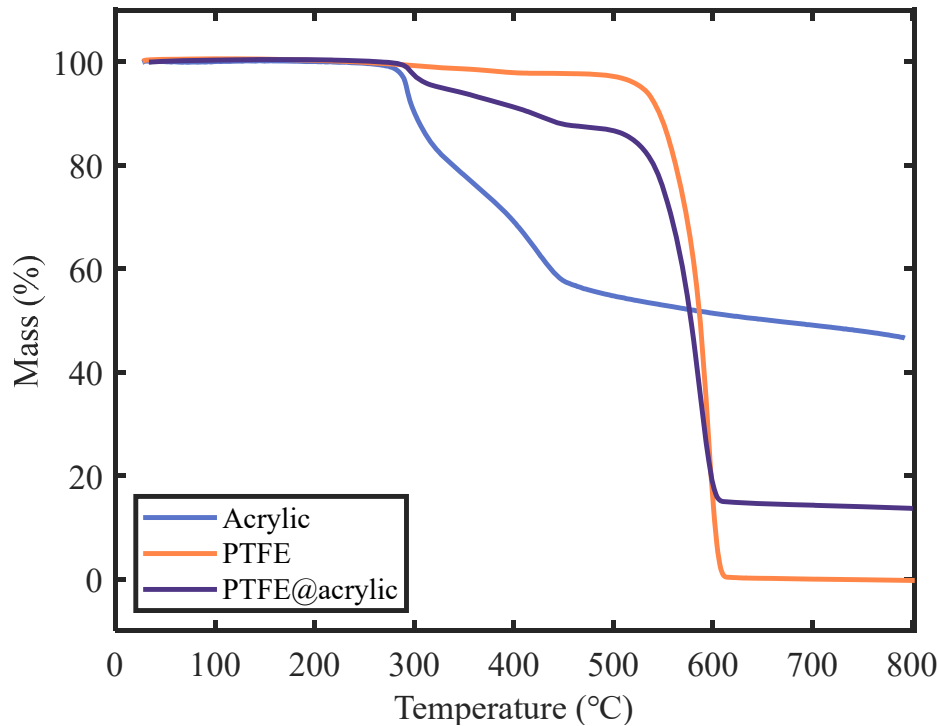
Figure 5.13 TGA curves of the acrylic-base felt, PTFE, and PTFE coated felt

5.2.2 Effect of PTFE coating on sample mechanical properties

The stiffness of the samples prepared under different PTFE concentration conditions is shown in Figure 5.14. It can be observed that within the low concentration range of 0%–12%, the samples exhibited similarly low bending forces with almost no differences. When PTFE concentrations were increased to 30% and 60%, the bending forces of samples significantly increased and correlated positively with concentration. This phenomenon is due to the fibers' inability to deform during pyrolysis, because of the adhesive effects of PTFE between the fibers. As mentioned above, the overall mechanical behavior of the nonwoven fiber network is influenced by the interplay of fiber stretching, fiber bending, and cross-link rotation deformations. Evidently, the solid PTFE filling between the fibers hindered fiber curling and

cross-link rotation during pyrolysis, resulting in increased stiffness of the obtained carbon felt.
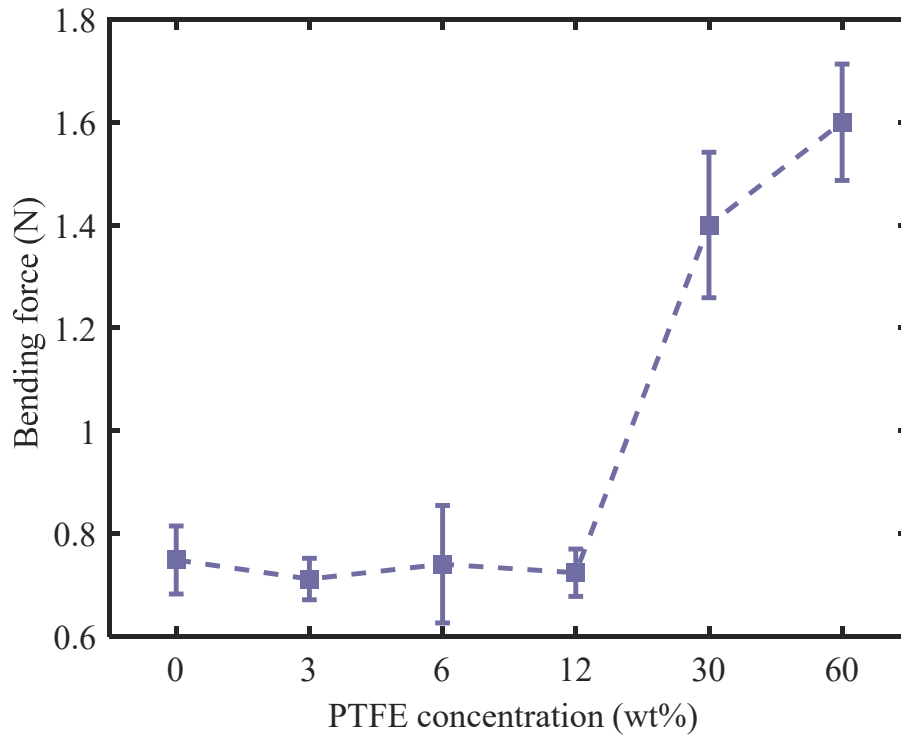
Figure 5.14 Stiffness of the carbon felts obtained with different concentration PTFE coating

The tensile strength and modulus of the samples are shown in Figure 5.15. In comparison to uncoated samples, low PTFE concentrations of 3%–12% resulted in lower tensile strength. When concentrations increased to 30% and 60%, the tensile strength was slightly higher than that of the uncoated samples. The enhancement of the samples' modulus due to the coating was more pronounced. Low PTFE concentrations modestly increased the modulus by about 10 MPa, whereas high concentrations significantly increased the modulus, from 15 MPa to 76.4 MPa. Such a marked increase in modulus can be attributed to the control exerted by PTFE on fiber deformation during pyrolysis, as discussed in the previous section, which led to increased stiffness in the carbon felt samples. However, since PTFE was mostly converted into gaseous products after carbonization, it did not significantly improve the tensile strength of the samples.
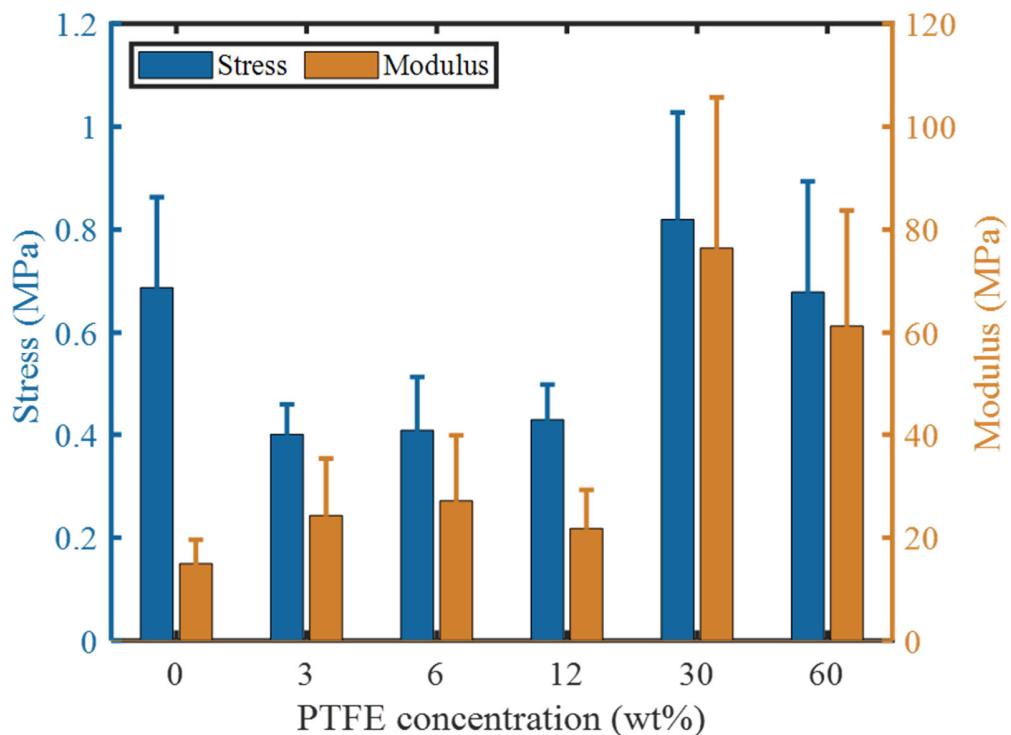
Figure 5.15 Tensile properties of the carbon felts obtained with different concentration PTFE coating

5.2.3 Effect of PTFE coating on sample electrical conductivity

The coating and filling of PTFE may have altered the distribution of the fibers within the carbon felt, which can change the conductive network formed by the carbon fibers. Therefore, we studied the impact of the PTFE coating on the conductivity of samples. The changes in conductivity with PTFE concentration are shown in Figure 5.16. It was found that conductivity slightly increased with increasing PTFE concentration. At the same time, samples with the coating exhibited greater variation in results. This may be due to the inability of the fibers to naturally contract and curl during pyrolysis, which led to significant differences between each sampling point.
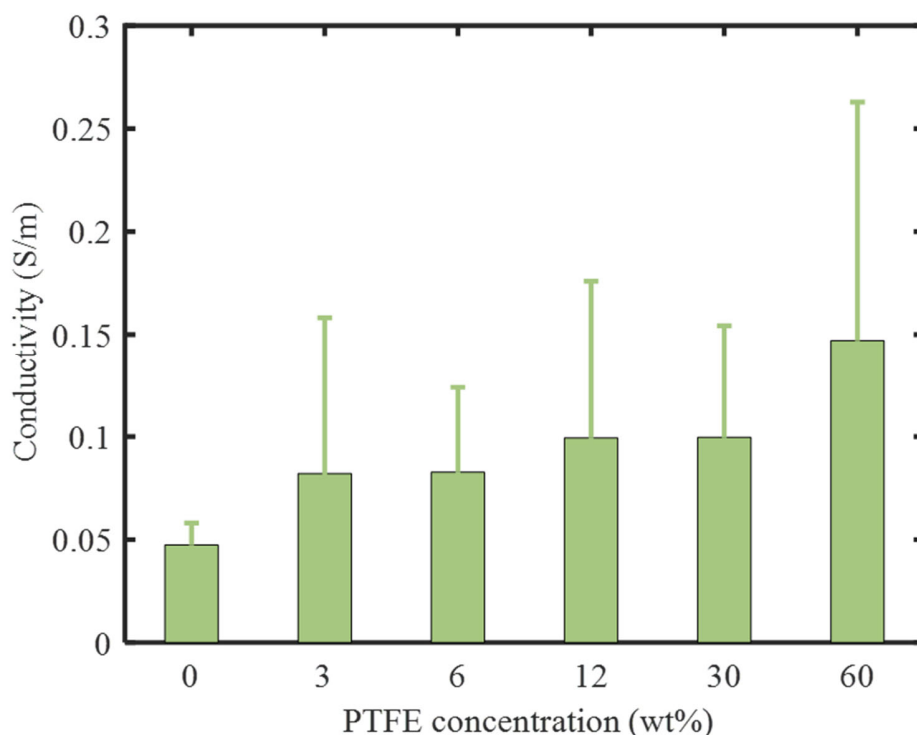
Figure 5.16 Electrical conductivity of the carbon felts obtained with different concentration PTFE coating

In summary, through the study of the morphology, mechanical properties, and electrical properties of PTFE-coated samples, we found that low-concentration coatings had a minimal impact on the performance of the resulting carbon felt. High-concentration coatings, while increasing the material's modulus and conductivity, led to a loss of flexibility in the carbon felt, potentially significantly limiting its range of applications. Therefore, in subsequent work of this dissertation, to prepare flexible carbon felt, we used precursors without additional PTFE coatings, as the thin PTFE layer on one side of the raw material is believed to have a negligible impact on the performance of carbon felt.

5.3 Flexible carbon felt characterization and properties.

After exploring the process during carbonization, we established the optimal process for preparing flexible conductive carbon felt. In this section, the carbon felt prepared using the edge-loading mode was characterized, and its EMI shielding and resistive heating properties were studied.

5.3.1 Morphology and structure characterization

The SEM images of the carbon felts obtained are illustrated in Figure 5.17. The carbon fibers obtained from the acrylic-based precursors underwent a change in their fineness, exhibiting a finer structure with increasing carbonization temperature. This transformation can be attributed to the depletion of hydrogen and nitrogen in acrylic as the degree of carbonization escalated, resulting in fiber shrinkage. Moreover, when carbonized at 1100°C, the carbon fibers displayed prominent wrinkles on their surface. Wrinkles on the surface of fibers can serve several advantageous purposes in material science. Firstly, they contribute to an increase in the overall surface area of the fiber, which in turn enhances processes such as adsorption, absorption, and exchange. Secondly, these wrinkles also bolster the strength and rigidity of the fibrous material, rendering it better suited to withstand external forces and pressures. Furthermore, the presence of microscale indentations and protrusions on the fiber surface aids in improving adhesion.
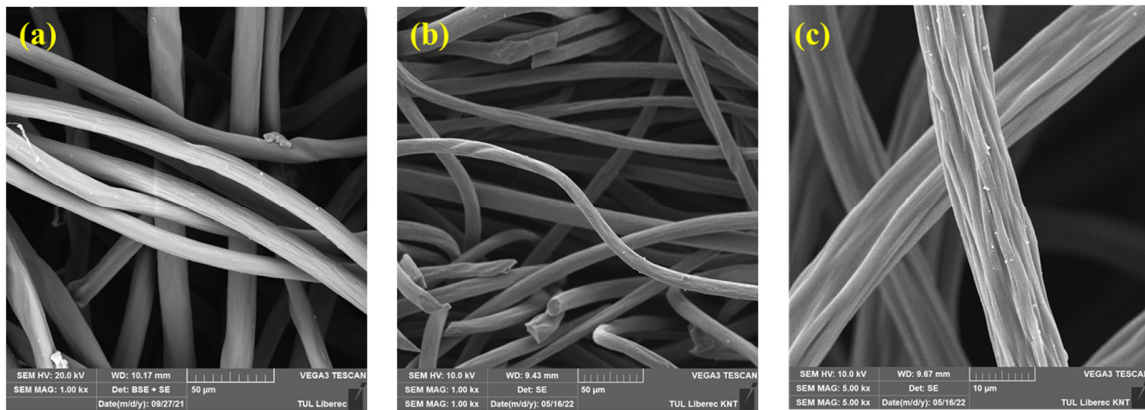
Figure 5.17. Fiber morphology of the carbon felts. SEM images of precursor acrylic fiber(a), AC_800(b), and AC_1100(c)

The distribution of carbon fiber diameters was analyzed using ImageJ software applied to SEM images. Figure 5.18 shows that as the carbonization temperature increased from 800°C to 1100°C, the average fiber diameter decreased from 12.74 μm to 9.2 μm. With the temperature elevation, the fiber diameter distribution tended to follow a normal distribution pattern, indicating that higher carbonization temperatures were conducive to optimizing the fiber fineness distribution. The fineness of the fibers directly impacts the physical and

mechanical properties of the carbon felt, while also influencing its porosity and specific surface area. A higher porosity is considered advantageous for the reflection of electromagnetic waves within the carbon felt, thereby enhancing shielding effectiveness[99].
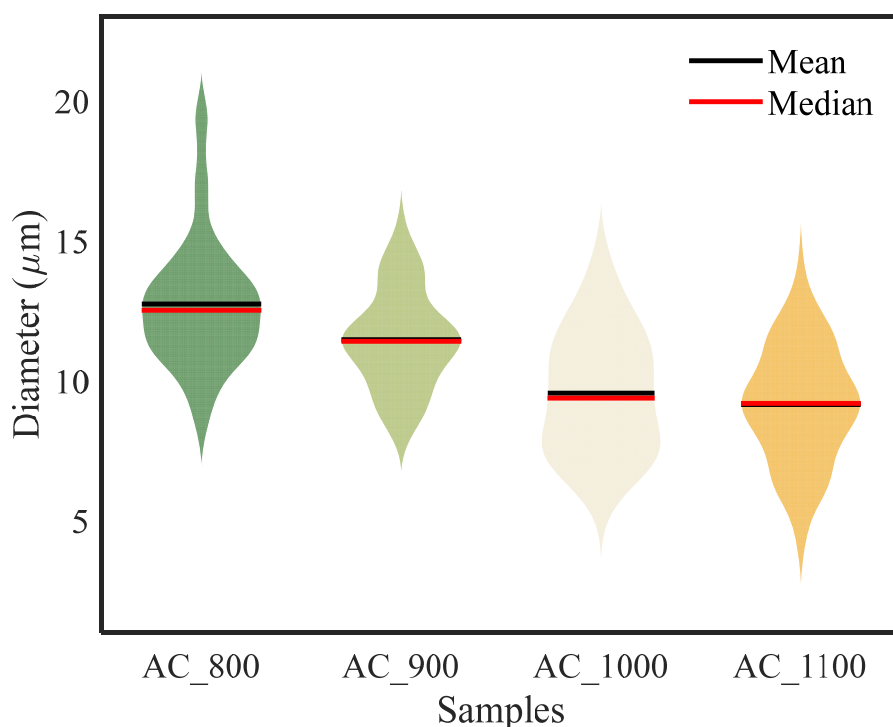
Figure 5.18 Fiber diameter distribution of the carbon felts

In addition to fiber morphology, the porosity of carbon felts also plays a significant role in influencing their properties, including filtration and separation capabilities. The porosity and associated parameters of samples prepared at different temperatures are listed in Table 5.1. As the carbonization temperature increased from 800 to 1100°C, it was found that the porosity increased from 83.39% to 93.91%. Simultaneously, the fiber density increased from 1.24 to 1.69 g/cm^3. The increase in porosity may be attributed to two mechanisms. One can be explained by the aforementioned changes in fiber morphology and fiber fineness. With the increase in carbonization temperature, the fibers gradually contract and became finer, naturally increasing the proportion of internal voids within the carbon felt. The other mechanism is that during high-temperature carbonization, the polymer undergoes

decomposition, releasing gases and volatile substances, resulting in the formation of pores. The relationship between porosity and temperature was modeled using a straight line as linear regression model (Figure 5.19), resulting in an R^2 value of 0.86. This R^2 value indicates that the straight line model has a certain degree of explanatory power for the relationship between porosity and temperature, but it is not perfect. The relatively low R^2 value obtained may be attributed to several factors. It is important to acknowledge that temperature may not be the sole determinant of pore volume. Other unconsidered factors or variables might also play significant roles in influencing the porosity.

Table 5.1 Porosity of the carbon felts

Sample	AC_800	AC_900	AC_1000	AC_1100
Porosity (%)	83.39	90.52	92.5	93.91
Fiber density (g/cm^3)	1.24	1.37	1.56	1.69
Thickness (mm)	2.11	2.11	2	1.89
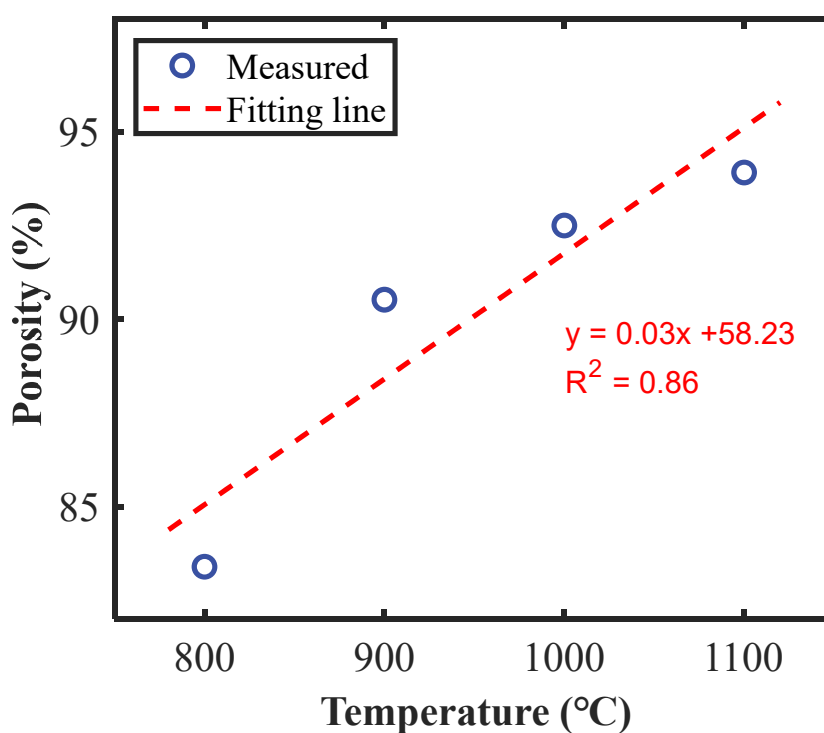
Figure 5.19 Porosity of carbon felts

The Raman spectrum of the obtained carbon felt is depicted in Figure 5.20. Typically, the D band at 1350 cm^{-1} is attributed to defects and disordered carbon structure, while the G band at 1580 cm^{-1} is induced by the sp^2 hybridization of carbon. The peak intensity ratio of the D band to the G band (I_D/I_G) is considered to be linearly correlated with the inverse of the in-plane crystal size. Thus, this indicator can be utilized to quantify the amount of ordered graphite structure [100]. After fitting the obtained spectra with a Gaussian function, the I_D/I_G ratio of the resulting samples decreased from 1.45 to 1.05 as the carbonization temperature increased from 800 °C to 1000 °C. This indicates that due to the removal of non-carbon elements such as oxygen and a reduction in the number of defects, the carbon structure within the fibers is transitioning from a mixed-bonded amorphous carbon to a predominantly sp^2-bonded carbon [101].
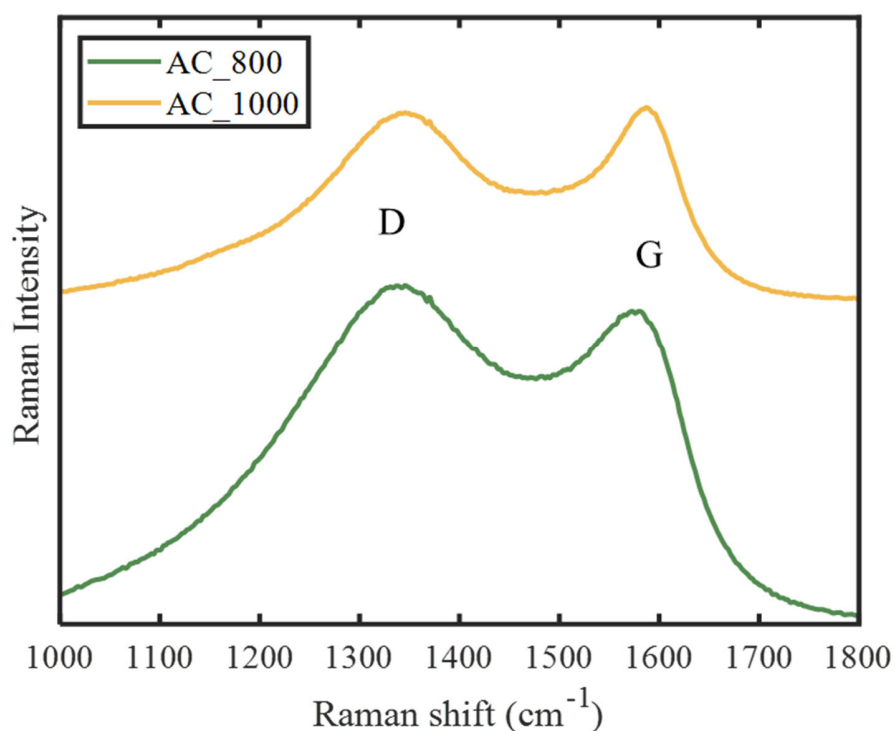
Figure 5.20 Raman spectrum of the carbon felts

To investigate the crystalline structure of the obtained carbon felts, XRD analysis was conducted. As shown in the Figure 5.21, both carbonized samples exhibited distinct peaks at

approximately 25.5° and 43.4°. The strongest diffraction peak was observed at 25.5°, corresponding to the (002) graphite basal plane reflection, indicating the presence of a hexagonal graphite structure.[43]. The diffraction peaks observed at 43.4° were attributed to the (100) diffraction of the graphite structure [102]. Furthermore, the peak at 43.4° became sharper with increasing carbonization temperature, indicating a more ordered arrangement of carbon atoms along the (100) plane. In summary, we found that increasing the carbonization temperature facilitated the attainment of higher crystallinity or structural order within the fibers, which would be advantageous for enhancing the electrical and thermal properties of the samples.
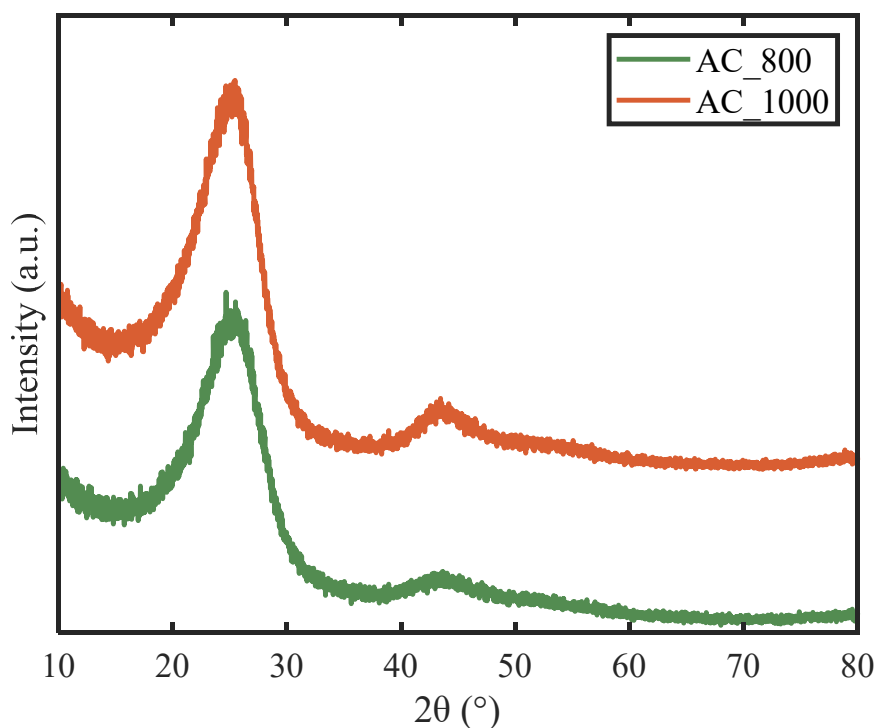
Figure 5.21 XRD spectra of carbon felts

5.3.2 EMI shielding behavior

Figure 5.22 illustrates the EMI shielding effectiveness (SE) of a single-layer carbon felt in the frequency range from 30 MHz to 3 GHz. It is clear that the total SE increases with the rise in carbonization temperature. As the carbonization temperature increases from 800 to

1100 °C, the EMI SE significantly rose from 17-20 dB to 42-57 dB. In accordance with the general requirements for EMI SE in textile materials, all samples in this study, with the exception of AC_800, demonstrated an "excellent" rating. AC_800 was characterized as "very good"[103].
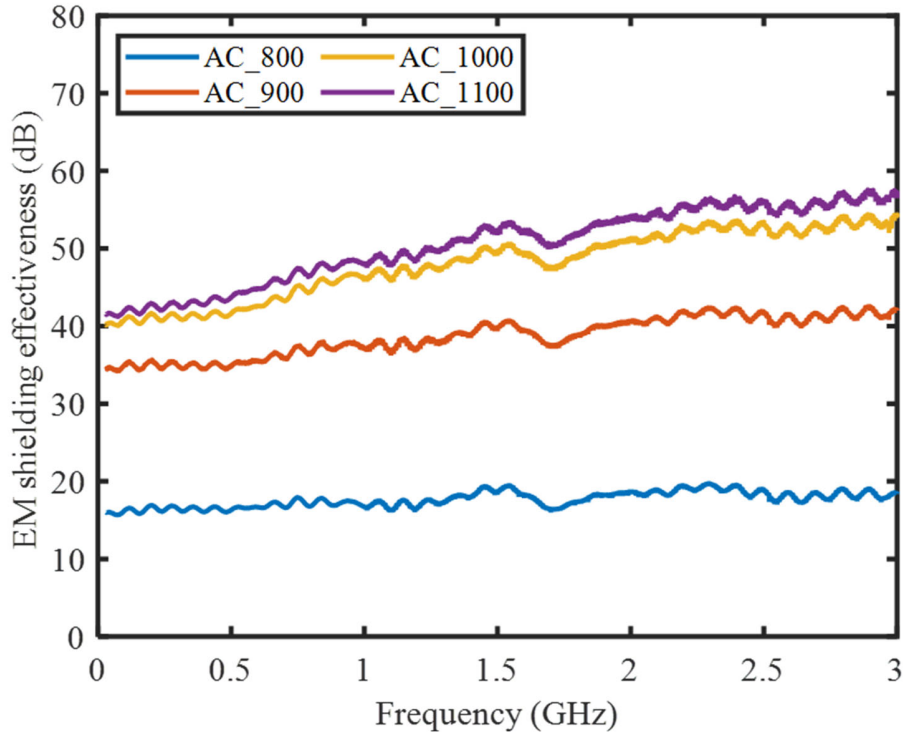
Figure 5.22 Total EMI shielding effectiveness from 30MHz to 3GHz of the carbon felts

In Figure 5.23, the reflection SE (SE_R), absorption SE (SE_A) and total SE (SE_T) of at the frequency of 1.5 GHz of the carbon felts is displayed. The SE_A and SE_T of each sample were found increased with the increase in carbonization temperature. The SE_R, however, remained at about 10 dB after the temperature reached 900 °C. Therefore, it can be said that the samples carbonized at temperatures above 900°C showed an increase in SE_T with increasing temperature, primarily due to the growth in SE_A. A high SE_A can often mislead the assessment of shielding mechanisms, creating the false impression that absorption is the dominant mechanism [104].
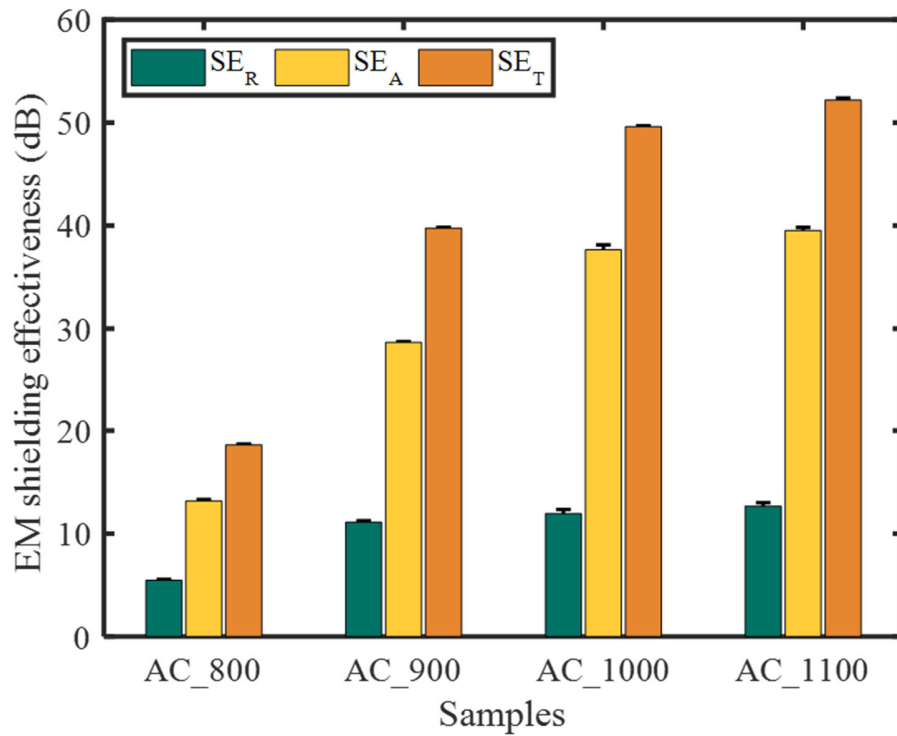
Figure 5.23 SER, SEA, and SET at 1.5 GHz of the carbon felts

To further investigate the role of EM wave reflection and absorption, the power coefficients were calculated and shown in Figure 5.24 [104]. The coefficients R of the samples increased with temperature while the coefficients A decreased. R was observed to be much larger than A, proving that reflection dominated the attenuation of the incident EM waves. An increase in carbonization temperature is typically accompanied by improved electrical conductivity. Therefore, carbon felt with the highest conductivity was most effective at reflecting EM waves. The surface electrical conductivity of material plays a pivotal role in determining the reflection of EM waves. This phenomenon arises from the direct interaction between the mobile charge carriers on the surface of conductive materials and incident EM waves, resulting in the reflection of EM waves due to impedance mismatch at the interface [105]. Literature suggested that when the EMI shielding SE exceeds 50 dB, the reflectivity (R value) of EMI shielding materials often exceeds 0.9, indicating a reflection rate exceeding 90% [106].
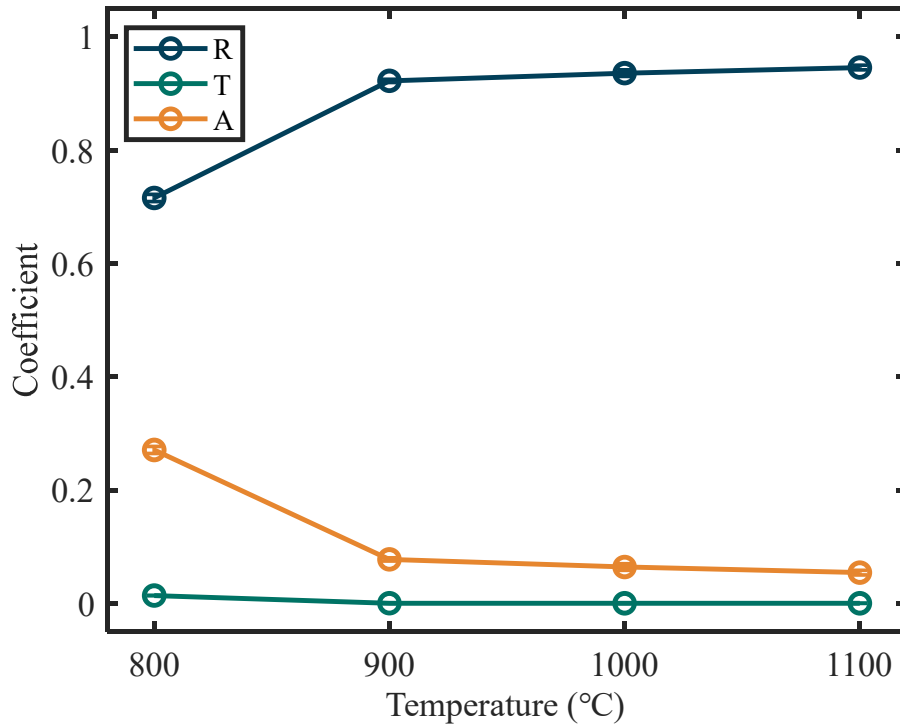
Figure 5.24 Power coefficients at 1.5 GHz of the carbon felts

When designing EMI shielding materials, light weight and thickness should also be considered. Therefore, we adopted the concept of a specific SE value (divide the SE_T by the density and thickness of the material) to compare the shielding performance of materials in a more comprehensive way [107]. Figure 5.25compares the specific SE values of this work with those reported in other literatures. Due to the low density of the carbon fibers, the high porosity of the carbon felts and the remarkable SE_T, the specific SE values of the carbon felts sample AC_1000 and AC_1100 in this work outstandingly outperform the other reported materials, including carbon nanotube [108][109], graphene [110][111][112], carbon black [109], carbon foam [113], carbon nanofiber mat [78], metal foam [114], and MXene [107].
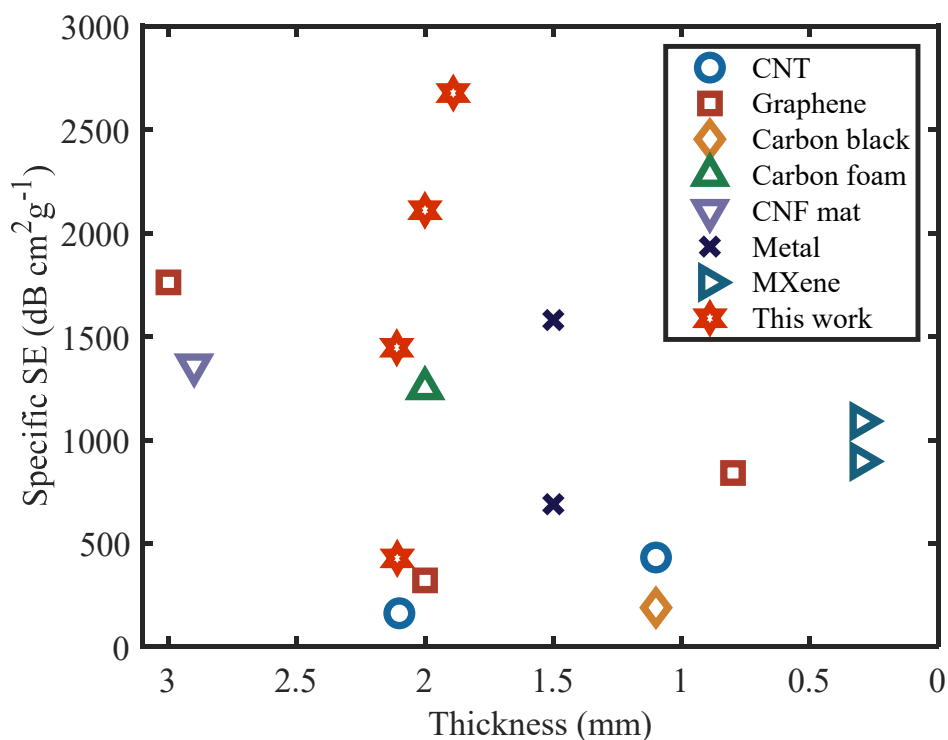
Figure 5.25 Comparison of the specific SE as a function of the thickness

In summary, the prepared carbon felt exhibits excellent EMI shielding performance and, due to its flexibility and lightweight nature, has great potential for a wide range of applications.

5.3.3 Electrical resistive heating performance

The varying response of different samples to different applied voltages is shown in Figure 5.26. The temperature rose as the voltage increased, in accordance with Joule's Law. Among them, the sample AC_1100 reached a high temperature of nearly 200 °C at a 3 V and 0.9 A, indicating that this sample exhibited a responsive and broad range of temperatures for heating under voltage. Under the same applied voltage, the heat generation temperature increased with the elevation of carbonization temperature. This phenomenon can be attributed to the higher electrical conductivity of the sample, as previously described. The graphite layers inside the carbon felt had an irregular arrangement, and the higher graphitization promoted the formation of a dense conductive network in the structure. When a voltage was applied, the graphite layer heated up due to Joule heating. At this point, the graphite layer acquired vibrational energy and diffused the thermal energy in a common vibrational mode throughout

54

the system, raising the temperature of the sample [9]. The heat was then transferred to the surroundings by conduction or radiation, resulting in an increase in the surrounding temperature.
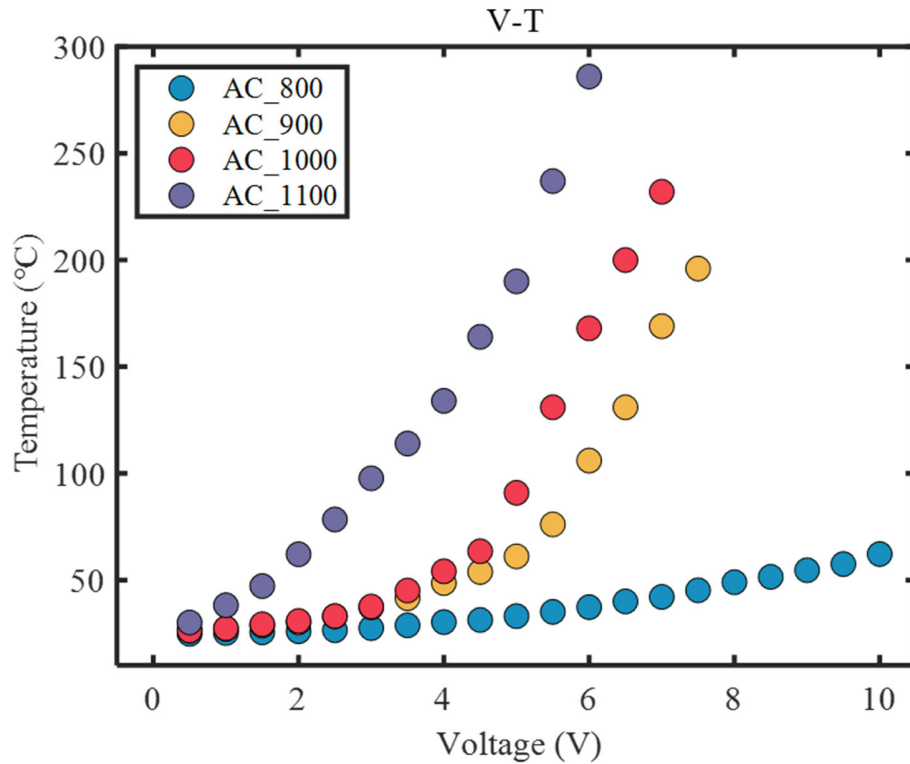
Figure 5.26 Changes of heating temperature of carbon felts as functions of the applied voltage

Additionally, the relationship between power and temperature was analyzed, as shown in Figure 5.27. From the power-temperature curves of different samples, it can be observed that as the carbonization temperature increased, the slope became steeper. In other words, at the same power level, samples with higher carbonization temperatures can achieve higher resistive heating temperatures. This suggests that the electrical energy efficiency of the samples can be adjusted through parameters in the preparation process. Heating efficiency is a key parameter for evaluating the performance of electric heaters and is defined as the ratio of temperature rise per unit area to input power. The heating efficiencies of samples AC_900, AC_1000, AC_1100 in this work were calculated to be 204.4, 195.2, and 448.6 $°C\ W^{-1}\ cm^2$,

respectively. Such high heating efficiencies have surpassed many others reported using higher cost conductive materials such as nanosilver [115], carbon nanotubes [116], graphene [117], and MXene [118].
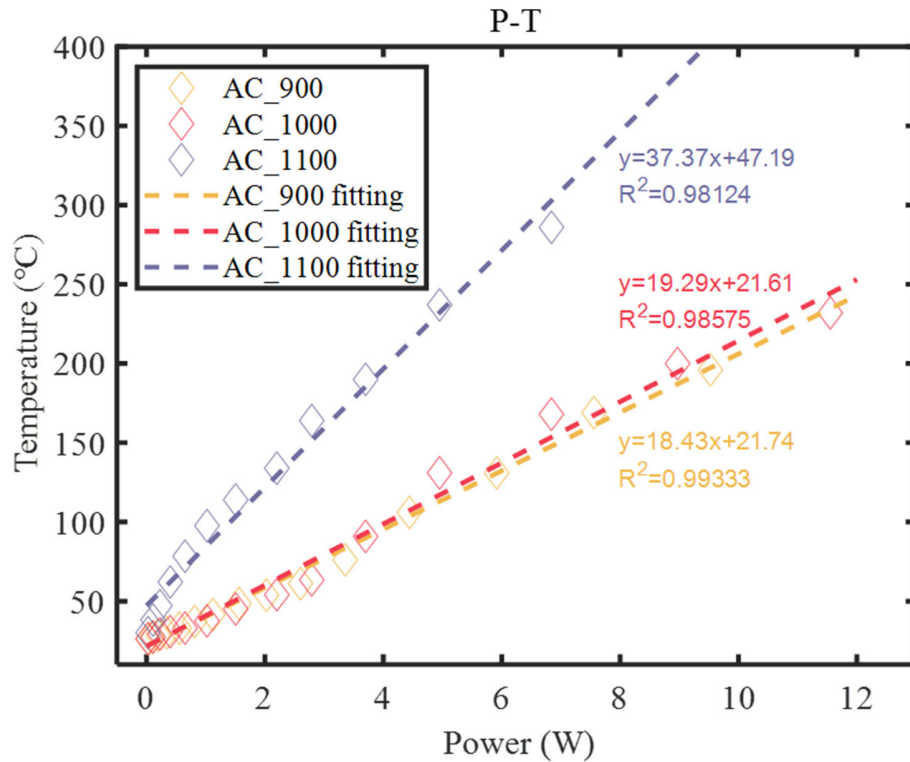
Figure 5.27 Changes of heating temperature of carbon felts as functions of electric power

Later, the heating and cooling behavior of the samples was investigated by applying a constant voltage (Figure 5.28). Considering that voltages in the range of 3-5V are more readily available in everyday life (from batteries, USB chargers, etc.), this study conducted heating experiments on the samples using 3V and 5V voltages. Under these voltage conditions, the AC_800 sample exhibited suboptimal heating performance, with a maximum temperature of only 35 °C reached. In contrast, the other two samples showed a significant increase in heating rate and reached much higher maximum temperatures. However, due to the thickness of the samples, it takes a considerable amount of time for the temperature to return to the initial temperature after the power was disconnected. These properties make the samples suitable for applications with different temperature requirements, such as lower

temperature for body temperature management, and higher temperature for sterilization and anti-icing.
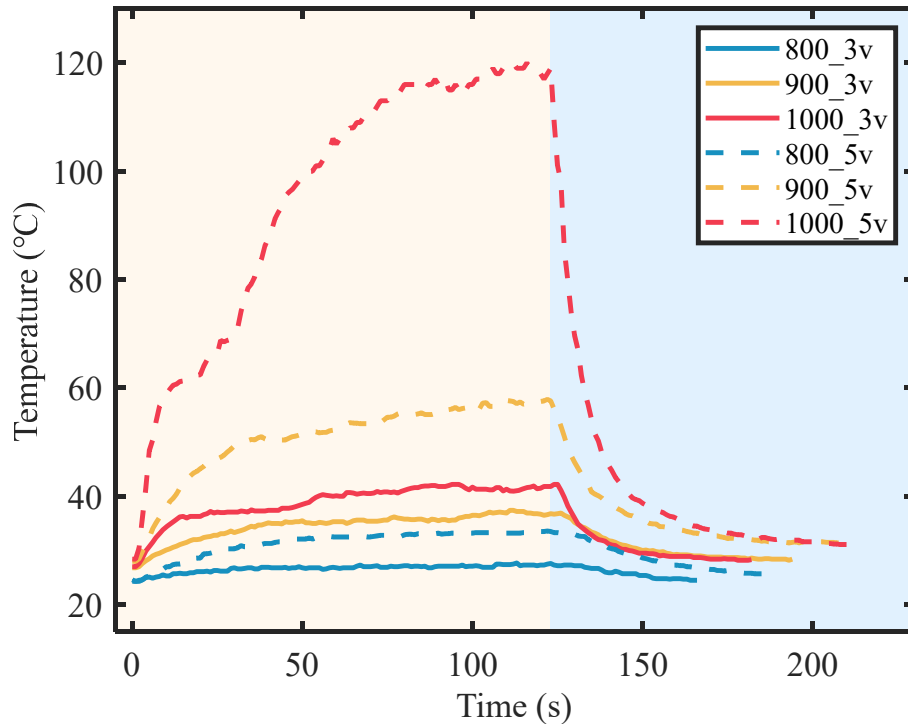
Figure 5.28 The time-temperature curve under a voltage of 3V and 5V

In practical use, the repeatability of heating performance is an important indicator, the cyclic heating performance is shown in Figure 5.29. The temperature-time curves of the sample varied slightly over the ten heating cycles, indicating a good repeatability of the heating performance. Furthermore, we studied the heating behavior of samples in different deformation states. As shown in the Figure 5.30, the samples exhibit stable heating performance in flat, bent, twisted, and even knotted states. This further demonstrated the excellent flexibility of the carbon felt samples, enabling them to meet various deformation requirements.
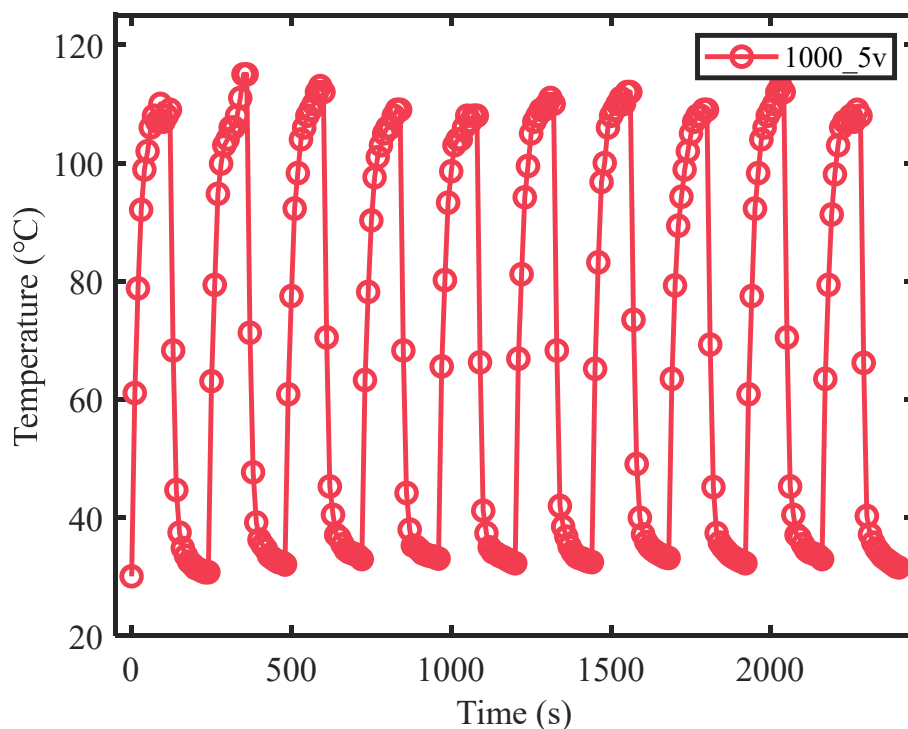
Figure 5.29 Heating cycles of sample AC_1000 at 5V
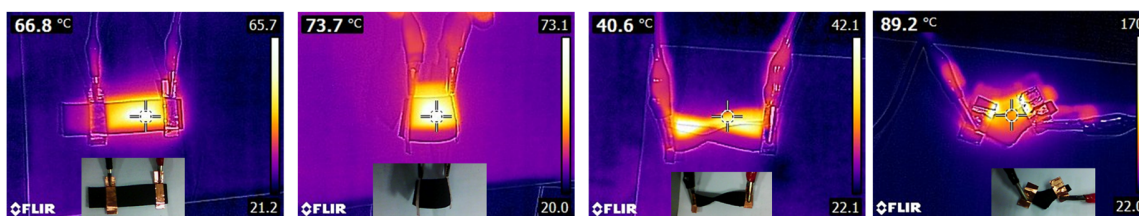
Figure 5.30 Heating performance of the carbon felt in flat, bent, twisted, and knotted states

In summary, the carbon felt studied in this work exhibits excellent electrical heating performance and can be customized to serve as a flexible heater material to meet various requirements by adjusting the preparation parameters.

5.3.4 Structural and chemical stability

We examined the change in resistance and resistive heating performance of the samples throughout in-situ testing during dynamic bending processes to assess their structural stability. Figure 5.31 illustrates the variation in sample resistance with bending cycles. The

resistances of AC_900, 1000, and 1100 samples remained stable within 4000 bending cycles, showing minimal decline. This demonstrated their remarkable structural stability under repeated bending. This can be attributed to the reduced brittleness of the internal fibers and the overall good flexibility of the carbon felt, where the bending deformation applied was not sufficient to cause fiber breakage. However, the AC_800 sample exhibited an initial increase in resistance during the first few bending cycles, followed by stabilization. This is consistent with the lower carbonization temperature leading to higher stiffness mentioned in the mechanical properties section above.
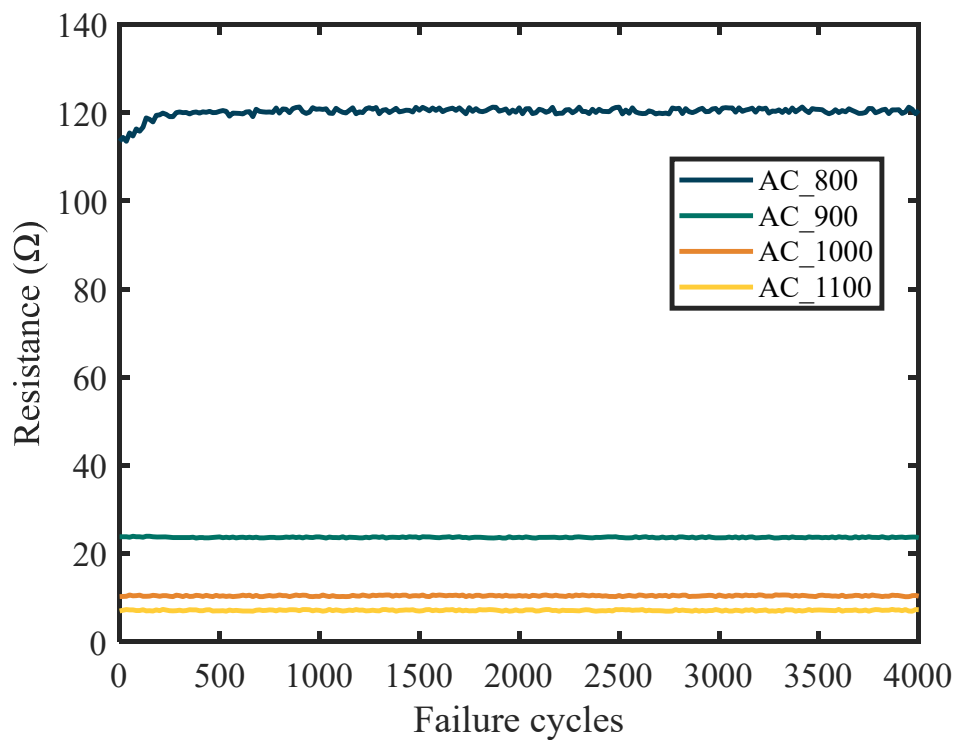
Figure 5.31 The variation of sample resistance with the number of bending cycles

Using the same equipment, resistive heating behaviors of the carbon felt during the bending cycle was also recorded and shown in Figure 5.32. The two selected samples both exhibited stable temperatures within 1000 bending cycles at different applied voltages. This demonstrates that even under heating conditions, the sample maintained the same stability of

its conductive network as at room temperature. This examination provides support for the potential application of carbon felts to deformable heaters in motion.
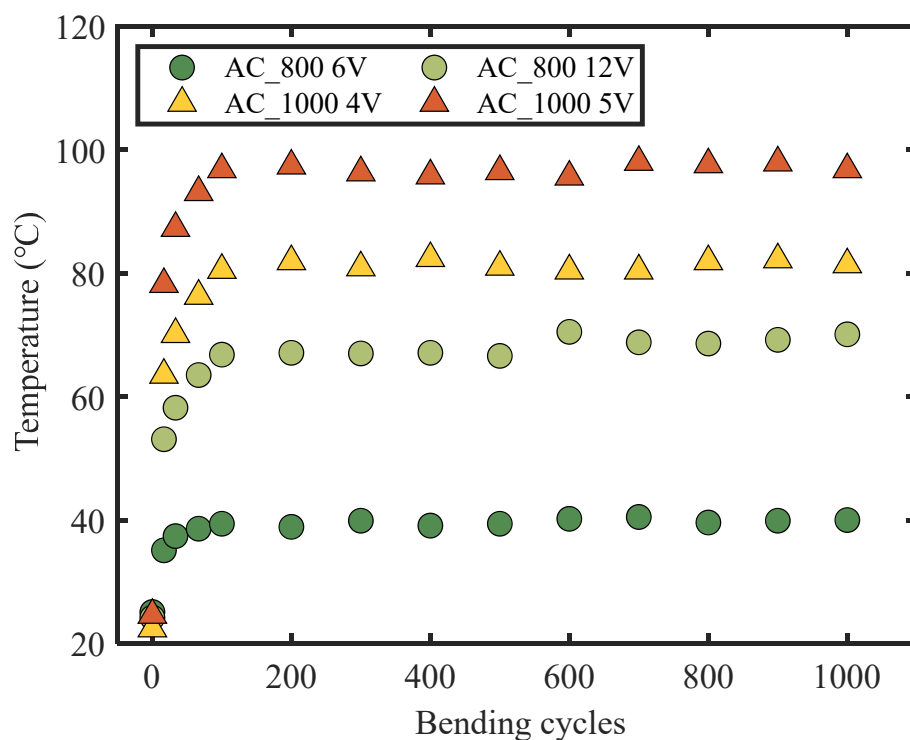
Figure 5.32 The variation of heating performance with the number of bending cycles

Then, the chemical stability of the carbon felts was evaluated by the change in electrical conductivity after immersion in acid and alkaline solutions. As can be seen from Figure 5.33, the conductivity of the carbon felts remained almost invariable after immersion for up to 30 h in solutions with pH values of 2 and 12, respectively. The lack of susceptibility to chemical degradation in carbon fiber materials is due to the presence of strong and stable carbon-carbon bonds and the ordered arrangement of fibrous carbon crystals.
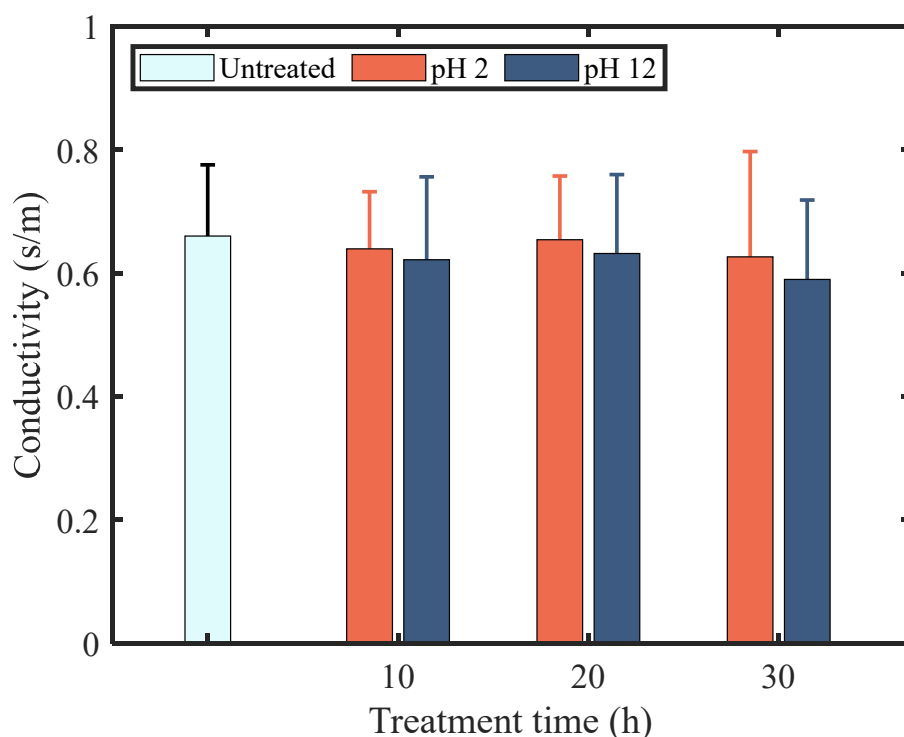
Figure 5.33 Changes in electrical conductivity after acid and alkali treatment

The above results demonstrate that the flexible carbon felt possesses good chemical and structural stability, maintaining the stability of its internal conductive pathways even under heating conditions and through multiple bending cycles. It has promising applications in fields such as wearable heaters and flexible EMI shielding materials.

5.4 Special application of the prepared carbon felt

As a flexible 3D conductive network, the manufactured carbon felt can be utilized not only for traditional conductor applications such as EMI shielding and electric heating but also as a respirator filter layer, taking advantage of the filtration properties of its raw materials. This part will explore the performance of carbon felt in this context, focusing on its suitability for use as a respirator filter layer.

5.4.1 Air permeability and breathability

As a potential respiratory filter material, the permeability and breathability of carbon felt need to be studied. Figure 5.34 shows the air permeability of the carbon felt at different

pressures. It is clear that the permeability correlated positively with pressure and carbonization temperature. The previous results of fiber fineness distribution can well explain the phenomenon that the permeability increased with the carbonization temperature. The decrease in fiber fineness has created more space within the fiber assembly, which facilitated the air flow and thereby improved air permeability. Additionally, linear regression was performed on permeability and pressure data. The results indicate that for all samples, the R^2 values of the linear regression fits were greater than 0.99. The R^2 value of 0.99 in our linear regression analysis signifies a strong linear correlation between permeability and pressure across all samples. Furthermore, the elevated R^2 value underscores the predictive capacity of the model, indicating its effectiveness in forecasting future data points.
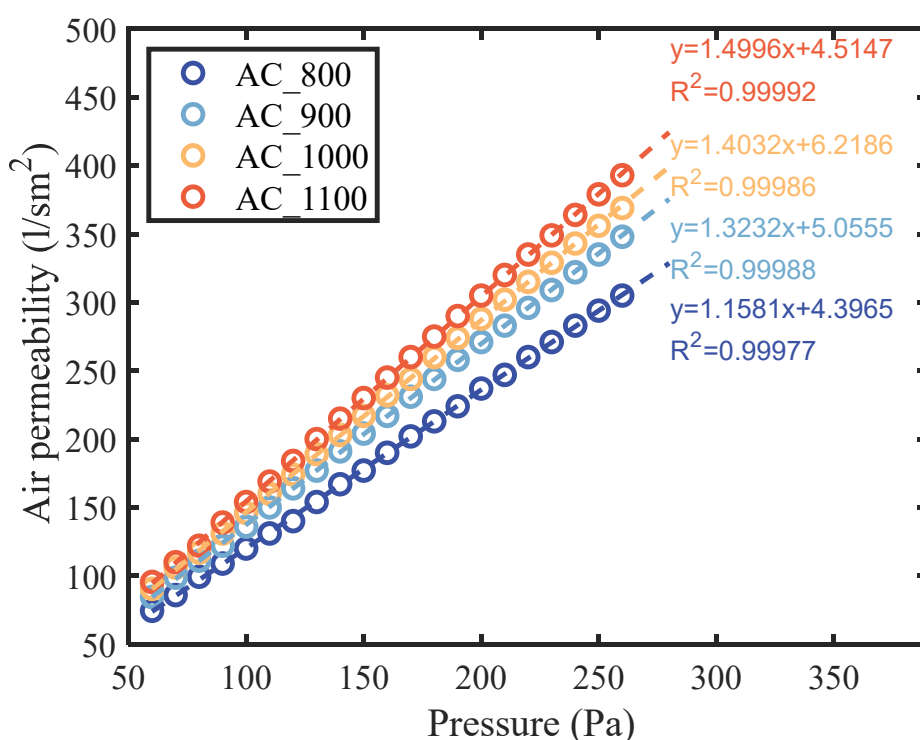
Figure 5.34 Air permeability of the carbon felts

Based on the good linear correlation between permeability and pressure, breathability was calculated through the permeability and precise respiratory filter area. The area of respiratory filter in this work is $35cm^2$. First, with the determination of the filter area, the volume of air per minute that can pass through the filter media at different pressures can be obtained.

Subsequently, a linear relationship between air permeability and pressure can be established. By using this linear relationship, we can assume the pressure required to achieve different air flows. The resulting breathability properties are listed in Table 5.2. Here, we assume that 100 Pa is critical value for breathing, which means that it can breathe smoothly when the value is below 100 Pa. From the data in the table, it can be noted that the samples AC_800 and 900 can satisfy the peace and walk human activity. While samples AC_1000 and 1100 can further ensure unhindered breathing during accelerated movement. In settings such as hospitals and virus laboratories, where respiratory filters are worn, the primary physiological activities of the wearer involve sitting and walking. Hence, the carbon felts prepared in this study can all ensure respiratory performance that accommodates essential human activities.

Table 5.2 Breathability (Pa) of the carbon felts

Air volume during various human activities	AC_800	AC_900	AC_1000	AC_1100
Peace 8 – 10 l/min	32-40	28-35	27-33	25-31
Walk 15 – 20 l/min	60-81	53-70	50-66	47-62
Accelerated movement 20 – 30 l/min	81-121	70-106	66-99	62-94
Medium work 30 – 40 l/min	121-161	106-141	99-133	94-125
Hard work 40 – 50 l/min	161-201	141-176	133-166	125-156
Extreme stress 50 – 120 l/min	201-483	176-423	166-398	156-375

5.4.2 Water vapor permeability

For respiratory filtration materials, it is imperative that they possess air permeability and undergo meticulous examination of their water vapor permeability performance to ensure prevention of water vapor condensation on a singular side of the material. Figure 5.35 illustrates the water vapor resistance (R_{et}) of samples prepared at various temperatures. As mentioned in the materials section, the precursor felt used in this study is coated with a layer of PTFE membrane on one side. Herein, the term "A side" denotes the side without the PTFE membrane, while "B side" signifies the side with the PTFE membrane. Evidently, the R_{et} values on A side decreased with the increasement of the carbonization temperature, attributable to the attainment of finer fibers and an augmented porosity. Interestingly, the carbonization temperature did not exert a notable impact on the water vapor resistance of the

B side. Research has indicated that during the carbonization of precursor mixtures containing PTFE and other polymers, PTFE evaporates at its decomposition temperature, thereby giving rise to the formation of microporous or mesoporous structures [119]. In this study, the carbonization temperatures employed for different samples were all above the decomposition temperature of PTFE. This can account for the lack of significant influence of carbonization temperature on the R_{et} of the side with the PTFE membrane. Furthermore, the introduction of PTFE resulted in a refinement of pore structures and optimization of the pathways for water vapor transmission through the fabric. As a result, the vapor resistances on the "B side" of the samples were significantly lower compared to the "A side". The R_{et} values of all samples on "B side" were consistently below 6, indicating a very good water vapor permeability (R_{et} range 0–6: very good or extremely breathable, 6–13: good or very breathable, 13–20: satisfactory or breathable, 20–30 unsatisfactory or slightly breathable, 30 + unsatisfactory or not breathable) [120][121]. The R_{et} values on the "A side" of the samples, all falling within the range of 6 to 13, signified good water vapor permeability and breathability. Therefore, in terms of the breathable and water vapor permeability, the obtained samples meet the requisites for utilization in respiratory filtration systems.
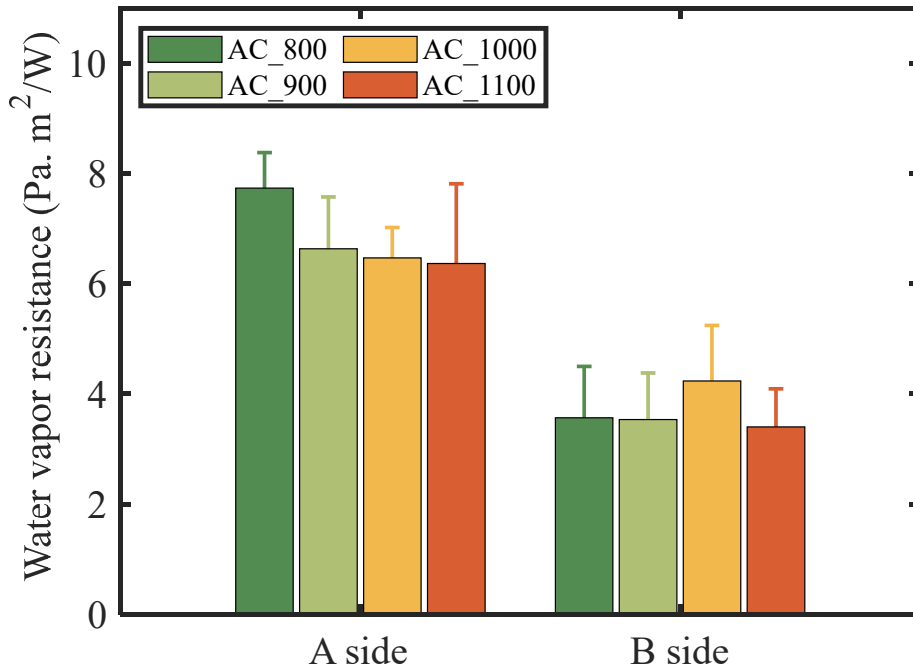
Figure 5.35 Water vapor resistance of the carbon felts

5.4.3 Filtration efficiency

After studying the permeability, the gas filtration performance was examined to assess their potential suitability for respiratory filter applications. The filtration efficiency of carbon felt samples for particles of different sizes is shown in Figure 5.36. It can be observed that for particles with a diameter less than 1 μm, the filtration efficiency of all samples was relatively low, below 50%. With the increase in particle size, there was a noticeable improvement in the filtration efficiency of all the samples. At the same time, the filtration efficiency was found to be positively influenced by the carbonization temperature. The AC_1100 sample, in particular, achieves a filtration efficiency of 93.8% for particles with a size of 1.8 μm. This is because the increase in carbonization temperature led to a reduction in fiber diameter and the formation of wrinkles on the fiber surface. These two factors synergistically increased the fiber surface area and the porosity of the carbon felt.
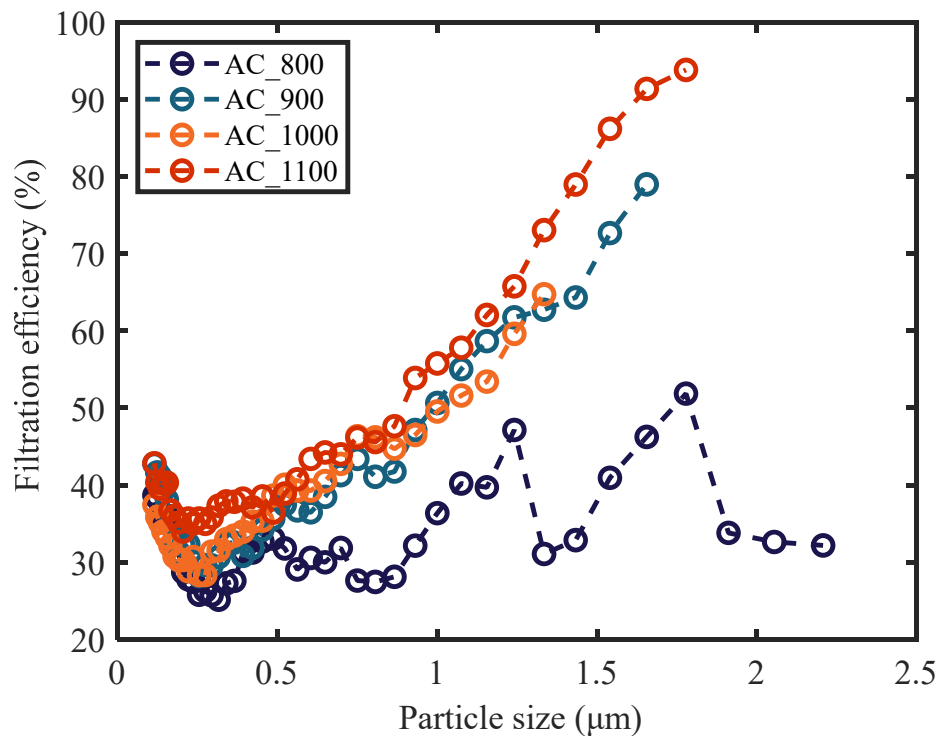
Figure 5.36 Filtration efficiency of the carbon felts

The primary filtration mechanisms of fibrous materials for particles include Brownian diffusion, interception, and inertial impaction[122]. The diffusion mechanism refers to the irregular motion of particles due to Brownian forces when the particle size is small (<0.1 μm), ultimately leading to particle collection on the surface of fibers. The interception mechanism is characterized by the trajectory of particles closely aligning with the fluid streamlines. Once the gap between the particle center and the fiber surface is smaller than the particle radius, the particle is captured by the fiber. Inertial impaction occurs when large-sized particles (>1 μm) cannot follow the original fluid streamlines due to inertia and directly collide with the fiber surface [123]. The primary filtration target of this respiratory filter is viral particles. While the size of individual viruses is extremely small (size around hundred nm), the actual transmission of infection often occurs through the emission of virus-containing aerosols during activities such as speaking, coughing, and sneezing. For example, SARS-CoV-2 virus RNA was primarily detected in aerosols within the >1 μm diameter range, with the majority of virus RNA detected in aerosols >4 μm in hospitals experiencing large-

scale COVID-19 outbreaks[124]. Therefore, here, inertial impaction is the predominant filtration mechanism. In this work, the increase in fiber surface roughness and specific surface area due to carbonization provided more sites for particle capture, thereby enhancing particle collection efficiency[125], as illustrated in the Figure 4.37. In summary, the filtration carbon felt prepared in this study can be tailored to meet the filtration requirements for particles of different sizes by adjusting the preparation parameters.
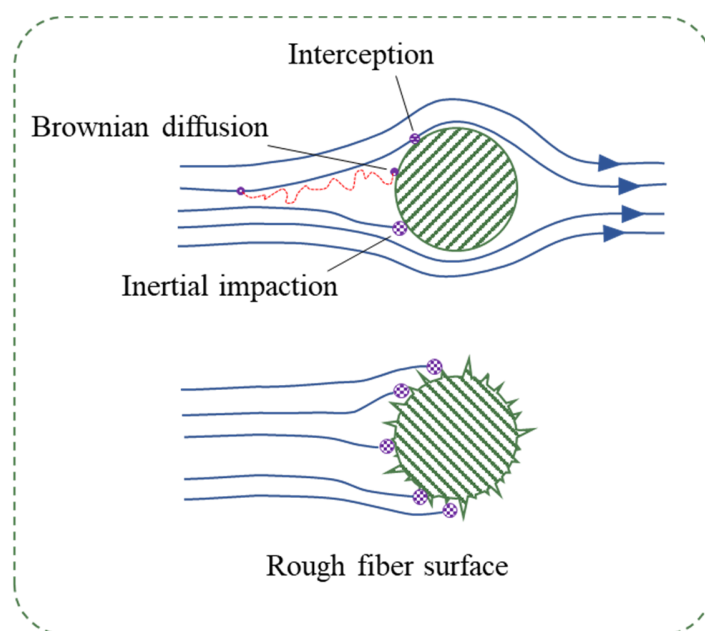
Figure 5.37 Filtration mechanisms of the carbon felt

5.4.4 Resistive heating for disinfection

After filtration, viruses may remain viable within the filter layer for a period of time. If left unaddressed during this period, they continue to pose a potential health hazard to the users of respiratory filters. Hence, it is imperative to promptly disinfect the respiratory filter layer. Among the disinfection methods, high-temperature treatment stands out as an effective and reliable approach. Here, carbon felt not only serves as a filtration layer but also functions as an electric heater due to its excellent electrical conductivity. In prior section the resistance heating performance of carbon felts have been studied. When the carbon felt serves as a filtration layer, it needs to be integrated into respirators. Therefore, this study first investigated the influence of different electrode configurations on the thermal distribution of

carbon felts embedded within respirator. Upon determining the optimal electrode configuration, the heating behavior under electrical current was further examined.

Typically, during resistive heating processes, electrodes are positioned in parallel on either side of the sample to achieve uniform heat distribution. However, in this study, the respirator design was circular. Therefore, we experimented with various electrode configurations to ensure both feasibility within the respirator and uniform heat distribution across the sample. The three different electrode connection methods are illustrated in Figure 5.38. From the infrared image, it can be observed that when the electrodes were connected to the sample in a circumferential (I) or point (II) manner, significant localized heating occurred in the vicinity of the electrodes. When the electrodes were connected in an arc shape (III), the heat distribution in the carbon felt was relatively uniform. Therefore, symmetrically arc-shaped electrodes were designed and positioned within the respirator, and subsequent experiments were conducted using this configuration.
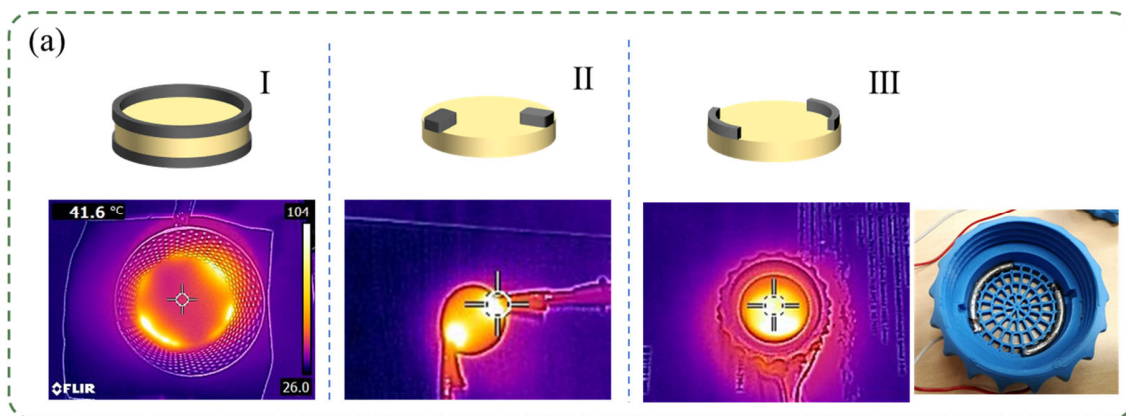
Figure 5.38 Different electrode configurations with carbon felt and their corresponding electrical heating distribution

The heating and cooling performance of the carbon felt under constant voltage was studied to ascertain its potential for achieving disinfection purposes in practical applications. Based on safety and practical feasibility considerations, a voltage of 3V was selected for testing. The time-temperature curve is depicted in Figure 5.39. After applying voltage, the temperature of the samples rapidly increased and stabilized upon reaching a steady-state

temperature. The steady-state temperatures of the four samples were approximately 45°C, 80°C, 105°C, and 188°C, respectively. Subsequently, the power supply was disconnected, and the temperature of the samples decreased. However, samples with higher steady-state temperatures did not reach room temperature within 120 seconds, as the thickness of the samples and being placed inside the respirator hindered heat dissipation. Some studies have provided recommendations for thermal inactivation of coronaviruses. Taking the example of the COVID-19, they suggested that virus inactivation can be achieved at temperatures of above 75 °C for 3 minutes, above 65 °C for 5 minutes, or above 60 °C for 20 minutes [126]. Hence, it can be stated that samples with carbonization temperatures exceeding 900°C in this study exhibited resistive heating characteristics capable of virus inactivation under low voltage of 3 V.
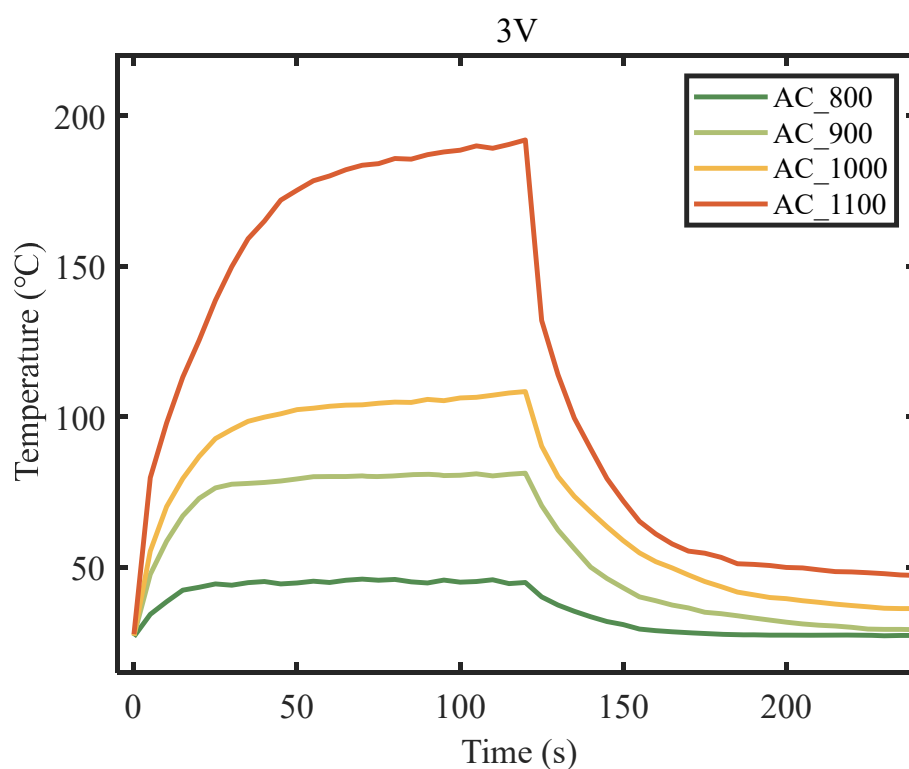
Figure 5.39 Time-temperature curve of carbon felts for disinfection

Lastly, the heating durability of the samples was assessed through heating cycle tests on sample AC_1000. During the heating and cooling cycles, both the heating equilibrium temperatures and the cooling temperatures of the sample exhibited minimal differences

69

(Figure 5.40). This observation underscored the robust repeatability and durability of the heating performance of carbon felt, rendering it suitable for repeated utilization as both a filtration layer and a high-temperature disinfection apparatus.
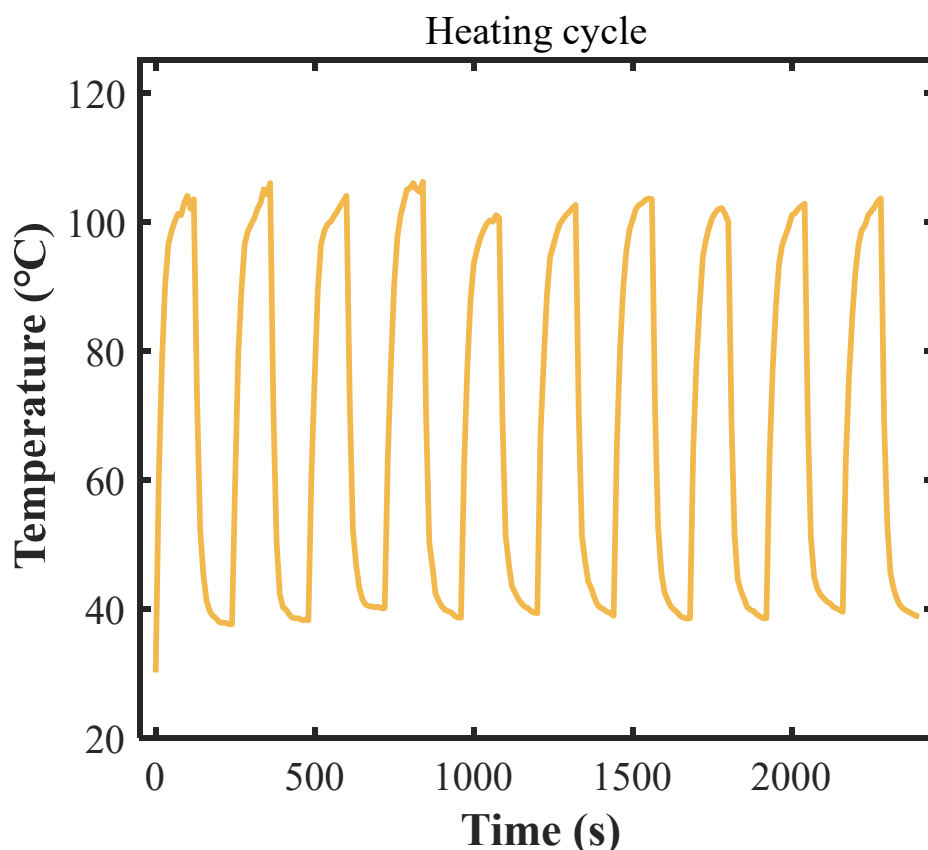
Figure 5.40 Heating and cooling cycles under a voltage of 3V

5.4.5 Antibacterial properties

In addition to its filtration and disinfection functionalities, as an integral component of a respirator, its antibacterial properties warrant scrutiny. Quantitative assessment of the bactericidal activity of the carbon felt was conducted, targeting Staphylococcus aureus and Escherichia coli. The results depicted in Figure 5.41 demonstrated that the duration of sample mixing significantly reduced the colony counts of both bacterial strains. The carbon felt exhibited higher bactericidal activity against Escherichia coli compared to Staphylococcus aureus (Figure 5.42). After 24 hours of treatment, Escherichia coli was completely eradicated, while the reduction rate in colony count for Staphylococcus aureus was 69%. For carbon

fiber filtration layers, researchers generally believe that the antibacterial activity of carbon fibers is limited, and become breeding grounds for pathogenic microorganisms after filtering air [127]. The retention of pathogens on the fiber surface may lead to secondary air pollution. Therefore, a large body of literature reported various methods for antimicrobial finishing of fiber surfaces [127][128][129][130]. However, the carbon fibers in this study exhibited antimicrobial activity even without antimicrobial treatment, which could be attributed to: 1) the morphology of the fibers, 2) the bacterial repulsion induced by their electrostatic charge, and 3) their surface chemical properties [131]. In fact, previous literature has also reported antimicrobial activity in carbon fiber samples, however, it may not have been significant enough to draw attention [132][133]. Despite this, further exploration is needed to elucidate the precise antimicrobial mechanisms of the carbon felt in this study.
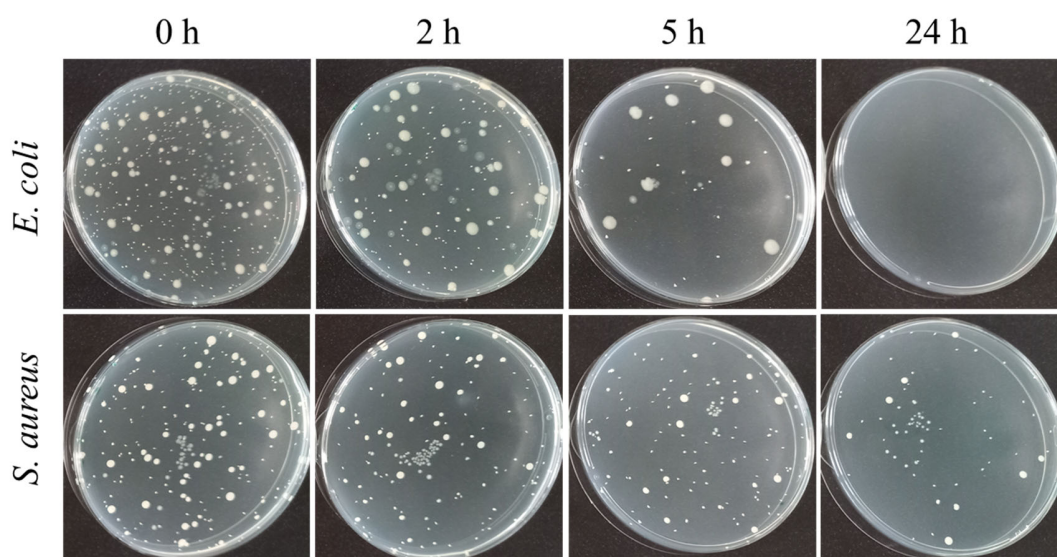
Figure 5.41 Digital images of bacterial strains grown on agar media.
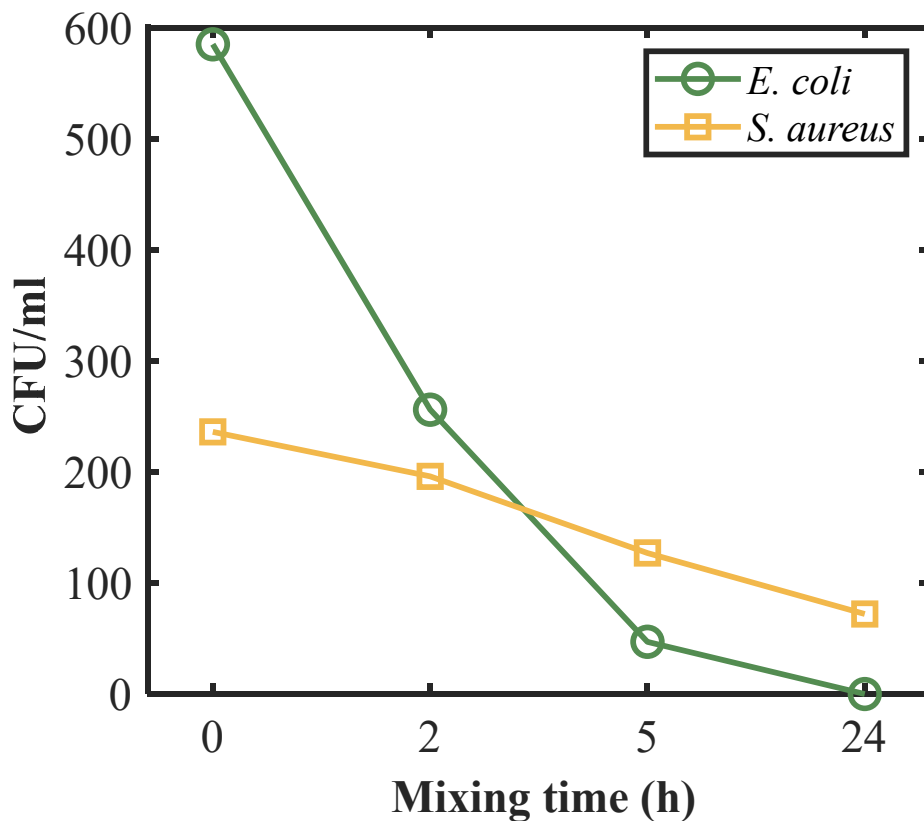
Figure 5.42 CFU changes with mixing time

In summary, the exceptional electrical conductivity of carbon felt enables its use not only as a respirator filter layer but also for high-temperature electric heating and sterilization. Its breathability and water vapor permeability ensure comfort when used as a respirator filter layer. Filtration efficiency and antibacterial testing results indicate that carbon felt achieves over 90% efficiency in filtering inhalable particles, while its antibacterial properties effectively inhibit microbial growth. The designed respirator filter shows great potential for application in various environments.

Chapter 6 Conclusion

The conclusion of this dissertation can be approached from the following perspectives.

6.1 Controlled pyrolysis of PTFE-coated acrylic-based felt

In this work, carbon felt was first prepared using waste acrylic-based felt as a precursor through controlled pyrolysis. The effects of different loading conditions on raw materials during the pyrolysis process on the shrinkage rate, mechanical properties, and electrical properties of the resulting carbon felt were studied. The results showed that applying edge load to the sample during the carbonization stage helps reduce the shrinkage rate of the final product, thereby allowing the carbon felt to gain flexibility and form a well-constructed conductive network. To investigate the impact of PTFE coating on the pyrolysis of acrylic-based felt, acrylic-based felt was coated with different concentrations of PTFE and subsequently subjected to pyrolysis. By examining the morphology, mechanical properties, and electrical properties of the PTFE-coated samples, we found that higher coating concentrations had a greater impact on the performance of the resulting carbon felt. Although high coating concentrations increased the modulus and electrical conductivity of the material, they also led to a loss of flexibility in the carbon felt, potentially severely limiting its application scope. Thus, it can be considered that a thin PTFE layer on one side of the raw material has a negligible impact on the shrinkage and mechanical properties of the carbon felt.

6.2 Flexible carbon felt characterization and properties

By characterizing the morphology and structure of carbon felts prepared at different carbonization temperatures under the edge load mode, it was found that as the carbonization temperature increased, the fibers became finer and wrinkled, and the porosity of the carbon felt increased. Additionally, high temperatures facilitated higher crystallinity within the fibers and the formation of an ordered graphite structure. The resulting carbon felt achieved a high EMI shielding effectiveness of 55 dB and a specific shielding effectiveness value of 2676.9 dBcm²g⁻¹ due to the formation of a dense, highly conductive network and high porosity. Additionally, the carbon felt demonstrated excellent heating efficiency and high heating rates in resistive heating tests. Finally, structural stability was studied through a self-

designed experiment. The results indicated that the carbon felt could maintain internal conductive pathway stability through multiple bending cycles even under heating conditions. The flexible carbon felt, with its lower manufacturing cost, good chemical and structural stability, and breathability, shows potential for a wide range of applications in wearable heaters, flexible EMI shielding, and other related fields.

6.3 Special application of the prepared carbon felt

This work also investigated the feasibility of converting acrylic-based filter felts into carbon felts for use in respiratory filtration layers. The excellent electrical conductivity of carbon felt allows it to be used not only as a respiratory filtration layer but also for high-temperature electrical disinfection. The design of the mask body and corresponding electrode configuration enabled controlled resistive heating performance, ensuring the reliability of high-temperature disinfection of the carbon felt. The comfort of the carbon felt as a respiratory filtration layer was determined through breathability and water vapor permeability tests. Filtration efficiency and antibacterial testing results indicated that the carbon felt achieved over 90% filtration efficiency for inhalable particles and effectively inhibited microbial growth due to its antibacterial properties. This method of reusing waste textiles maintains consistency in the use of textiles before and after reuse, simplifying the recycling process of waste acrylic fibers while reducing the manufacturing cost of respiratory filters. The designed respiratory filter has immense potential for applications in various environments, including hospitals and virology research institutes.

6.4 Future work

- Using molten salt-assisted carbonization method to increase the porosity and specific surface area of the resulting carbon felt.
- A ramping heating strategy may be employed during the carbonization stage to further improve the mechanical properties of the carbon felt.
- Refining the load during the carbonization process to apply tension as uniformly as possible across the fibers.

References

[1] Khayyam H., et al., PAN Precursor Fabrication, Applications and Thermal Stabilization Process in Carbon Fiber Production: Experimental and Mathematical Modelling. *Progress in Materials Science*, 2020, 107, 100575, https://doi.org/10.1016/j.pmatsci.2019.100575.

[2] Kopeć M., et al., Polyacrylonitrile-Derived Nanostructured Carbon Materials. *Progress in Polymer Science*, 2019, 92, 89–134, https://doi.org/10.1016/j.progpolymsci.2019.02.003.

[3] Brown K.R., et al., Carbon Fibers Derived from Commodity Polymers: A Review. *Carbon*, 2022, 196, 422–39, https://doi.org/10.1016/j.carbon.2022.05.005.

[4] Su Y., et al., Application of Modified Graphite Felt as Electrode Material: A Review. *Carbon Letters*, 2023, 33, no. 1, 1–16, https://doi.org/10.1007/s42823-022-00414-x.

[5] Huong Le T.X., et al., Carbon Felt Based-Electrodes for Energy and Environmental Applications: A Review. *Carbon*, 2017, 122, 564–91, https://doi.org/10.1016/j.carbon.2017.06.078.

[6] He Zhangxing, et al., Effects of Nitrogen Doping on the Electrochemical Performance of Graphite Felts for Vanadium Redox Flow Batteries. *International Journal of Energy Research*, 2015, 39, no. 5, 709–16, https://doi.org/10.1002/er.3291.

[7] Chen T., et al., Effects of Needle-Punched Felt Structure on the Mechanical Properties of Carbon/Carbon Composites. *Carbon*, 2003, 41, no. 5, 993–99, https://doi.org/10.1016/S0008-6223(02)00445-1.

[8] Jiang T., et al., Highly Thermally Conductive and Negative Permittivity Epoxy Composites by Constructing the Carbon Fiber/Carbon Networks. *Composites Communications*, 2023, 39, 101560, https://doi.org/10.1016/j.coco.2023.101560.

[9] Singh K., and V. Baheti, Electromagnetic Interference Shielding and Ohmic Heating Applications of Carbonized Nonwoven Fabrics Prepared from Blended Fibrous Wastes. *Diamond and Related Materials*, 2023, 133, 109708, https://doi.org/10.1016/j.diamond.2023.109708.

[10] Sundqvist B., Carbon under Pressure. *Physics Reports*, 2021, 909, 1–73, https://doi.org/10.1016/j.physrep.2020.12.007.

[11] Shi L., et al., Confined Linear Carbon Chains as a Route to Bulk Carbyne. *Nature Materials*, 2016, 15, no. 6, 634–39, https://doi.org/10.1038/nmat4617.

[12] Sengupta R., et al., A Review on the Mechanical and Electrical Properties of Graphite and Modified Graphite Reinforced Polymer Composites. *Progress in Polymer Science*, 2011, 36, no. 5, 638–70, https://doi.org/10.1016/j.progpolymsci.2010.11.003.

[13] Field J.E., The Mechanical and Strength Properties of Diamond. *Reports on Progress in Physics*, 2012, 75, no. 12, 126505, https://doi.org/10.1088/0034-

4885/75/12/126505.

[14] Chung D.D.L., Carbon Materials: Science and Applications. *MRS Bulletin*, 2019, 44, no. 8, https://doi.org/10.1557/mrs.2019.196.

[15] Newcomb B.A., Processing, Structure, and Properties of Carbon Fibers. *Composites Part A: Applied Science and Manufacturing*, 2016, 91, 262–82, https://doi.org/10.1016/j.compositesa.2016.10.018.

[16] Wu X., et al., Recent Progress in the Synthesis of Graphene/CNT Composites and the Energy-Related Applications. *Journal of Materials Science & Technology*, 2020, 55, 16–34, https://doi.org/10.1016/j.jmst.2019.05.063.

[17] Heidarinejad Z., et al., Methods for Preparation and Activation of Activated Carbon: A Review. *Environmental Chemistry Letters*, 2020, 18, no. 2, 393–415, https://doi.org/10.1007/s10311-019-00955-0.

[18] Shirvanimoghaddam K., et al., Death by Waste: Fashion and Textile Circular Economy Case. *Science of The Total Environment*, 2020, 718, 137317, https://doi.org/10.1016/j.scitotenv.2020.137317.

[19] Diddi S., et al., Exploring Young Adult Consumers' Sustainable Clothing Consumption Intention-Behavior Gap: A Behavioral Reasoning Theory Perspective. *Sustainable Production and Consumption*, 2019, 18, 200–09, https://doi.org/10.1016/j.spc.2019.02.009.

[20] Lopatina A., et al., Re-Use of Waste Cotton Textile as an Ultrafiltration Membrane. *Journal of Environmental Chemical Engineering*, 2021, 9, no. 4, 105705, https://doi.org/10.1016/j.jece.2021.105705.

[21] Rahman S.S., et al., Sustainable Applications of Textile Waste Fiber in the Construction and Geotechnical Industries: A Retrospect. *Cleaner Engineering and Technology*, 2022, 6, 100420, https://doi.org/10.1016/j.clet.2022.100420.

[22] Šajn N., Environmental Impact of the Textile and Clothing Industry. What Consumers Need to Know. *European Parliamentary Research Service*, 2019, no. January, https://www.europarl.europa.eu/portal/en.

[23] Kant R., Textile Dyeing Industry an Environmental Hazard. *Natural Science*, 2012, 04, no. 01, 22–26, https://doi.org/10.4236/ns.2012.41004.

[24] Leal Filho W., et al., A Review of the Socio-Economic Advantages of Textile Recycling. *Journal of Cleaner Production*, 2019, 218, 10–20, https://doi.org/10.1016/j.jclepro.2019.01.210.

[25] Titirici M.-M., et al., Sustainable Carbon Materials. *Chemical Society Reviews*, 2015, 44, no. 1, 250–90, https://doi.org/10.1039/C4CS00232F.

[26] Xia M., et al., Conversion of Cotton Textile Wastes into Porous Carbons by Chemical Activation with ZnCl2, H3PO4, and FeCl3. *Environmental Science and Pollution*

Research, 2020, 27, no. 20, 25186–96, https://doi.org/10.1007/s11356-020-08873-3.

[27] Tian D., et al., Multifaceted Roles of FeCl2 on Pore Formation of Polyester Fabric Wastes-Based Activated Carbon. *Colloids and Surfaces A: Physicochemical and Engineering Aspects*, 2020, 598, no. February, 124756, https://doi.org/10.1016/j.colsurfa.2020.124756.

[28] Nahil M.A., and P.T. Williams, Activated Carbons from Acrylic Textile Waste. *Journal of Analytical and Applied Pyrolysis*, 2010, 89, no. 1, 51–59, https://doi.org/10.1016/j.jaap.2010.05.005.

[29] --- Surface Chemistry and Porosity of Nitrogen-Containing Activated Carbons Produced from Acrylic Textile Waste. *Chemical Engineering Journal*, 2012, 184, 228–37, https://doi.org/10.1016/j.cej.2012.01.047.

[30] Chen W., et al., Pyrolysis Behavior and Pore-Forming Mechanism During Reuse of Textile Waste Flax by Activation. *Waste and Biomass Valorization*, 2020, 11, no. 8, 4259–68, https://doi.org/10.1007/s12649-019-00770-2.

[31] Gu S., et al., Fabrication of Porous Carbon Derived from Cotton/Polyester Waste Mixed with Oyster Shells: Pore-Forming Process and Application for Tetracycline Removal. *Chemosphere*, 2021, 270, 129483, https://doi.org/10.1016/j.chemosphere.2020.129483.

[32] Xu Z., et al., Highly Mesoporous Activated Carbon Synthesized by Pyrolysis of Waste Polyester Textiles and MgCl2: Physiochemical Characteristics and Pore-Forming Mechanism. *Journal of Cleaner Production*, 2018, 192, 453–61, https://doi.org/10.1016/j.jclepro.2018.05.007.

[33] Chen W., et al., Porosity and Surface Chemistry Development and Thermal Degradation of Textile Waste Jute during Recycling as Activated Carbon. *Journal of Material Cycles and Waste Management*, 2019, 21, no. 2, 315–25, https://doi.org/10.1007/s10163-018-0792-8.

[34] Xu Z., et al., Highly Porous Activated Carbon Synthesized by Pyrolysis of Polyester Fabric Wastes with Different Iron Salts: Pore Development and Adsorption Behavior. *Colloids and Surfaces A: Physicochemical and Engineering Aspects*, 2019, 565, 180–87, https://doi.org/10.1016/j.colsurfa.2019.01.007.

[35] Yuan Z., et al., Mesoporous Activated Carbons Synthesized by Pyrolysis of Waste Polyester Textiles Mixed with Mg-Containing Compounds and Their Cr(VI) Adsorption. *Colloids and Surfaces A: Physicochemical and Engineering Aspects*, 2018, 549, 86–93, https://doi.org/10.1016/j.colsurfa.2018.04.008.

[36] Xu Z., et al., Insights into the Pyrolysis Behavior and Adsorption Properties of Activated Carbon from Waste Cotton Textiles by FeCl3-Activation. *Colloids and Surfaces A: Physicochemical and Engineering Aspects*, 2019, 582, 123934, https://doi.org/10.1016/j.colsurfa.2019.123934.

[37] Chen W., et al., Pyrolysis Behavior and Pore-Forming Mechanism During Reuse of Textile Waste Flax by Activation. *Waste and Biomass Valorization*, 2020, 11, no. 8, 4259–68, https://doi.org/10.1007/s12649-019-00770-2.

[38] Xia M., et al., Conversion of Cotton Textile Wastes into Porous Carbons by Chemical Activation with ZnCl2, H3PO4, and FeCl3. *Environmental Science and Pollution Research*, 2020, 27, no. 20, 25186–96, https://doi.org/10.1007/s11356-020-08873-3.

[39] Silva T.L., et al., Mesoporous Activated Carbon Fibers Synthesized from Denim Fabric Waste: Efficient Adsorbents for Removal of Textile Dye from Aqueous Solutions. *Journal of Cleaner Production*, 2018, 171, 482–90, https://doi.org/10.1016/j.jclepro.2017.10.034.

[40] Sekiguchi A., et al., Nylon Recovery from Carpet Waste through Pyrolysis under the Presence of Zinc Oxide and the Roll-Milling Treatment. *Journal of Material Cycles and Waste Management*, 2014, 16, no. 2, 239–44, https://doi.org/10.1007/s10163-013-0179-9.

[41] Zhu X., et al., Hard Carbon Fibers Pyrolyzed from Wool as High-Performance Anode for Sodium-Ion Batteries. *JOM*, 2016, 68, no. 10, 2579–84, https://doi.org/10.1007/s11837-016-2064-1.

[42] Naeem S., et al., Removal of Methylene Blue from Aqueous Media Using Activated Carbon Web. *The Journal of The Textile Institute*, 2017, 108, no. 5, 803–11, https://doi.org/10.1080/00405000.2016.1191745.

[43] --- Development of Porous and Electrically Conductive Activated Carbon Web for Effective EMI Shielding Applications. *Carbon*, 2017, 111, 439–47, https://doi.org/10.1016/j.carbon.2016.10.026.

[44] Ali A., et al., Development of Silver Plated Electrically Conductive Elastomers Embedded with Carbon Black Particles Obtained from Kevlar Waste Source. *Polymer Testing*, 2022, 116, 107793, https://doi.org/10.1016/j.polymertesting.2022.107793.

[45] Karthik D., et al., Joule Heating of Carbon-Based Materials Obtained by Carbonization of Para-Aramid Fabrics. *C*, 2023, 9, no. 1, 23, https://doi.org/10.3390/c9010023.

[46] Singh K., and V. Baheti, Electromagnetic Interference Shielding and Ohmic Heating of Layered Structures of Activated Carbon Fabric and Metalized Fabric. *Synthetic Metals*, 2023, 298, 117439, https://doi.org/10.1016/j.synthmet.2023.117439.

[47] Li Y., and M. Zhang, Mechanical Properties of Activated Carbon Fibers. *Activated Carbon Fiber and Textiles*, 2017, Elsevier, 167–80, https://doi.org/10.1016/B978-0-08-100660-3.00006-7.

[48] Rahaman M.S.A., et al., A Review of Heat Treatment on Polyacrylonitrile Fiber. *Polymer Degradation and Stability*, 2007, 92, no. 8, 1421–32, https://doi.org/10.1016/j.polymdegradstab.2007.03.023.

[49] Houtz R.C., "Orlon" Acrylic Fiber: Chemistry and Properties. *Textile Research*

Journal, 1950, 20, no. 11, 786–801, https://doi.org/10.1177/004051755002001107.

[50] Grassie N., and R. McGuchan, Pyrolysis of Polyacrylonitrile and Related Polymers—III. Thermal Analysis of Preheated Polymers. *European Polymer Journal*, 1971, 7, no. 10, 1357–71, https://doi.org/10.1016/0014-3057(71)90032-2.

[51] Fitzer E., and D.J. Müller, The Influence of Oxygen on the Chemical Reactions during Stabilization of Pan as Carbon Fiber Precursor. *Carbon*, 1975, 13, no. 1, 63–69, https://doi.org/10.1016/0008-6223(75)90259-6.

[52] Ko T., The Influence of Pyrolysis on Physical Properties and Microstructure of Modified PAN Fibers during Carbonization. *Journal of Applied Polymer Science*, 1991, 43, no. 3, 589–600, https://doi.org/10.1002/app.1991.070430321.

[53] Trinquecoste M., et al., High Temperature Thermal and Mechanical Properties of High Tensile Carbon Single Filaments. *Carbon*, 1996, 34, no. 7, 923–29, https://doi.org/10.1016/0008-6223(96)00052-8.

[54] Salim N. V., et al., The Role of Tension and Temperature for Efficient Carbonization of Polyacrylonitrile Fibers: Toward Low Cost Carbon Fibers. *Industrial and Engineering Chemistry Research*, 2018, 57, no. 12, 4268–76, https://doi.org/10.1021/acs.iecr.7b05336.

[55] Xu J., et al., Effect of Tension during Stabilization on Carbon Fiber Multifunctionality for Structural Battery Composites. *Carbon*, 2023, 209, 117982, https://doi.org/10.1016/j.carbon.2023.03.057.

[56] Liu Y., et al., Gel-Spun Carbon Nanotubes/Polyacrylonitrile Composite Fibers. Part III: Effect of Stabilization Conditions on Carbon Fiber Properties. *Carbon*, 2011, 49, no. 13, 4487–96, https://doi.org/10.1016/j.carbon.2011.06.045.

[57] Wu M., et al., Optimization of Stabilization Conditions for Electrospun Polyacrylonitrile Nanofibers. *Polymer Degradation and Stability*, 2012, 97, no. 8, 1511–19, https://doi.org/10.1016/j.polymdegradstab.2012.05.001.

[58] Santos de Oliveira Junior M., et al., A Statistical Approach to Evaluate the Oxidative Process of Electrospun Polyacrylonitrile Ultrathin Fibers. *Journal of Applied Polymer Science*, 2017, 134, no. 43, 45458, https://doi.org/10.1002/app.45458.

[59] Sabantina L., et al., Stabilization of Electrospun PAN/Gelatin Nanofiber Mats for Carbonization. *Journal of Nanomaterials*, 2018, 2018, 1–12, https://doi.org/10.1155/2018/6131085.

[60] Nan W., et al., Mechanically Flexible Electrospun Carbon Nanofiber Mats Derived from Biochar and Polyacrylonitrile. *Materials Letters*, 2017, 205, 206–10, https://doi.org/10.1016/j.matlet.2017.06.092.

[61] Storck J.L., et al., Metallic Supports Accelerate Carbonization and Improve Morphological Stability of Polyacrylonitrile Nanofibers during Heat Treatment. *Materials*, 2021, 14, no. 16, 4686, https://doi.org/10.3390/ma14164686.

[62] --- Comparative Study of Metal Substrates for Improved Carbonization of Electrospun PAN Nanofibers. *Polymers*, 2022, 14, no. 4, 721, https://doi.org/10.3390/polym14040721.

[63] Wang X.-X., et al., Ti3C2 MXenes Meta-Film Switching Ultra-Broadband and High-Efficiency Green EMI Shielding. *Carbon*, 2023, 213, 118267, https://doi.org/10.1016/j.carbon.2023.118267.

[64] Verma R., et al., A Review on MXene and Its' Composites for Electromagnetic Interference (EMI) Shielding Applications. *Carbon*, 2023, 208, 170–90, https://doi.org/10.1016/j.carbon.2023.03.050.

[65] Fan B., et al., Salt-Templated Graphene Nanosheet Foams Filled in Silicon Rubber toward Prominent EMI Shielding Effectiveness and High Thermal Conductivity. *Carbon*, 2023, 207, 317–27, https://doi.org/10.1016/j.carbon.2023.03.022.

[66] Hu S., et al., The Novel Approach of EMI Shielding Simulation for Metal Coated Nonwoven Textiles with Optimized Textile Module. *Polymer Testing*, 2022, 114, 107706, https://doi.org/10.1016/j.polymertesting.2022.107706.

[67] --- Washable and Breathable Ultrathin Copper-Coated Nonwoven Polyethylene Terephthalate (PET) Fabric with Chlorinated Poly-Para-Xylylene (Parylene-C) Encapsulation for Electromagnetic Interference Shielding Application. *Textile Research Journal*, 2023, 93, no. 17–18, 3982–98, https://doi.org/10.1177/00405175231168418.

[68] Liu J., et al., Hydrophobic, Flexible, and Lightweight MXene Foams for High-Performance Electromagnetic-Interference Shielding. *Advanced Materials*, 2017, 29, no. 38, https://doi.org/10.1002/adma.201702367.

[69] Lu D., et al., Flexible, Lightweight Carbon Nanotube Sponges and Composites for High-Performance Electromagnetic Interference Shielding. *Carbon*, 2018, 133, 457–63, https://doi.org/10.1016/j.carbon.2018.03.061.

[70] Ju Z., et al., Flexible TiN/Co@Carbon Nanofiber Mats for High-Performance Electromagnetic Interference Shielding and Joule Heating Applications. *Carbon*, 2022, 196, 612–20, https://doi.org/10.1016/j.carbon.2022.05.034.

[71] Isari A.A., et al., Structural Design for EMI Shielding: From Underlying Mechanisms to Common Pitfalls. *Advanced Materials*, 2024, https://doi.org/10.1002/adma.202310683.

[72] Ali A., et al., Copper Electroless Plating of Cotton Fabrics after Surface Activation with Deposition of Silver and Copper Nanoparticles. *Journal of Physics and Chemistry of Solids*, 2020, 137, 109181, https://doi.org/10.1016/j.jpcs.2019.109181.

[73] Ghaffarkhah A., et al., High-Resolution Extrusion Printing of Ti3C2-Based Inks for Wearable Human Motion Monitoring and Electromagnetic Interference Shielding. *Carbon*, 2022, 191, 277–89, https://doi.org/10.1016/j.carbon.2022.02.003.

[74] Liu H., et al., Recent Progress in Morphological Engineering of Carbon Materials for Electromagnetic Interference Shielding. *Carbon*, 2021, 172, 569–96, https://doi.org/10.1016/j.carbon.2020.10.067.

[75] Lu H., et al., Flexible, Electrothermal-Driven Controllable Carbon Fiber/Poly(Ethylene-Co-Vinyl Acetate) Shape Memory Composites for Electromagnetic Shielding. *Composites Science and Technology*, 2021, 207, 108697, https://doi.org/10.1016/j.compscitech.2021.108697.

[76] Liang J., et al., Electromagnetic Shielding Property of Carbon Fiber Felt Made of Different Types of Short-Chopped Carbon Fibers. *Composites Part A: Applied Science and Manufacturing*, 2019, 121, 289–98, https://doi.org/10.1016/j.compositesa.2019.03.037.

[77] Hu Q., et al., Lightweight, Flexible, and Highly Conductive Recycled Carbon Fiber Felt for Electromagnetic Interference Shielding. *Journal of Alloys and Compounds*, 2023, 935, 168152, https://doi.org/10.1016/j.jallcom.2022.168152.

[78] Hong X., and D.D.L. Chung, Carbon Nanofiber Mats for Electromagnetic Interference Shielding. *Carbon*, 2017, 111, 529–37, https://doi.org/10.1016/j.carbon.2016.10.031.

[79] Guo Z., et al., Simultaneous Realization of Highly Efficient Electromagnetic Interference Shielding and Human Motion Detection in Carbon Fiber Felt Decorated with Silver Nanowires and Thermoplastic Polyurethane. *Journal of Materials Chemistry C*, 2021, 9, no. 21, 6894–903, https://doi.org/10.1039/D1TC01099A.

[80] Yin Z., et al., Cost-Effective Graphite Felt and Phosphorous Flame Retardant with Extremely High Electromagnetic Shielding. *Composites Part B: Engineering*, 2022, 236, 109819, https://doi.org/10.1016/j.compositesb.2022.109819.

[81] Tcharkhtchi A., et al., An Overview of Filtration Efficiency through the Masks: Mechanisms of the Aerosols Penetration. *Bioactive Materials*, 2021, 6, no. 1, 106–22, https://doi.org/10.1016/j.bioactmat.2020.08.002.

[82] Dunnett S., Filtration Mechanisms. *Aerosol Science*, 2013, Wiley, 89–117, https://doi.org/10.1002/9781118682555.ch5.

[83] Lorimier C., et al., Indoor Air Particulate Filtration onto Activated Carbon Fiber Media. *Journal of Environmental Engineering*, 2008, 134, no. 2, 126–37, https://doi.org/10.1061/(ASCE)0733-9372(2008)134:2(126).

[84] Hayashi T., et al., Characterization of Activated Carbon Fiber Filters for Pressure Drop, Submicrometer Particulate Collection, and Mercury Capture. *Journal of the Air & Waste Management Association*, 2000, 50, no. 6, 922–29, https://doi.org/10.1080/10473289.2000.10464136.

[85] Kim Y., et al., Wet-Laid Nonwoven of Activated Carbon Fiber for Gas Adsorption Layer in Face Masks. *Fibers and Polymers*, 2023, 24, no. 8, 2711–23, https://doi.org/10.1007/s12221-023-00230-8.

[86] Francelino I.G., et al., High Efficacy of Activated Carbon Fabric Filters and Masks Developed to Prevent the Inhalation of Microorganisms and Particles Associated with Respiratory Tract Infections. *Textile Research Journal*, 2023, 93, no. 3–4, 834–44, https://doi.org/10.1177/00405175221127313.

[87] Xiong S.-W., et al., Temperature-Adjustable F-Carbon Nanofiber/Carbon Fiber Nanocomposite Fibrous Masks with Excellent Comfortability and Anti-Pathogen Functionality. *Chemical Engineering Journal*, 2022, 432, 134160, https://doi.org/10.1016/j.cej.2021.134160.

[88] Wang Y., et al., Carbon Felt from Acrylic Dust Bags as Flexible EMI Shielding Layer and Resistive Heater. *Journal of Materials Research and Technology*, 2024, 28, 4417–27, https://doi.org/10.1016/j.jmrt.2024.01.077.

[89] Fridrichová L., A New Method of Measuring the Bending Rigidity of Fabrics and Its Application to the Determination of the Their Anisotropy. *Textile Research Journal*, 2013, 83, no. 9, 883–92, https://doi.org/10.1177/0040517512467133.

[90] Yang T., et al., Study on the Sound Absorption Behavior of Multi-Component Polyester Nonwovens: Experimental and Numerical Methods. *Textile Research Journal*, 2019, 89, no. 16, 3342–61, https://doi.org/10.1177/0040517518811940.

[91] Peng Q., et al., Preparation of Electrosprayed Composite Coated Microporous Filter for Particulate Matter Capture. *Nano Select*, 2022, 3, no. 3, 555–66, https://doi.org/10.1002/nano.202100186.

[92] Xiong X., et al., Transport Properties of Electro-Sprayed Polytetrafluoroethylene Fibrous Layer Filled with Aerogels/Phase Change Materials. *Nanomaterials*, 2020, 10, no. 10, 2042, https://doi.org/10.3390/nano10102042.

[93] Acem Z., et al., Surface Temperature of Carbon Composite Samples during Thermal Degradation. *International Journal of Thermal Sciences*, 2017, 112, 427–38, https://doi.org/10.1016/j.ijthermalsci.2016.11.007.

[94] Pei X., et al., Porous Network Carbon Nanotubes/Chitosan 3D Printed Composites Based on Ball Milling for Electromagnetic Shielding. *Composites Part A: Applied Science and Manufacturing*, 2021, 145, 106363, https://doi.org/10.1016/j.compositesa.2021.106363.

[95] Liang J., et al., Electromagnetic Shielding Property of Carbon Fiber Felt Made of Different Types of Short-Chopped Carbon Fibers. *Composites Part A: Applied Science and Manufacturing*, 2019, 121, no. March, 289–98, https://doi.org/10.1016/j.compositesa.2019.03.037.

[96] Zhang M., et al., Theoretical Prediction of Effective Stiffness of Nonwoven Fibrous Networks with Straight and Curved Nanofibers. *Composites Part A: Applied Science and Manufacturing*, 2021, 143, 106311, https://doi.org/10.1016/j.compositesa.2021.106311.

[97] Chen J., et al., The Catalytic Effect of Boric Acid on Polyacrylonitrile-Based Carbon Fibers and the Thermal Conductivity of Carbon/Carbon Composites Produced from Them. *Carbon*, 2010, 48, no. 8, 2341–46, https://doi.org/10.1016/j.carbon.2010.03.012.

[98] Naito K., et al., Enhancing the Thermal Conductivity of Polyacrylonitrile- and Pitch-Based Carbon Fibers by Grafting Carbon Nanotubes on Them. *Carbon*, 2010, 48, no. 6, 1849–57, https://doi.org/10.1016/j.carbon.2010.01.031.

[99] Singh A.K., et al., A Review of Porous Lightweight Composite Materials for Electromagnetic Interference Shielding. *Composites Part B: Engineering*, 2018, 149, 188–97, https://doi.org/10.1016/j.compositesb.2018.05.027.

[100] Zhang Y., et al., Rapid In Situ Polymerization of Polyacrylonitrile/Graphene Oxide Nanocomposites as Precursors for High-Strength Carbon Nanofibers. *ACS Applied Materials & Interfaces*, 2021, 13, no. 14, 16846–58, https://doi.org/10.1021/acsami.1c02643.

[101] Schuepfer D.B., et al., Assessing the Structural Properties of Graphitic and Non-Graphitic Carbons by Raman Spectroscopy. *Carbon*, 2020, 161, 359–72, https://doi.org/10.1016/j.carbon.2019.12.094.

[102] Meek N., and D. Penumadu, Nonlinear Elastic Response of Pan Based Carbon Fiber to Tensile Loading and Relations to Microstructure. *Carbon*, 2021, 178, 133–43, https://doi.org/10.1016/j.carbon.2021.03.012.

[103] Šafářová V., and J. Militký, Electromagnetic Shielding Properties of Woven Fabrics Made from High-Performance Fibers. *Textile Research Journal*, 2014, 84, no. 12, 1255–67, https://doi.org/10.1177/0040517514521118.

[104] Hwang U., et al., Quantitative Interpretation of Electromagnetic Interference Shielding Efficiency: Is It Really a Wave Absorber or a Reflector?. *ACS Omega*, 2022, 7, no. 5, 4135–39, https://doi.org/10.1021/acsomega.1c05657.

[105] Wu N., et al., Review on the Electromagnetic Interference Shielding Properties of Carbon Based Materials and Their Novel Composites: Recent Progress, Challenges and Prospects. *Carbon*, 2021, 176, 88–105, https://doi.org/10.1016/j.carbon.2021.01.124.

[106] Yang J., et al., Constructing 3D Expanded Graphite-Silver Segregated Network Structure for Ultra-Efficient EMI Shielding and Low Reflection. *Journal of Materials Research and Technology*, 2023, 23, 5115–26, https://doi.org/10.1016/j.jmrt.2023.02.105.

[107] Cheng H., et al., Ultrathin Flexible Poly(Vinylidene Fluoride)/MXene/Silver Nanowire Film with Outstanding Specific EMI Shielding and High Heat Dissipation. *Advanced Composites and Hybrid Materials*, 2021, 4, no. 3, 505–13, https://doi.org/10.1007/s42114-021-00224-1.

[108] Pande S., et al., Mechanical and Electrical Properties of Multiwall Carbon Nanotube/Polycarbonate Composites for Electrostatic Discharge and Electromagnetic Interference Shielding Applications. *RSC Advances*, 2014, 4, no. 27, 13839, https://doi.org/10.1039/c3ra47387b.

[109] Al-Saleh M.H., et al., EMI Shielding Effectiveness of Carbon Based Nanostructured Polymeric Materials: A Comparative Study. *Carbon*, 2013, 60, 146–56, https://doi.org/10.1016/j.carbon.2013.04.008.

[110] Agnihotri N., et al., Highly Efficient Electromagnetic Interference Shielding Using Graphite Nanoplatelet/Poly(3,4-Ethylenedioxythiophene)–Poly(Styrenesulfonate) Composites with Enhanced Thermal Conductivity. *RSC Advances*, 2015, 5, no. 54, 43765–71, https://doi.org/10.1039/C4RA15674A.

[111] Yan D.-X., et al., Efficient Electromagnetic Interference Shielding of Lightweight Graphene/Polystyrene Composite. *Journal of Materials Chemistry*, 2012, 22, no. 36, 18772, https://doi.org/10.1039/c2jm32692b.

[112] Song W.-L., et al., Flexible Graphene/Polymer Composite Films in Sandwich Structures for Effective Electromagnetic Interference Shielding. *Carbon*, 2014, 66, 67–76, https://doi.org/10.1016/j.carbon.2013.08.043.

[113] Moglie F., et al., Electromagnetic Shielding Performance of Carbon Foams. *Carbon*, 2012, 50, no. 5, 1972–80, https://doi.org/10.1016/j.carbon.2011.12.053.

[114] Ji K., et al., Fabrication and Electromagnetic Interference Shielding Performance of Open-Cell Foam of a Cu–Ni Alloy Integrated with CNTs. *Applied Surface Science*, 2014, 311, 351–56, https://doi.org/10.1016/j.apsusc.2014.05.067.

[115] Ji S., et al., Thermal Response of Transparent Silver Nanowire/PEDOT:PSS Film Heaters. *Small*, 2014, 10, no. 23, 4951–60, https://doi.org/10.1002/smll.201401690.

[116] Chu K., et al., Electrical and Thermal Properties of Carbon-Nanotube Composite for Flexible Electric Heating-Unit Applications. *IEEE Electron Device Letters*, 2013, 34, no. 5, 668–70, https://doi.org/10.1109/LED.2013.2249493.

[117] Sui D., et al., Flexible and Transparent Electrothermal Film Heaters Based on Graphene Materials. *Small*, 2011, 7, no. 22, 3186–92, https://doi.org/10.1002/smll.201101305.

[118] Wang Q., et al., Multifunctional and Water-Resistant MXene-Decorated Polyester Textiles with Outstanding Electromagnetic Interference Shielding and Joule Heating Performances. *Advanced Functional Materials*, 2019, 29, no. 7, https://doi.org/10.1002/adfm.201806819.

[119] Son I.-S., et al., Facile Fabrication of Mesoporous Carbon from Mixed Polymer Precursor of PVDF and PTFE for High-Power Supercapacitors. *Carbon*, 2020, 159, 283–91, https://doi.org/10.1016/j.carbon.2019.12.049.

[120] Nayak R., et al., Evaluation of Thermal, Moisture Management and Sensorial

Comfort Properties of Superabsorbent Polyacrylate Fabrics for the next-to-Skin Layer in Firefighters' Protective Clothing. *Textile Research Journal*, 2018, 88, no. 9, 1077–88, https://doi.org/10.1177/0040517517697640.

[121] Wang D., et al., Evaluation of the Wearing Comfort Properties for Winter Used Electromagnetic Interference Shielding Sandwich Materials. *Journal of Industrial Textiles*, 2023, 53, 152808372311598, https://doi.org/10.1177/15280837231159869.

[122] Bai H., et al., Theoretical Model of Single Fiber Efficiency and the Effect of Microstructure on Fibrous Filtration Performance: A Review. *Industrial & Engineering Chemistry Research*, 2021, 60, no. 1, 3–36, https://doi.org/10.1021/acs.iecr.0c04400.

[123] Fan J., et al., Dimensionless Study of the Fiber Arrangement on Particle Filtration Characteristics in a Multi-Fiber Filter. *Journal of Industrial Textiles*, 2023, 53, https://doi.org/10.1177/15280837231200030.

[124] Kohanski M.A., et al., Review of Indoor Aerosol Generation, Transport, and Control in the Context of COVID-19. *International Forum of Allergy & Rhinology*, 2020, 10, no. 10, 1173–79, https://doi.org/10.1002/alr.22661.

[125] Payen J., et al., Influence of Fiber Diameter, Fiber Combinations and Solid Volume Fraction on Air Filtration Properties in Nonwovens. *Textile Research Journal*, 2012, 82, no. 19, 1948–59, https://doi.org/10.1177/0040517512449066.

[126] Abraham J.P., et al., Using Heat to Kill SARS-CoV-2. *Reviews in Medical Virology*, 2020, 30, no. 5, https://doi.org/10.1002/rmv.2115.

[127] Kang S., et al., Hierarchical ZnO Nano-Spines Grown on a Carbon Fiber Seed Layer for Efficient VOC Removal and Airborne Virus and Bacteria Inactivation. *Journal of Hazardous Materials*, 2022, 424, 127262, https://doi.org/10.1016/j.jhazmat.2021.127262.

[128] Yoon K.Y., et al., Antimicrobial Effect of Silver Particles on Bacterial Contamination of Activated Carbon Fibers. *Environmental Science & Technology*, 2008, 42, no. 4, 1251–55, https://doi.org/10.1021/es0720199.

[129] Sim K.M., et al., Development and Evaluation of Antimicrobial Activated Carbon Fiber Filters Using Sophora Flavescens Nanoparticles. *Science of The Total Environment*, 2014, 493, 291–97, https://doi.org/10.1016/j.scitotenv.2014.06.002.

[130] Jung J.H., et al., Preparation of Airborne Ag/CNT Hybrid Nanoparticles Using an Aerosol Process and Their Application to Antimicrobial Air Filtration. *Langmuir*, 2011, 27, no. 16, 10256–64, https://doi.org/10.1021/la201851r.

[131] Wilk S., et al., The Addition of Carbon Nanotubes Modifies the Biological, Physicochemical, and Electrical Properties of Carbon Nanofiber Composites. *Chemical Engineering Journal*, 2023, 455, 140617, https://doi.org/10.1016/j.cej.2022.140617.

[132] Le Pape H., et al., Evaluation of the Anti-Microbial Properties of an Activated Carbon Fibre Supporting Silver Using a Dynamic Method. *Carbon*, 2002, 40, no. 15, 2947–54, https://doi.org/10.1016/S0008-6223(02)00246-4.

[133] Huang E., et al., Disinfection of Escherichia Coli by a Reactive Electrochemical Membrane System Involving Activated Carbon Fiber Cloth (ACFC). *Water*, 2019, 11, no. 3, 430, https://doi.org/10.3390/w11030430.

Research Outputs

Journal paper

[1] **Wang, Y**., Hu, S., Tunáková, V., Niamlang, S., Chvojka, J., Venkataraman, M., ... & Ali, A. (2024). Carbon felt from acrylic dust bags as flexible EMI shielding layer and resistive heater. Journal of Materials Research and Technology, 28, 4417-4427.

[2] **Wang, Y**., Baheti, V., Yang, K., Yang, T., Wiener, J., & Militký, J. (2021). Utility of whiskerized carbon fabric surfaces in resistive heating of composites. Polymer Composites, 42(6), 2774-2786.

[3] **Wang, Y**., Baheti, V., Khan, M. Z., Viková, M., Yang, K., Yang, T., & Militký, J. (2022). A facile approach to develop multifunctional cotton fabrics with hydrophobic, self-cleaning and UV protection properties using ZnO particles and fluorocarbon. The Journal of The Textile Institute, 113(10), 2238-2248.

[4] **Wang, Y**., Khan, M. Z., Li, S., Novotná, J., Viková, M., Stuchlík, M., ... & Petru, M. (2023). A novel approach to fabricate durable superhydrophobic and UV protective cotton fabrics using fly ash and graphene nanoplatelets. Cellulose, 1-16.

[5] **Wang, Y**. F., Baheti, V., Yang, K., Venkataraman, M., & Yang, T. (2020). Study on Ohmic Heating Behavior of Fly Ash Filled Carbon Woven/Epoxy Resin Composite. Journal of Fiber Bioengineering and Informatics, 13(1), 1-11.

[6] Yang, T., Hu, L., Xiong, X., **Wang, Y**., Wang, X., Petrů, M., ... & Militký, J. (2021). A comparison of fabric structures for carbon fiber reinforced composite: Laminated and orthogonal woven structures. Polymer Composites, 42(10), 5300-5309.

[7] Peng, Q., Tan, X., Xiong, X., **Wang, Y**., Novotná, J., Shah, K. V., ... & Militky, J. (2023). Insights into the large-size graphene improvement effect of the mechanical properties on the epoxy/glass fabric composites. Polymer Composites, 44(11), 7430-7443.

[8] Yang, T., Xiong, X., **Wang, Y**., Mishra, R., Petrů, M., & Militký, J. (2021). Application of acoustical method to characterize nonwoven material. Fibers and Polymers, 22, 831-840.

[9] Yang, K., Zhang, X., Venkataraman, M., Chen, K., **Wang, Y**., Wiener, J., ... & Militky, J. (2024). Thermal behavior of flexible and breathable sandwich fibrous polyethylene glycol (PEG) encapsulations. Textile Research Journal, 00405175241236494.

[10] Yang, K., Wiener, J., Venkataraman, M., **Wang, Y**., Yang, T., Zhang, G., ... & Militky, J. (2021). Thermal analysis of PEG/Metal particle-coated viscose fabric. Polymer Testing, 100, 107231.

[11] Karthik, D., Militky, J., **Wang, Y**., & Venkataraman, M. (2023). Joule Heating of Carbon-Based Materials Obtained by Carbonization of Para-Aramid Fabrics. C, 9(1), 23.

[12] Hu, S., Wang, D., Venkataraman, M., Křemenáková, D., Militký, J., Yang, K., **Wang Y**., Palanisamy, S. (2023). Enhanced electromagnetic shielding of lightweight copper-coated nonwoven laminate with carbon filament reinforcement. Journal of Engineered Fibers and Fabrics, 18, 15589250231199970.

[13] Ali, A., Azeem, M., Noman, M. T., Amor, N., Militky, J., Petru, M., & **Wang, Y**. (2022). Development of silver plated electrically conductive elastomers embedded with carbon black particles obtained from Kevlar waste source. Polymer Testing, 116, 107793.

[14] Yang, K., Zhang, X., Wiener, J., Venkataraman, M., **Wang, Y**., Zhu, G., ... & Militky, J. (2022). Nanofibrous membranes in multilayer fabrics to avoid PCM leakages. ChemNanoMat, 8(10), e202200352.

[15] Baheti, V., & **Wang, Y**. (2021). Ohmic heating and mechanical stability of carbon fabric/green epoxy composites after incorporation of fly ash particles. Materials Today Communications, 26, 101710.

[16] Khan, M. Z., Militky, J., Petru, M., Ali, A., **Wang, Y**., & Kremenakova, D. (2021). Hydrothermal Growth of TiO2 Nanoflowers on PET Fabrics for Functional Applications. Journal of Fiber Bioengineering and Informatics, 14(4), 199-210.

[17] Yang, K., Venkataraman, M., Karpiskova, J., Suzuki, Y., Ullah, S., Kim, I. S., ... & Yao, J. (2021). Structural analysis of embedding polyethylene glycol in silica aerogel. Microporous and Mesoporous Materials, 310, 110636.

[18] Yang, K., Venkataraman, M., **Wang, Y. F**., Xiong, X. M., Yang, T., Wiener, J., ... & Yao, J. M. (2020). Thermal performance of a multi-layer composite containing peg/laponite as pcms. Journal of Fiber Bioengineering and Informatics, 13(2), 61-68.

Book chapter

[1] **Wang, Y**., Militký, J., & Periyasamy, A. P. (2021). 5 Disinfection Mechanisms of UV. Textiles and Their Use in Microbial Protection: Focus on COVID-19 and Other Viruses.

[2] **Wang, Y.,** Ali A., Venkataraman M., & Militký, J. (2022). A Review on Flexible Carbon-based Conductive Polymer Nanocomposites for Stretchable Strain Sensors. Selected Topics in Fibrous Materials Science, 261-286.

[3] **Wang, Y**., Venkataraman, M., & Militký, J. (2023). Flexible Carbon-Based Nanocomposites. Advanced Multifunctional Materials from Fibrous Structures, 199-225.

Conference paper

[1**] Wang Y**.-F., Karthik D., Yang K., Yang T., Xiong X.-M., Baheti V., Militký J. Electrical heating properties of carbon fabric/green epoxy composites filled with fly ash (2019) Textile Bioengineering and Informatics Symposium Proceedings 2019 - 12th Textile Bioengineering and Informatics Symposium, TBIS 2019, pp. 44 – 51.

[2] **Y.-F. Wang**, V. Baheti, K. Yang, S. Hu, D. Wang, X.-D. Tan, T. Yang and J. Militký, "Electrical heating properties of various carbonized textile structures," in: Text. Bioeng. Informatics Symp. Proc. 2020 - 13th Text. Bioeng. Informatics Symp. TBIS 2020, pp. 99–106, 2020.

[3] **Y.-F. Wang**, J. Militky, A.P. Periyasamy, M. Venkataraman, V. Baheti, K. Yang, S. Hu, D. Wang, X.-D. Tan, T. Yang, T. Yang and Q.-Y. Peng, "Disinfection mechanisms of UV light and ozonization," Text. Bioeng. Informatics Symp. Proc. 2020 - 13th Text. Bioeng. Informatics Symp. TBIS 2020, pp. 173–180, 2020.

[4] **Y. Wang,** M. Venkataraman, V. Baheti, K. Yang, T. Yang, S. Hu, J. Wiener, J. Militký, Structural stability of carbon fiber composite heating elements functionalized with ZnO whiskers. Autex Conference 2021.

[5] **Wang Y.-F**., Venkataraman M., Peng Q.-Y., Yang K., Hu S., Militký J. Development of Polydimethylsiloxane (PDMS) /Copper-coated Graphite Elastomer for Strain Sensors (2022) Textile Bioengineering and Informatics Symposium Proceedings 2022 - 15th Textile Bioengineering and Informatics Symposium, TBIS 2022, pp. 8 – 15.

[6] **Wang, Yuanfeng**, Mohanapriya Venkataraman, and Jiri Militky. "Resistive heating performance of waste cotton-derived carbon obtained by salt-assisted hydrothermal carbonization." AUTEX 2022: 21st World Textile Conference AUTEX 2022-AUTEX Conference Proceedings, Lodz University of Technology Press, Lodz 2022, ISBN 978-83-66741-75-1.